



HAL
open science

Micro- and nano-patterning of conducting polymers for biomedical applications

Mohammed Elmahmoudy

► **To cite this version:**

Mohammed Elmahmoudy. Micro- and nano-patterning of conducting polymers for biomedical applications. Other. Université de Lyon, 2017. English. NNT : 2017LYSEM027 . tel-01844247

HAL Id: tel-01844247

<https://theses.hal.science/tel-01844247>

Submitted on 19 Jul 2018

HAL is a multi-disciplinary open access archive for the deposit and dissemination of scientific research documents, whether they are published or not. The documents may come from teaching and research institutions in France or abroad, or from public or private research centers.

L'archive ouverte pluridisciplinaire **HAL**, est destinée au dépôt et à la diffusion de documents scientifiques de niveau recherche, publiés ou non, émanant des établissements d'enseignement et de recherche français ou étrangers, des laboratoires publics ou privés.



N°d'ordre NNT: 2017LYSEM027

THESE de DOCTORAT DE L'UNIVERSITE DE LYON
opérée au sein de
l'Ecole des Mines de Saint-Etienne

Ecole Doctorale N° 488
Sciences, Ingénierie, Santé
Spécialité de doctorat : Microélectronique
Discipline : Bioélectronique Organique

Soutenue publiquement le 16/10/2017, par:
Mohammed ELMAHMOUDY

Micro- et Nano-patterning de Polymères Conducteurs pour des Applications Biomédicales

Devant le jury composé de :

De Mello, John	Professeur, Imperial College London	Président et rapporteur
Offenhäusser, Andreas	Professeur, Forschungszentrum Jülich	Rapporteur
Dufour, Isabelle	Professeur, Université de bordeaux	Examinatrice
Inal, Sahika	Professeur assistante, King Abdullah University of Science and Technology	Examinatrice
Gkoupidenis, Paschalis	Group leader, Max Plank Institute for polymer research	Examineur
Malliaras, George	Professeur, Ecole des Mines de Saint-Etienne	Directeur de thèse
Sanaur, Sébastien	Professeur assistant, Ecole des Mines de Saint-Etienne	Co-directeur de thèse

This thesis is dedicated to my lovely mother and siblings

NNT:

Mohammed ELMAHMOUDY

Micro- and Nano-Patterning of Conducting Polymers for Biomedical Applications

Speciality: Organic Bioelectronics

Keywords: Bioelectronics, PEDOT:PSS, Nano-patterning, Microelectronics

Abstract:

Bioelectronics uses electrical signals to interact with biological systems. Sensors that allow for electrical read-out of important disease markers, and implants/stimulators used for the detection and treatment of pathological cellular activity are only a few examples of what this technology can offer. Due to their intriguing electroactive and mechanical properties, organic electronics or π -conjugated materials have been extensively explored regarding their use in bioelectronics applications. The interest in organic electronic materials stemmed from their soft and flexible nature which dampens the mechanical properties mismatch with tissue. This less “foreign” surface enhances the signal transfer to/from cells *in vitro*. The attractive mixed electronic/ionic conductivity feature of conducting polymers enables coupling between the electronic charges in the bulk of the organic films with ion fluxes in biological medium. The prototypical material of organic bioelectronics is the conducting polymer poly(3,4-ethylenedioxythiophene) (PEDOT) doped with polystyrene sulfonate (PSS). PEDOT:PSS is commercially available, water-dispersible conjugated polymer complex that can be cast into films of high hole and cation conductivity, good charge storage capacity, biocompatibility, and chemical stability. In the present work we investigate an approach to tailor the mechanical, electrical, and electrochemical properties of PEDOT:PSS and study their impact on the performance of organic electrochemical transistors. In addition, we study the effect of micro-structuring and nano-patterning on the electrochemical impedance of PEDOT:PSS-coated gold electrodes for future neural recordings and stimulation. Moreover we demonstrate the use of micro-patterned PEDOT:PSS in cell adhesion and migration.

NNT:

Mohammed ELMAHMOUDY

Micro et Nano-patterning de Polymères Conducteurs pour des Applications Biomédicales

Spécialité: Bioélectronique Organique

Mots clés: Bioélectronique, PEDOT:PSS, Nano-patterning, Microélectronique

Résumé:

La bioélectronique utilise des signaux électriques pour interagir avec des systèmes biologiques. Les capteurs qui permettent la lecture électrique de marqueurs de maladies importantes et les implants/stimulateurs utilisés pour la détection et le traitement d'activité cellulaire pathologique ne sont que quelques exemples de ce que cette technologie peut offrir. Du fait de leurs propriétés électro-actives et mécaniques fascinantes, l'électronique organique ou les matériaux conjugués π ont été largement exploités dans le domaine de la bioélectronique. L'intérêt pour les matériaux électroniques organiques provient de leur nature douce et flexible qui amortit les désagrégations mécaniques à l'interface avec les tissus. Cette surface moins "étrangère" améliore le transfert de signal vers / en provenance des cellules *in vitro*. Le mélange intéressant entre conductivité électronique et ionique de ces polymères conducteurs permet le couplage entre les charges électroniques présentes dans le volume des films organiques avec les flux ioniques du milieu biologique. Le matériau prototypique de la bioélectronique organique est le polymère conducteur poly(3,4-éthylènedioxythiophène) (PEDOT) dopé avec du polystyrène sulfonate (PSS). Le PEDOT: PSS, disponible dans le commerce, est un complexe de polymères conjugués qui peut se disperser dans l'eau, être coulé sous forme de films biocompatibles très conducteurs comprenant des trous et des cations, doté d'une bonne capacité de stockage de charge et d'une bonne stabilité chimique. Dans ce rapport, nous étudierons une approche pour moduler les propriétés mécaniques, électriques et électrochimiques du PEDOT: PSS et étudier leur impact sur la performance des transistors électrochimiques organiques. Par ailleurs, nous évaluerons l'effet de la micro-structuration et du nano-patterning sur l'impédance électrochimique des électrodes en or recouvertes de PEDOT: PSS utiles pour de futurs enregistrements et stimulations neurales. Enfin, nous démontrerons l'utilisation du PEDOT:PSS à micro-motifs pour l'adhésion et la migration de cellules.

Acknowledgment

I would like to start off by thanking George Malliaras, the director of my thesis, for his outstanding and wise supervision of my Phd and his continuous professional and personal support. You gave us, PhD candidates and post-docs, the opportunity to learn and develop without pressuring anyone in anyway. You have created a work environment where everyone felt at home and gave us the necessary motivation to keep on the good work with the freedom to explore and satisfy our curiosity.

Thanks to Sébastien Sanaur for establishing the project and bringing the fund and doing all the necessary work to make it happen. And mostly for giving me the great opportunity to join the amazing Department of Bioelectronics (BEL).

A special thanks to Roisin Owens for her personal and professional support and for leading the department for the last period of my PhD.

I would like to thank all my colleagues from the BEL for being cooperative, and for making the department a very rich place for scientific discussions and exchange. You have definitely made the group a better place, and gave it all the fun and positive energy needed to keep it going and producing excellent work that is recognized worldwide. Names including the visiting professors and students; Xenofon Strakosas, Thomas Lonjaret, Marc Ramuz, Mar FERRO, Rod O'Connor, Alexandra Rutz, Ilke Uguz, Mary Donahue, Paschalis Gkoupidenis, Vincenzo F Curto, Christopher Proctor, Sahika INAL, Usein Ismailov, Donata Iandolo, Yi zhang, Charalampos Pitsalidis, Ana Sanchez, Esma Ismailova, Dimitrios A Koutsouras, Eloïse Bihar, Marcel Brändlein, Anna-Maria Pappa, Shahab Rezaei Mazinani, Jolien Pas, Magali Ferro, Aimie Pavia, Isabel del Agua, Gerwin Dijk, Viviana Fascianella, Loig Kergoat, Carol Chan, Helena Gleskova, David Martin, Jon de Mello, Alberto Salleo, Miriam Huerta, Clemens STOLZ, Jacob Friedlein, david ohayon, Michel Fiocchi, Adam WILLIAMSON, Susan Daniel, Nathan Schaefer, Takamatsu SEIICHI, Gaëtan Scheiblin, Sofia Drakopoulou,

Amale Ankhili, Federica MARIANI, Timothée Roberts, Silvia Battistoni, Julie, Patrick FOURNET, Margaret BRENNAN, Yingxin, Manu, Maria, Simon Régal, liza klots, Jonathan Rivnay, and Daniel Corzo. As well as Pierre Leleux from Panaxium startup for the active support in the clean room and fruitful discussions.

I specially thank people who I had the pleasure to work with on common projects; Sahika INAL, Alexandra RUTZ, Ilke UKUZ, Mary DONAHUE, Vincenzo CURTO, Magali FERRO, Rodney O'CONNOR, Adel HAMA, and Isabel DEL-AGUA-LOPEZ. In addition to my collaborators; Martina SCHMIDT from University of Bayreuth, Germany, and Anne CHARRIER from CINAM, CNRS, Aix-Marseille University, France.

I would like to also thank Bastien MARCCHIORI, Mohamed SAADAOU, and Cyril CALMES from Flexible Electronics Department (FEL) for their help and support. As well as the clean room staff; Gaëlle RONDEAU, Sylvain NOLOT, Jessica MAZUIR, Thierry CAMILLONI, and Jean-Philippe for taking care of the safety and security in the clean room area and their efforts in keeping the machines up and running.

Special thanks to Philippe Lalevée, the director of the Center of Microelectronics Georges Charpak of the Provence, and the platform Micro-Packs, for his great support during my PhD and for his efforts in managing our école and providing a productive environment for work.

Not to forget the great people behind the scene, the administration stuff; Véronique VILLAREAL for her great help though out my PhD, as well as Michelle Gillet, and Anaïs BALAGUER. Aurélie and Johanne at the front desk. And Gracien COUNOT and Christophe LECOINTE from the IT office, as well as melodie CAYOL and LAGAIZE Richard from the logistics office.

I would like to also thank the Agence Nationale de la Recherche for supporting my PhD project financially (grant number: ANR-14-CE08-0006).

To my mother, Mervat SALAH, you have been my strength and inner sound of wisdom. You have given me and my siblings, the example of protecting the pure kind human nature along

the years and through any conditions. You gave us the example of the strength, the patience, and the strive to success. Being a single mother of four for 26 years, you have seen a lot of challenges, and lot of distressing moments and situations, you have been the super mama who made it through all. You have made everyone impressed by how far you could take us. You have been self-ignoring to provide for us and make us as happy as possible. We love you and appreciate who you are. All what I have acquired from you through the years gave me strength and persistence to be the man I am today, and this has been always a support for me during my PhD work.

To my siblings, Ahmed, Amr, and Rana, you are the rock stars. You have gone so far in your lives, and made me look up to you. You have been always the support system that I could rely on. You gave me and the family all the needed support while I was busy working on my Phd and being so far away. You have created sustained the ecosystem for the family, thank you really and truly. You have been always there for anything I needed. Your presence has made a huge difference, and I wish I can pay you back a little of what you have given me.

Last, but not least, I would like to give very special thanks to my partner Douaa Mckadm. You give me all the emotional support, encouragement, and love to stay focused on my PhD work. At my many very low points, you saw the bright side of things, and you gave me the right analysis, and told me the exact words that kept me moving. You are such a positive adorable cheerful smart person. Even though my PhD drained me out of energy for extended periods of time, and stressed me and changed my moods, you have been always understanding and absorbing. And most of all, you have been always my mirror; you made me learn more things about myself, and understand more who I am and what I really need and want in life. Intelligent strong loving women like you can build nations and civilizations. I love you, and I wish I can make you always happy.

Table of Content

Chapter 1	10
PEDOT:PSS for Biomedical Applications.....	10
1.1. Introduction	10
1.2. Synthesis and Deposition.....	12
1.2.1 Electrochemical Approach.....	12
1.2.2 Chemical Approach	14
1.2.2.1 Synthesis.....	14
1.2.2.2 Deposition	15
1.3. Properties	18
1.3.1 Film Structure and Mechanical Properties.....	18
1.3.2 Electrical properties	22
1.3.3 Stability	26
1.4. Applications.....	31
1.4.1 Electrophysiology	33
1.4.2 Tissue Engineering.....	44
1.4.3 Biosensing.....	48
1.4.4 Drug Delivery	52
1.5. Conclusions and Future Directions.....	57
References	59
Chapter 2	67
Tailoring the Electrochemical and Mechanical Properties of PEDOT:PSS Films for Bioelectronics.....	67
2.1 Introduction	67
2.2 Results and Discussion	70
2.2.1 Effect of the cross-linker on electrical properties	70
2.2.2 Cross-linked PEDOT:PSS properties in aqueous environment	72
2.3 Conclusion	79
2.4 Experimental Section.....	79
References	83
Supporting Information	85
Chapter 3	89
Facile Nano-Patterning of PEDOT:PSS Thin Films	89
3.1 Introduction	89

3.2 Results and Discussion	92
3.3 Conclusion	101
3.4 Experimental Section.....	101
References	104
Supporting Information	105
Chapter 4	109
Designing Low Impedance Amorphous PEDOT:PSS Electrodes For Neural Recordings ...	109
4.1 Introduction	109
4.2 Results and Discussion	112
4.3 Conclusion	117
4.4 Experimental Section.....	117
References	121
Chapter 5	122
Linear Cell Migration on Micro-Patterned Conducting Polymers.....	122
5.1 Introduction	122
5.2 Results and discussion	124
5.3 Conclusion	133
5.4 Experimental Section.....	134
References	138
Supporting Information	140
Chapter 6	142
Conclusion and outlook	142
Appendix	146
List of Publications and Conferences	151

Chapter 1

PEDOT:PSS for Biomedical Applications

1.1. Introduction

The field of electronics has had a great impact in the field of medicine. Electronic devices such as glucose monitors, pacemakers, defibrillators, cochlear implants, and deep brain stimulators are resulting into quality of life improvements for millions around the world. Traditionally, electronics have been built from inorganic electronic materials such as silicon and metals, which have drastically different properties (chemical, mechanical, electrical) than those of biological materials. Recently, organic electronic materials are being increasingly investigated for their potential to interface with biological systems.^[1,2] Advantages of organics include a chemical structure that is rather similar to that of biological molecules, “softer” mechanical properties than their inorganic counterparts, and the capability to conduct ionic charges.

Conjugated polymers possess alternating single and double bonds that form π molecular orbitals along the polymer backbone.^[3] They can be doped to become conducting, resulting into excess holes or electrons in these orbitals that can move along the polymer backbone as well as between adjacent polymer chains. The doping process is described as oxidation or reduction of the conjugated polymer, or as *p*-type and *n*-type doping, respectively. At any case, counter ions (dopands) are present in the film to compensate the excess electronic charge. There are several types of conducting polymers, based on polypyrrole, polythiophene, and polyaniline. The applications of these conducting polymers in

biomedical applications are extensive.^[4] This review will focus on the polymer poly(3,4-ethylenedioxythiophene) doped with poly(styrene sulfonate) (PEDOT:PSS) due to its ubiquitous use. In this system, PEDOT is the π -conjugated polymer and it is doped *p*-type by the polyanion PSS (**Figure 1**).

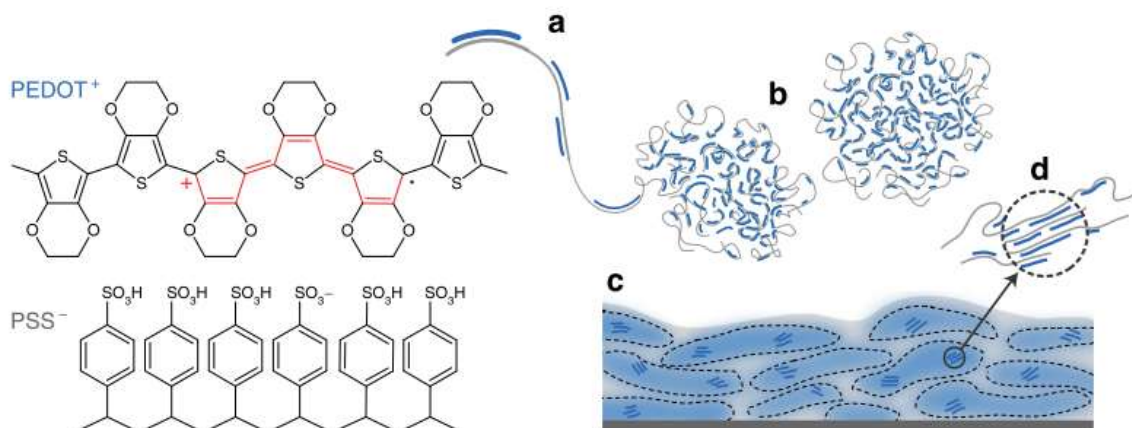


Figure 1. PEDOT:PSS structure and morphology. The chemical structure of PEDOT:PSS and commonly described microstructure of the conducting polymer system (a) synthesis onto PSS template, (b) formation of colloidal gel particles in dispersion and (c) resulting film with PEDOT:PSS-rich (blue) and PSS-rich (grey) phases. (d) Aggregates/crystallites support enhanced electronic transport. Reproduced with permission.^[5] Copyright 2015, Nature publishing group.

PEDOT:PSS is the most commonly used conducting polymer in organic electronics due to its high conductivity, accessibility (easy to synthesize and commercially available), and facile film deposition. Besides these advantages, PEDOT:PSS is cytocompatible, has a lower Young's modulus than traditional electronic materials, and shows mixed ionic/electronic conductivity, all of which are favorable properties for interfacing with biological systems. PEDOT:PSS can be synthesized by chemical and electrochemical routes, and can be deposited in a variety of ways to yield structures of different form factors including thin films, fibers and 3D porous scaffolds. Many of these deposition methods are inexpensive and rely on equipment that is readily available. Moreover, its properties can be tuned over a wide range through the incorporation of various additives.

In this review, we begin by outlining the synthesis and deposition of PEDOT:PSS as these two processes have a large impact on the resulting properties. We will then overview film structure, mechanical and electrical properties, and discuss stability issues. Finally, we will go over the broad range of applications in field such as electrophysiology, biosensing, tissue engineering and drug delivery.

1.2. Synthesis and Deposition

There are two main types of synthetic routes of PEDOT:PSS; chemical polymerization and electrochemical polymerization – both initiate an oxidation reaction of the monomer EDOT. Both have been widely used in biomedical applications, and the application often dictates the choice of fabrication method. Electrochemical polymerization and deposition occur simultaneously, whereas chemically-polymerized PEDOT:PSS results in a aqueous dispersion, which can be deposited in a great variety of ways. Here, we will briefly discuss each synthetic route as well as how PEDOT:PSS from each method is deposited for device fabrication.

1.2.1 Electrochemical Approach

Electrochemical polymerization is an easy and fast technique for depositing PEDOT:PSS on conductive surfaces such as gold. It also allows selective deposition on specific areas where a metallic film is present. This a convenient method to pattern PEDOT:PSS, as opposed to multi-step photolithographic techniques, but also requires a conductive substrate, which can limit its use in some devices. This process is typically performed in an electrochemical cell with a three-electrode configuration. A working electrode, reference electrode and counter electrode are submersed in a solution of the monomer 3,4-ethylenedioxythiophene (EDOT) and poly(styrene sulfonate) sodium salt in deionized water.^[6,7] EDOT monomers are oxidized by the metal electrode and form a cation. These cations combine together to form oligomers and chains that eventually precipitate on

the electrode (**Figure 2**).^[7,8] Polymerization can be done in potentiostatic (constant potential), galvanostatic (constant current) or potentiodynamic modes. PEDOT:PSS films electrochemically deposited in the galvanostatic mode were found to be more uniform when compared to those deposited in potentiostatic mode (**Figure 3**).^[6] In both modes, an edge effect was observed and this led to thicker deposition along the circumference of the electrodes. The edge effect is due to a non-uniform current distribution on the electrodes and is more pronounced when operating in potentiostatic mode.^[6] The deposition time, current density and solution concentration contribute to the thickness of the electrochemically deposited film. For instance, the film thickness is directly proportional to the deposition charge (ex. for 1 μm at 5 μC). In another study, a potentiodynamic mode was used to polymerize PEDOT:PSS by scanning potentials using cyclic voltammetry.^[9] When compared to the films obtained by galvanostatic and potentiostatic modes, the potentiodynamic films were relatively more homogenous.



Figure 2. Electrical polymerization process. (a) The metal electrode oxidizes the EDOT monomers creating radical cations. (b) These radical cations combine, creating dimers, trimers, and higher oligomers. (c) As the molecular weight of the polymer chains increase they become insoluble, precipitating onto the metal electrode surface. Adapted with permission.^[8] Copyright 2016, the Royal Society of Chemistry.

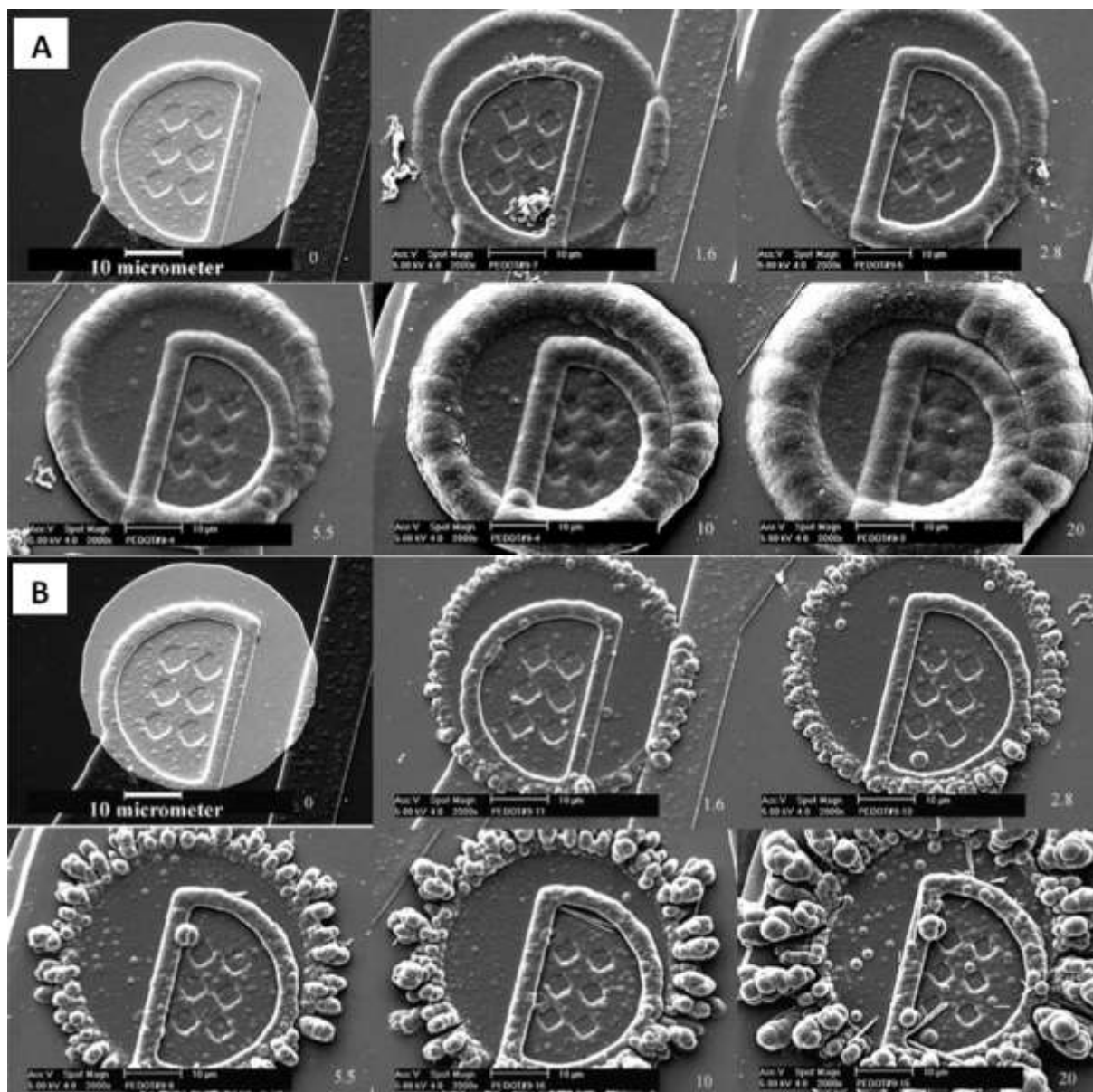


Figure 3. Electrochemical growth of PEDOT :PSS on the microelectrode sites of neural probes (a) galvanostatic (b) potentiostatic. Numbers on the right corner of each image indicate the deposition charge on each site (in μC). Adapted with permission.^[6] Copyright 2003, Elsevier.

1.2.2 Chemical Approach

1.2.2.1 Synthesis

PEDOT can be chemically synthesized via several synthetic routes^[10] with the aid of oxidizing agents such as iron (III) chloride or nitride and peroxodisulfates^[11]. Obtaining a stable aqueous dispersion is assisted by the presence of PSS. Due to its polar nature stemming from its sulfonic acid groups, PSS helps solvate PEDOT in the form of

PEDOT:PSS complexes.^[11,12] The resulting dispersion is very stable and has a long shelf-life, which has facilitated its commercialization. Several commercialized formulations exist (e.g. Heraeus Clevios™, Agfa Orgacon, Sigma Aldrich), allowing easy processing and reproducible film formation.^[12]

The weight ratio between the thiophene groups and sulfonic acid groups for commercially available PEDOT:PSS (Heraeus Clevios™) is about 1:2.5; however, there is only a single charge introduced on every 3-4 thiophene groups. The fact that the charge ratio and mass ratio of chemicals do not match shows that the PSS is always added in excess.^[12-14] Although not required for doping/charge balance, excess PSS is required for stabilizing the PEDOT:PSS dispersion by forming PSS shells around the PEDOT:PSS gel-like particles to prevent aggregation through electrostatic repulsion.^[12,15]

1.2.2.2 Deposition

Chemically-polymerized aqueous dispersions of PEDOT:PSS can be deposited in a great variety of ways. Deposition methods include conventional coating techniques such as drop casting, spin-coating, solution-shearing, doctor-blading, ink-jetting, electro-spinning and spraying.^[12] Every technique might require some optimization of the PEDOT:PSS dispersion content to obtain a uniform film. Additionally, solution viscosity, surface tension, and adhesion to the substrate must also be considered and optimized. Dispersion additives have a direct impact on these parameters and will be discussed in Section 1.3.2.^[16,17]

Drop casting is the simplest coating technique, which includes only two basic steps: casting the polymer on a substrate and drying. The greatest advantage of this technique is that no machines are required. However, films obtained by drop casting are relatively thick (depending on the viscosity and substrate wettability) and lack homogeneity along the substrate.

Spin-coating PEDOT:PSS is typically used for thin film applications and often used as part of photolithographic fabrication in which PEDOT:PSS can be patterned with μm -scale

resolution. Unlike drop casting, spin-coating yields very homogenous films of up to ~300 nm thick from a single layer and ~800 nm from multiple layers.^[12] In contrast to electrochemical deposition, spin coating yields more homogeneous PEDOT:PSS coatings, particularly at the edges of the film. It can be used to coat large substrates, with high reproducibility.^[12] In this technique, the substrate is placed on a rotating sample holder and then the solution is drop cast on it before or while the holder is rotating. The thickness of the polymer film decreases with rotation speed (rpm) and increases with solution viscosity.^[18] The spin coating step is usually followed by a drying step to remove the excess water content and some solvent additives. This drying step can be done by thermal treatment or by applying vacuum. A drawback of this technique is generating significant material waste since most of the used solution is excessive and is ejected during the process. Further details of polymer spin-coating, in terms of both physical and chemical properties, are described in the following review.^[19]

Doctor blading is another technique used for film formation of homogenous thicknesses. In this technique, the blade (or knife) is placed parallel to a substrate with a certain gap that defines the film thickness. Afterwards, the solution is placed in front of the knife which then starts moving along the substrate. In comparison to spin coating, the material loss using doctor blading is negligible, and the range of thicknesses (10 μm to 500 μm) obtained is much higher.

Solution shearing deposition is a similar technique to doctor blading and has been used for organic polymer deposition.^[20-22] In this technique, the solution is placed in-between two surfaces. The bottom surface is a heated substrate treated to be hydrophilic, while the upper surface is a silicon blade treated to be hydrophobic. The top plate is designed to move parallel to the substrate at a controlled speed. This movement leads to exposing some solution to air, and with heat provided by the bottom blade, the solvent can evaporate to form the film. The obtained film contains crystallized sites that propagate along with the direction of shearing. This technique was shown to be scalable up to areas of 5 x 5 cm. Shearing speed, temperature,

and solution properties are all parameters that can be tuned in this technique. Like spin coating, the deposited thickness using this technique is inversely proportional with the shearing speed. Shearing parameters have been changed to tune film morphology and composition: 20 to 250 nm thicknesses were obtained from shearing speeds of 0.02 to 4 mm/sec.^[23] In comparison to spin coating, shearing deposited PEDOT:PSS is more conductive and more transparent.^[23]

Inkjet printing is an additive solution deposition technique that has also been used for depositing PEDOT:PSS.^[24–26] This technology allows direct patterning of the ink on a variety of substrates including those that are rigid, flexible, or stretchable.^[24,27] This technology consists of computer-aided design, ink preparation, printing, and curing by heat or UV light.^[25,27] Thickness of inkjet-printed films can be tuned by the number of printed layers. A thickness of 190 nm was obtained from two layers of PEDOT:PSS, but this is dependent on ink composition and process parameters.^[26] In addition to its low cost, other advantages of this technique include minimal material loss and the ability to pattern without expensive masks that are used in photolithography.^[28]

Spray deposition techniques such as airbrush spraying, electro-spraying, and ultrasonic spraying have been used for depositing PEDOT:PSS; however, most of their applications were only focused on organic photovoltaic devices, which is out of the focus of this review.^[29–34] Other form factors of PEDOT:PSS include the fabrication of microfibers using wet-spinning,^[35,36] brushing onto textiles^[37] and scaffolds using freezing templating.^[38]

The great variety of deposition methods gives flexibility in fabricating PEDOT:PSS into a variety of forms and device structures. Desired material properties (e.g. morphology, electrical properties, adhesion to substrate), patterned features, and thickness also further dictate deposition method.

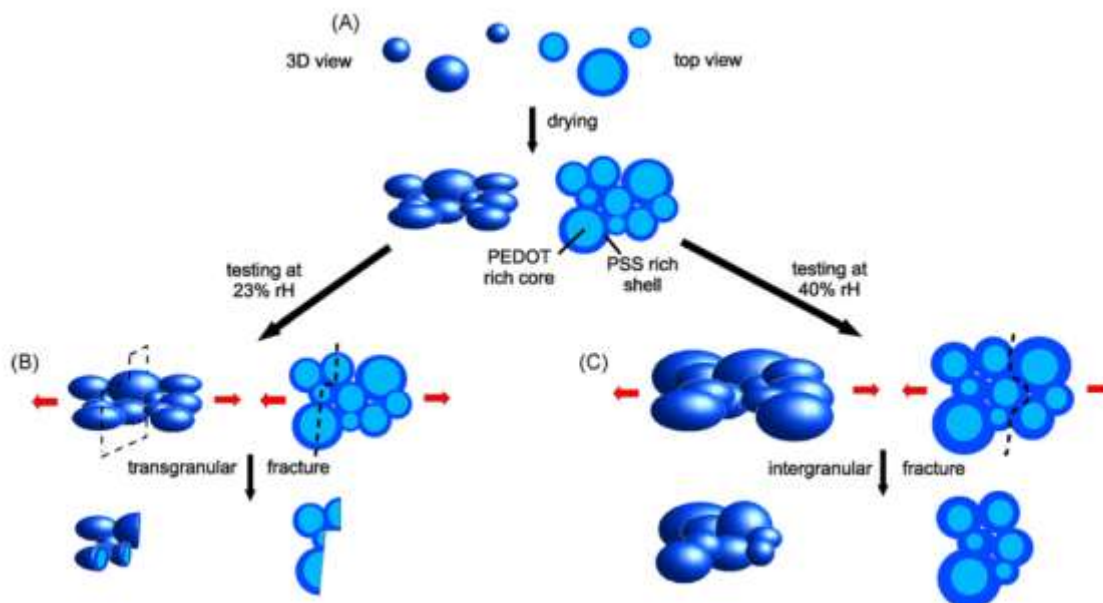


Figure 1. Comprehensive schematic overview of the proposed models: (A) PEDOT:PSS forms spherical gel particles in aqueous dispersions. Upon drying a solid film consisting of lentil-like shaped grains develops. (B) At low relative humidity, e.g. 23% rH the hydrogen bonds in the PSS rich shell are very strong and therefore external tensile forces lead to a transgranular brittle fracture and therefore smooth fracture surfaces. (C) At higher relative humidity, e.g. 40% rH the hygroscopic PSS takes up water which causes the hydrogen bonds to be weakened and also leads to a swelling of the film. Upon exertion of external tensile forces individual PEDOT:PSS grains can slide by each other and therefore intergranular plastic fracture takes place. The fracture surface is rough with rather spherical grains forming the outer layer. Reproduced with permission.^[39] Copyright 2009, Elsevier.

1.3. Properties

The vast majority of work on the determination of properties of PEDOT:PSS has been on spin coated films of chemically-polymerized PEDOT:PSS, owing to the application of this material in a variety of organic electronic devices such as light emitting diodes and solar cells. The properties of electrochemically polymerized PEDOT:PSS, on the other hand, have received less attention.

1.3.1 Film Structure and Mechanical Properties

PEDOT:PSS particles have been repeatedly described as having a “pancake” morphology, as shown in Figure 1, and this also describes the bulk morphology of PEDOT:PSS spin coated thin films.^[5,40–42] Experiments combining anisotropic conductivity measurements with scanning tunneling microscopy and atomic force microscopy revealed the

presence of PEDOT-rich particles of 20-25 nm in diameter and 5-6 nm in height separated by PSS lamellas.^[41] These findings were supported by scanning tunneling electron microscopy on PEDOT:PSS thin films (25 nm thick), which revealed the same distribution and sizes of the PEDOT:PSS particles.^[40] By using energy dispersive X-ray spectroscopy, the PSS shell around the individual PEDOT clusters was found to be 5-10 nm.^[40] Ultraviolet photoelectron spectroscopy has also been used to study the surface morphology of PEDOT:PSS thin films. This spectroscopy method can differentiate between PEDOT and PSS by their binding energies.^[43] Authors found that the PSS concentration at the surface is 3 folds higher than expected and that the PSS concentration in the bulk is lower than its concentration at the surface.^[43,44]

One of the main advantages of PEDOT:PSS is its soft nature compared to inorganic conductors. This softness allows PEDOT:PSS films to be conformable and even stretchable in some cases.^[16,45] PEDOT:PSS films swell when immersed in water or placed in a humid environment, and their thickness increases accordingly.^[11,12] Swelling also helps increase ionic mobility in the film.^[46] Additionally, the swelling is responsible for a reduction in the electrochemical impedance of PEDOT:PSS-coated metal electrodes, as discussed in detail in Section 1.3.2. For these reasons, swelling is a very important property of PEDOT:PSS films for biomedical application.

A general morphological model for the swelling of PEDOT:PSS films^[39] was proposed assuming the films contained PEDOT-rich particles and PSS shells (**Figure 4**).^[40] At low relative humidity, the model states that the hydrogen bonds in the PSS shells are strong, and the film exhibits brittle fracture that propagates through the grains.^[40] At a higher humidity, PSS shells absorb water and the inter-distance between the shells increases; therefore, hydrogen bonds between PSS shells diminish and so does the mechanical strength of the film.^[40] A few studies have quantified the swelling of PEDOT:PSS films when immersed in water^[46,47], and their findings are summarized in **Table 1**.

Several studies have investigated the mechanical properties of PEDOT:PSS using techniques such as tensile testing, peak force quantitative nanomechanical property mapping (QNM) and strain-induced buckling instability (SIEBIMM).^[16,35,39,48,49] **Table 2** summarizes Young's modulus values of PEDOT:PSS in different conditions of humidity as well as in water.

Cross-linkers are often added to PEDOT:PSS to increase film stability. Film stability is required for biomedical devices that are immersed in aqueous solutions. Not only must the films maintain their integrity, but also they should have strong adhesion to the substrate. Furthermore, the use of cross-linkers can increase the mechanical properties of films. A few cross-linkers of PEDOT:PSS have been demonstrated to date.

3-glycidoxypropyltrimethoxysilane (GOPS) is often used as a cross-linker for PEDOT:PSS films.^[50-52] GOPS allows strong film integrity and strong adhesion to the substrate when immersed in aqueous solutions.^[53] Increasing the GOPS concentration in PEDOT:PSS films increases the mechanical strength as shown in Table 2 but at the expense of conductivity.^[53] Divinylsulfone (DVS) is another chemical additive that was recently used as a low temperature cross-linker for PEDOT:PSS.^[54] In contrast to GOPS, DVS only had a very small effect on conductivity while enhancing the mechanical properties and film integrity.^[54]

Aside from cross-linkers, other additives may be used to change the mechanical properties and swelling. Some researchers have blended polyvinyl alcohol (PVA) with PEDOT:PSS to increase its flexibility, ductility, and durability.^[55-57] The Young's modulus of pure PVA films was increased from 41.3 MPa to 1.63 GPa by increasing the concentration of PEDOT:PSS from 0% to 50%.^[58] The increase in PEDOT:PSS ductility resulting from PVA addition was countered by a decrease in tensile strength, Young's modulus, and conductivity since PVA is insulating and decreases contact between the PEDOT-rich regions.^[55,59]

Table 1. The swelling of PEDOT:PSS in water

PEDOT:PSS Form	Additives	Measurement Technique	Swelling	References
Thin film	-	AFM	660% \pm 90%	Duc et al. ^[47]
Thin film	1% GOPS	AFM	40% \pm 1%	Duc et al. ^[47]
Thin film	1% GOPS	AFM	35% \pm 4%	Stavriniidou et al. ^[46]

Table 2. The mechanical properties of PEDOT:PSS thin films, pristine and with additives

PEDOT:PSS Form	Additives	Specific Conditions	Measurement Technique	Young's modulus	References
Microfibers	-	Room temp.	Tensile test	1.1 \pm 0.3 GPa	Okuzaki et al. ^[35]
Cast film	3% EG	50% rH / 25 °C	Strain gauge Stress-Strain curves	1.8 \pm 0.2 GPa	Okuzaki et al. ^[35]
Pipetted film	-	40%rH	Tensile test	2.7 GPa	Lang et al. ^[39,48]
Pipetted film	-	50%rH	Tensile test	2.0 GPa	Lang et al. ^[39,48]
Pipetted film	-	23% rH/ 22 °C	Tensile test	2.8 \pm 0.5 GPa	Lang et al. ^[39]
Pipetted film	-	40% rH/ 22 °C	Tensile test	1.9 \pm 0.02 GPa	Lang et al. ^[39]

Pipetted film	-	55% rH/ 22 °C	Tensile test	0.9 ± 0.2 GPa	Lang et al. ^[39]
Thin film	-	-	SIEBIMM*	0.8 ± 0.1 to 1.02 ± 0.2 GPa	Greco et al. ^[16]
Thin film	-	23 to 30% rH	Buckling method	2.26 ± 0.05 GPa	Tahk et al. ^[60]
Electrochemically deposited PEDOT thin film	-	25 °C	PeakForce QNM**	2.6 ± 1.4 GPa	Qu et al. ^[49]
Electrodeposited film	-	-	NanoIndentat ion	3.23 ± 1 GPa	Baek et al. ^[61]
Cast film	PEDOT:PSS(50%)/ PVA	40 ± 2% rH	Tensile test	1.632GPa	Chen et al. ^[55]

* SIEBIMM stands for strain-induced buckling instability for mechanical measurements.

** QNM stands for quantitative nanomechanical property mapping.

1.3.2 Electrical properties

PEDOT:PSS exhibits intrinsic electronic conduction properties.^[12] The conductivity of PEDOT:PSS is usually deduced from the sheet resistance measured from a flat film deposited on a non-conducting supporting layer using the 4-points probe technique or the transmission line method.^[16,62] The weight ratio of PEDOT to PSS alters the charge density on PEDOT and results in a change in the conductivity.^[12] The conductivity of PEDOT:PSS films is highly anisotropic: the lateral conductivity is three times higher than the vertical conductivity.^[41] This difference is due to film morphology, as PEDOT-rich particles, of about 20-25 nm in

diameter and 5-6 nm in height, are separated by PSS lamellas, which have weak electrical conduction.^[41]

The conductivity of commercial, aqueous PEDOT:PSS (pristine) ranges from 10^{-5} to 10^1 S/cm and can even exceed 1000 S/cm with certain additives.^[12] Several methods have been investigated to enhance the electrical conductivity of PEDOT:PSS films including treatments with light and heat as well as the treatments with ionic liquids, salt solutions, acids, organic solvents, and surfactants.^[63] A comprehensive summary of the conductivity values of treated PEDOT:PSS versus pristine PEDOT:PSS was presented in a recent review.^[63] Here, we will only highlight the three most widely used solvent additives used for enhancing the conductivity of PEDOT:PSS.^[63]

Dimethyl sulfoxide (DMSO) is a high-boiling point, polar solvent used for enhancing the conductivity of PEDOT:PSS.^[64–72] DMSO was first added to PEDOT:PSS dispersions in 2002.^[73] By adding one-part DMSO to three parts PEDOT:PSS (v/v), the conductivity was increased by 2 orders of magnitude, from ~ 0.8 S/cm to ~ 80 S/cm.^[73] This increase in conductivity is believed to be due to remaining DMSO that increases the separation of positive and negative charges on the PSS and PEDOT, respectively, and thereby reduces the electrostatic interactions between the chains (“screening effect”).^[73] Since then, many works have investigated the effect of solvents on the conductivity and morphology of PEDOT:PSS films.^[63–69,74–76] By adding DMSO, PEDOT-rich grains become enlarged and were more uniformly distributed in films. The increase in conductivity was attributed to these morphological changes.^[65] For inkjet-printed PEDOT:PSS films, the conductivity of PEDOT:PSS was increased by four orders of magnitude by adding 5% DMSO to the ink.^[70,77] The additional increase in conductivity was due to a three-fold increase in PEDOT particle size.^[77]

Used in a similar fashion as DMSO, ethylene glycol (EG) is another high-boiling point, polar solvent used for increasing the conductivity of PEDOT:PSS

films.^[43,45,47,55,56,60,61,66] It was demonstrated that by adding 7% EG, there was an increase of ~3 orders of magnitude in the conductivity of PEDOT:PSS films.^[78] Later, a 100-fold enhancement in the conductivity was observed when adding or when treating with EG.^[79] The mechanism of this increased conductivity was found to be from a change in the conformation of coiled PEDOT chains: from more compacted coils to either more expanded coils or linear chains. Furthermore, PEDOT chains changed from a benzoid structure (contributing to a coil conformation) to a quinoid structure (contributing to a linear chains) as revealed by Raman spectroscopy. In another study, authors reported an increase of more than 100 fold in the PEDOT:PSS conductivity (from 6 to 800 S/cm) with the addition of 5% EG.^[5] They suggested that this increase in conductivity was due to increased aggregation of PEDOT particles and tighter π -stacking.^[5] In other groups, researchers suggested that the PEDOT particle size increased and became more homogeneously packed.^[75,80] All of these studies relate the increase in PEDOT:PSS conductivity with EG addition to a change in the PEDOT:PSS film morphology, either due to stronger PEDOT particle interactions or due to more linear PEDOT chains.

Another example of the organic solvents used for improving the conductivity of PEDOT:PSS is sorbitol (a sugar alcohol).^[75,81–85] With the addition of sorbitol, PEDOT:PSS conductivity was increased by 2 orders of magnitude due to an increase in the PEDOT particle size.^[75] In the PEDOT:PSS dispersion, sorbitol undergoes a chemical conversion to 1,6-anhydrosorbitol and the PEDOT:PSS particle size increases, both of which contribute to improving conductivity.^[84]

In neural recordings and other electrophysiology applications, the electrode impedance is an important indicator of how well an electrode will capture signals. Therefore, analyzing and understanding the mechanism of charge transport and electrochemical impedance is crucial for designing and optimizing the performance of such devices.^[86] PEDOT:PSS coatings are known to dramatically decrease the impedance of metallic electrodes, especially

in the low frequency range (by ~ 2 orders of magnitude).^[6,87,88] This drop in the impedance is due to the mixed electronic and ionic conductivity in PEDOT:PSS; PEDOT-rich regions (electrically-conducting) facilitate and increase opportunities for charge exchange while the high water content of PEDOT:PSS imparts high ionic conductivity.

The complex electrochemical impedance curve of a PEDOT:PSS thin film is typically composed of two regions, a capacitance-dominated region at low frequencies and a resistance-dominated region at high frequencies.^[88] The transition between these two regions happens at a characteristic frequency (f_c). The f_c of a gold electrode shifts to lower values when coated with PEDOT:PSS (from 10 kHz to 100 Hz for 0.5 x 0.5 mm electrode, 350 nm PEDOT:PSS layer thickness).^[87] The impedance curve can be modeled by a simple RC or R(RC) circuit model, where R corresponds to the solution resistance (R_s), and C corresponds to the film capacitance. Since PEDOT:PSS swells in aqueous media and liquid electrolytes can enter the film, the charge transport can be understood in terms of volumetric capacitance (C_v : capacitance per unit volume).^[89] It was reported that capacitance scales with the volume of PEDOT:PSS films and this causes lower impedance.^[88] The volumetric capacitance of PEDOT:PSS can be understood as follows (**Figure 5**):^[90] PEDOT chains carry holes and PSS chains carry the sulfonate anions that balance these holes.^[90] Upon applying a positive bias, the cations from the electrolyte move inside the PEDOT:PSS film and replace the holes (Figure 5a). The volumetric capacitance can be estimated by treating the injected cations and sulfonate anions pairs as elementary capacitors. In Figure 5b, the holes/anion sites are represented as a group of planes perpendicular to the film surface and distanced by an average spacing α .^[90] The authors suggest that every plane represents a double layer capacitance ($C'_{DL}=C/A$, capacitance per unit area), and they deduced the volumetric capacitance as $C^*=C'_{DL}/\alpha$.^[90] This study suggested that the PEDOT volumetric capacitance can be enhanced by bringing the hole/anion sites closer together by adding dopants that are smaller than PSS or by blending with nanomaterials with high charge densities.^[90]

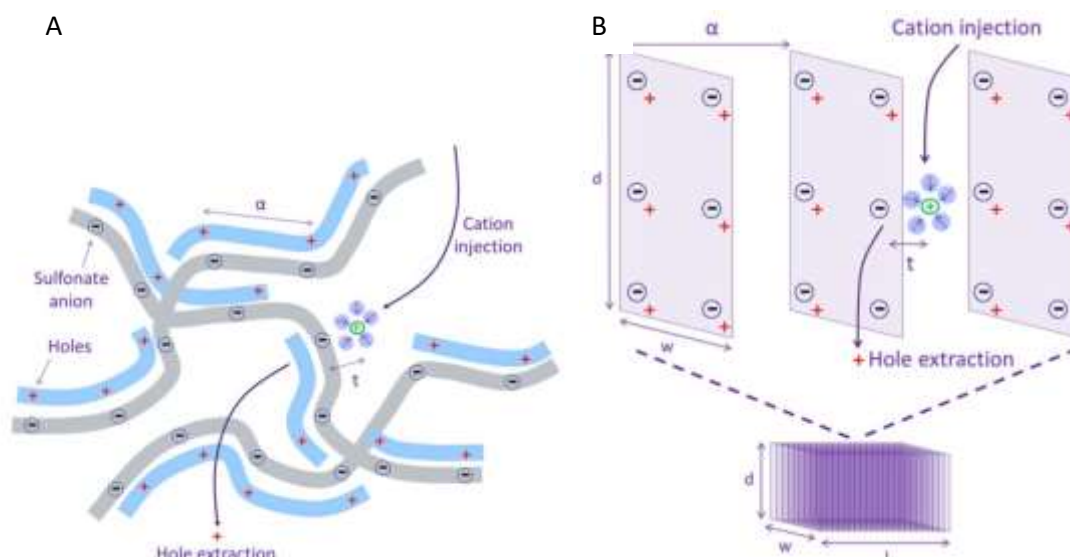


Figure 5. (a) Schematic showing the dedoping process caused by ion injection, where a is the average site distance. (b) Schematic showing an array of plates against which ions pile up to form double layer capacitors. Adapted with permission.^[90] Copyright 2016, John Wiley and Sons.

1.3.3 Stability

As will be discussed more extensively in the following section, PEDOT:PSS-based devices have been utilized with cells and tissues and have been implanted in the body. Unlike standard electronics, these conditions necessitate their performance submerged in an aqueous environment. Differing greatly from a simple salt solution, cell culture media and *in vivo* conditions are quite complex. Furthermore, operation is at physiological temperature (37 °C), which again differs from the common condition of room temperature. The stark contrast of between traditional electronics and bioelectronics warrants investigation of device performance at such conditions, especially for long periods of time. Parameters such as method of deposition, adhesion with the substrate, operation conditions (stimulation, recording, continuous, pulsed) and environment have a profound influence of stability. In this section, we discuss reports of PEDOT:PSS performance in simulated biological environments as well as *in vivo*.

In vitro studies with cells and tissues as well as *in vivo* implantations often require sterilization, particularly if the studies are carried out over time as opposed to one discrete measurement. Long-term stability measurements of PEDOT:PSS devices, discussed below,

should be conducted sterile to avoid any confounding factors, such as bacterial and fungal growth and subsequently, biofouling of electrode sites. Many polymers cannot survive or are deeply affected by clinical sterilization procedures such as ethylene oxide, autoclave, and hydrogen peroxide. In a recent study, the effects of various sterilization methods of PEDOT:PSS were studied.^[91] No apparent differences in surface roughness of spin coated PEDOT:PSS electrodes were observed with heat steam sterilization. Furthermore, mean impedance at 1 kHz across tested electrodes increased only slightly, and transconductance in OECTs was found to change very little. It is important to note these are annealed (140 °C), cross-linked films, and this processing seems necessary for film integrity to be maintained after autoclave. In another sterilization method, H₂O₂ gas plasma was devastating to performance leading to non-functional devices in which PEDOT:PSS delaminated from underlying metal, even though this sterilization method utilizes far lower temperatures than autoclave.^[91]

Early work with PEDOT:PSS first investigated the conducting polymer performance in phosphate-buffered saline (PBS) at room temperature for short-term periods *in vitro*. Electrochemically-polymerized films^[92] and coatings on gold^[93,94] and PtIr wire arrays^[95] as well as chemically-polymerized PEDOT:PSS on track-etch membranes^[96] observed little (~20% loss in electroactivity) to no changes for up to 2 weeks or with 1,000 of cycles of stimulation. Authors studying electrochemically deposited PEDOT:PSS on Pt electrodes did, however, find differences in performance with coatings of varied thickness when continuously stimulated for 2 weeks in PBS.^[97] Thirty electrodes of different thicknesses showed some cracking in the PEDOT:PSS films as well as delamination. Cracking only occurred in the films of intermediate thickness while the only films that delaminated were the thickest ones. The appearance of cracks did occur in the thickest films as well, but at an earlier time point, preceding delamination. The conductivity of PEDOT:PSS also diminished with stimulation time, and delaminated PEDOT:PSS coincided with electrical characterization

that were similar or identical to Pt properties. Even electrodes that did not display any obvious signs of damage still showed changes in electrical properties, including decreased charge capacity, peak shift, and peak separation. The authors note peak separation can be from a change in ion diffusivity, which may be a result of microstructural changes in the film.

Others have also investigated the performance of PEDOT:PSS at physiological temperature or at other elevated temperatures in PBS *in vitro*. These elevated temperatures (~60-70 °C) simulate long-term polymer aging at 37 °C; these protocols are based off standard protocols for assessing polymer degradation in medical devices.^[98] At 67 °C for 28 days, which simulates 32 weeks at 37 °C, impedance at 1 kHz increased by 27 kΩ, and the maximum negative voltage in response to 5 μA increased by 350 mV in PEDOT:PSS coated PtIr microwire arrays (75 μm in diameter). However, large, clinical PEDOT:PSS coated Pt electrodes (3x6 mm) were not found to degrade at 13 weeks of elevated temperature, corresponding to 2 years *in vivo*. It was suggested the delamination could have been the main contributor to the degradation in performance microwires while macrowires remained similar, but this was not tested.^[95] In electropolymerized PEDOT:PSS on gold electrodes in a flexible polyimide-based array, stimulation was conducted in PBS at 37 °C. Electrodes were stable for at least 7 weeks of continuous stimulation with no significant change in impedance after 4.2 billion bipolar current pulses. No significant changes were observed in the unstimulated experiments lasting over 10 months.^[99] Adhesion to the underlying substrate was cited as an issue in another study of electrochemically-polymerized PEDOT:PSS on ITO or gold.^[93] In PBS at 37 °C, all 9 PEDOT:PSS films on ITO delaminated within 2 weeks while only 1 of 9 PEDOT:PSS films on Au had delaminated by 35 days. Interestingly, no delamination was observed when PEDOT:PSS films on ITO were incubated in deionized water or 10 mM H₂O₂ at 37 °C. Hydrogen peroxide was investigated in order to simulate oxidative stress that can occur at sites of biomaterial implantation.^[100] The electroactivity of PEDOT:PSS rapidly declined around 10-15 days in dilute H₂O₂.^[93] The decline was attributed to over-oxidation of

PEDOT in which the double bonds of the polymer backbone are broken and result in a loss of conjugation and conductivity. In other long-term stability studies, electrochemically deposited PEDOT:PSS on gold-parylene C neural probes displayed slight increases and variations in the mean impedance over the course of 6 months in artificial cerebral spinal fluid (ACSF), but never exceeded 100 k Ω for 1 kHz.^[101] With PEDOT:PSS electrochemically deposited on carbon fibers, the average impedance started at 143 k Ω , but over the course of a simulated time of 172.2 days (over 24 weeks) in PBS at 60 °C, the impedance increased gradually to ~1920 k Ω .^[102]

PEDOT:PSS neural electrodes, for both recording and stimulation, have been tested in a few *in vivo* studies in both mice and rats. On microfabricated silicon shanks (PEDOT:PSS electrochemically deposited onto gold recording sites), there was a decrease in performance (decreasing single unit and multiunit yields, signal amplitude and signal-to-noise ratio) within the first two months but remained stable for the remaining two months of the study.^[103] Impedance also fluctuated in the first month, but increased steadily until ~2 M Ω at 1 kHz. In another study of electropolymerized PEDOT:PSS on silicon neural probes, the mean impedance was typically less than 1 M Ω at 1 kHz over the course of over 6 weeks after initial increase in impedance that occurred early within the first few days.^[104] This quick initial impedance increase was also observed with PtIr wire arrays with electropolymerized PEDOT:PSS.^[95] Starting at ~65 k Ω , impedance at 1 kHz increased over 9 days but then slowly decreased to ~550 k Ω . Importantly, the impedance still remained ~200 k Ω lower than bare metal electrodes.^[95]

The above *in vivo* studies were conducted with conventional neural probes, which are made of inorganic materials that far exceed the stiffness of surrounding brain tissue and therefore are thought to contribute to tissue damage and the prolonged immune response to neural probes. Recent efforts are being made to make smaller and more flexible probes aimed at minimizing tissue damage and improving biocompatibility. These probes will be discussed

further in the following sections, but with regards to chronic performance *in vivo*, flexible probes have recently shown potential for improved performance over conventional probes. In microfabricated neural probes composed of parylene C and PEDOT:PSS coated gold, electrode impedance began at 10-25 k Ω for 1 kHz.^[101] Impedance increased by only a factor of 2, and stable recordings were obtained for 30 weeks. Throughout the study, 70-90% of electrodes were functional but varied with time. In another study, the choice of substrate was shown to have an impact on neural recording performance. PEDOT:PSS on glassy carbon outperformed PEDOT:PSS on Pt when fabricated in polyimide microelectrode arrays.^[105] Results from these two studies underscore the importance of device properties and material choice that may affect PEDOT:PSS performance, especially long-term.

Cited as potential issues from many of the above studies, PEDOT:PSS delamination can be prevented with strategies to improve adhesion to the underlying substrates, typically metal. Adding the silane cross-linker GOPS in enough quantity to PEDOT:PSS dispersions results in a strong adhesion to glass substrates as well as metal surfaces such as gold. It is important to note that these surfaces are pre-activated by plasma oxygen cleaning or other chemical cleaning methods. As noted in one of the studies above, ITO is a more challenging surface for PEDOT:PSS or PEDOT:PSS:GOPS adhesion. To overcome this, ITO surface functionalization with GOPS is used by sonicating a pre-activated ITO substrate in a solution containing water, ethanol, and GOPS (unpublished results). The created GOPS layer on ITO surface bonds with the GOPS content in the PEDOT:PSS:GOPS blend, forming a stable adhesion. On Pt microwires, PEDOT:PSS was electrochemically deposited after a coating poly(vinyl alcohol)/poly(acrylic acid) inter-penetrating polymer networks. Mechanical and electrochemical stabilities were improved over PEDOT:PSS alone with notably improved adhesion on Pt that prevented delamination.^[106] Adhesion of PEDOT:PSS coatings can also be improved to a variety of substrates (Pt, Ir, ITO) when electrochemical polymerization is conducted with amine-functionalized EDOT to produce a P(EDOT-NH₂) layer on the

electrode, facilitated by amine-metal adsorption, and onto which additional PEDOT was polymerized and covalently linked.^[107] In a method for inducing mechanical rather than chemical adhesion, nanostructured IrO_x and Pt improved adhesion of PEDOT:PSS coatings^[108].

In summary, PBS does not seem to alter PEDOT:PSS performance nor does increasing temperature or stimulation. Long-term performance of PEDOT:PSS in PBS is obtainable *in vitro*. Thickness of coatings, substrate adhesion, and electrode surface area influence degradation properties mostly through cracking or delamination. Unobservable microstructural changes in the polymer, which change impedance, have yet to be thoroughly investigated. Oxidative environments, mimetic of inflamed tissue, can be devastating to the electrical performance of PEDOT:PSS. Liquid media containing more complex factors, such as hydrogen peroxide, that mimic the *in vivo* environment need to be investigated further. As well, the potential of PEDOT:PSS on more flexible and more biocompatible neural probes is a very promising avenue and will likely see performance exceeding that of PEDOT:PSS on stiff neural probes due to better tissue compatibility. Certainly, several strategies should be investigated to minimize the drastic impedance increase observed with implanted PEDOT:PSS.

1.4. Applications

PEDOT:PSS has been utilized in several forms for biomedical applications. The first example and the most widely used is the coating of PEDOT:PSS on electrodes for recording as well as stimulation of electroactive cells and tissues. As discussed above, the conducting polymer coating decreases the electrode impedance by increasing the effective area of the electrode and also increases the charge injection limit; thus, recording and stimulation performances are improved. The fabrication of arrays with PEDOT:PSS electrodes have a

broad impact in that they can be used to study biology as well as providing therapy or treatment.

PEDOT:PSS has also been utilized in organic electrochemical transistors (OECTs). OECTs have proven most useful for recording low amplitude signals (electrophysiology) or low concentrations of the desired analyte (biosensing) in that these devices can provide high signal amplification. First reported in 1984, the OECT consists of a polymer channel with source and drain electrodes. The channel is in contact with an electrolyte, in which a gate electrode is immersed.^[109] Application of a gate voltage drives ions from the electrolyte into the channel and changes its conductivity. This ion-to-electron transduction mechanism makes OECTs useful transducers for biological applications. OECTs and their various applications are discussed at greater length in the following review^[110] while this review will specifically focus on those based on PEDOT:PSS.

One key advantage of using PEDOT:PSS-based devices for recording and stimulation, either through electrodes or OECTs, is the ability to use varying substrates, including those that are cheap, flexible, and biocompatible. Various fabrication methods, as discussed above, lend the way to scale-up and commercialization at low costs. Compared to bare metal electrodes, conducting polymer coatings decrease electrode impedance and afford recording sites of smaller surface areas and therefore, a greater recording site density can be achieved on a device of certain dimensions. Finally, as will be discussed further in examples of tissue interfacing, fabrication of devices on flexible substrates is key for improving biocompatibility.

Other, less frequently explored form factors include free-standing films, porous or tubular scaffolds, fibers, nanowires^[111] and particles. Films and scaffolds are useful for interfacing electronics with cells. While films can be used for *in vitro* cell culture, scaffolds provide a three-dimensional environment that is more mimetic of the body. Furthermore, 3D scaffolds are used in tissue-engineered implants. Tubular scaffolds have mostly been proposed as nerve conduits. Alternatively, fibers can serve as soft and flexible electrodes for

electrophysiology. PEDOT:PSS particles can serve as sites for nucleation in electrochemical polymerization or in colloidal inks for printed electronics. Here, we discuss applications of all of the above PEDOT:PSS devices in highlighted examples.

1.4.1 Electrophysiology

1.4.1.1. Implantable Devices

Electrophysiology with implantable devices includes neural recordings - electrocorticography ECoG (from surface of brain) and stereoelectroencephalography SEEG (penetrating brain tissue) - as well as intramuscular electromyography EMG. Requirements for implantable electronics vary greatly from those for cutaneous electrophysiology, which is discussed in the next section. Neural electronics are the most widely studied of implantable bioelectronic devices. Neural electrodes serve those in basic science with the important task of uncovering the complexity of how the brain works. For the application of neural electrodes, Brain-Machine Interfaces (BMI) have been proposed and investigated with great success. Recording of brain activity can be translated to cursor control – including for speech and wheelchair control, movement of an artificial limb, and muscle stimulation for movement of a patient's own paralyzed limb.^[112,113] Especially for the brain, the softest tissue in our body, developing soft, flexible and small probes^[114] are of pressing importance to the field of chronic BMIs, which has traditionally used metal and silicon probes with poor biocompatibility^[115,116]. PEDOT:PSS has been used as both a coating of these metal wires and silicon shank probes and more recently, have been used on electrodes on flexible substrates.

In 2003, the ability of PEDOT:PSS to improve biological interfacing of metal electrodes was first demonstrated. PEDOT:PSS was electrodeposited on gold electrodes and was found to decrease the impedance by nearly two orders of magnitude.^[94] This study would also include the first demonstration of *in vivo* neural recordings with PEDOT:PSS, which was used to coat penetrating Michigan-style silicon electrodes for acute measurements in a guinea pig.

PEDOT:PSS has also been electrochemically applied to tips of 7 μm diameter carbon fibers (**Figure 6**).^[117] In contrast to traditionally used silicon shanks or metal microwires, these fibers served as an all organic-based fiber providing higher compliance and a smaller device footprint for minimizing brain damage in neural recordings. The coated fibers were one order of magnitude less stiff than silicon neural probes. When compared to uncoated probes, only PEDOT:PSS coated devices were able to detect single unit activity in the motor cortex of rats. The devices demonstrated a high signal-to-noise ratio and were stable over 5 weeks.

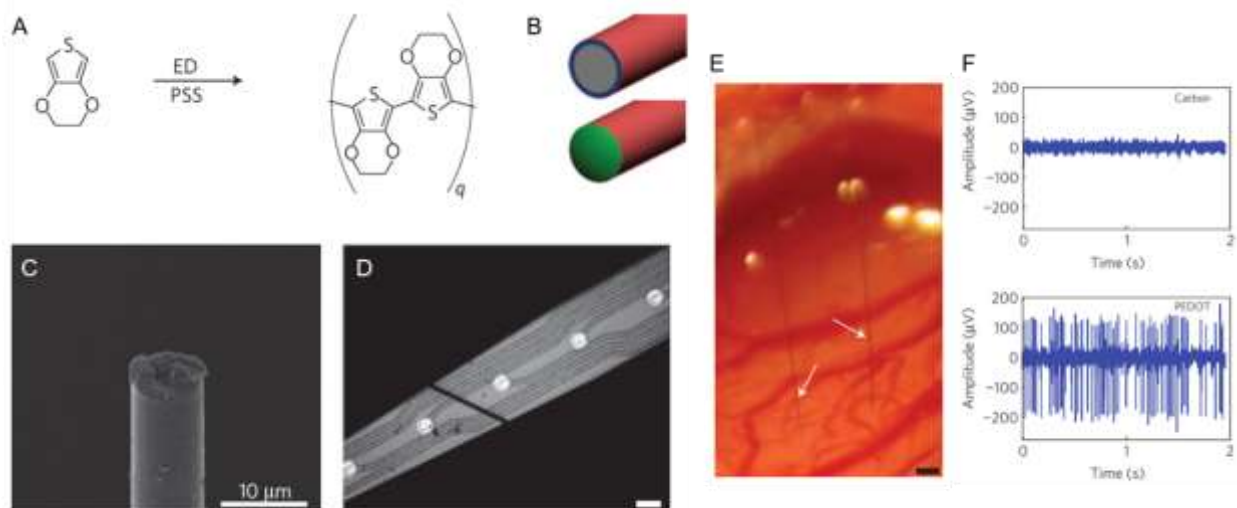


Figure 6. PEDOT:PSS coated carbon fibers for ultra-small, implantable neural probes. A) Electrochemical deposition of PEDOT:PSS on carbon fibers B) carbon fibers were coated with poly(p-xylylene) and poly((p-xylylene-4-methyl-2-bromoisobutyrate)-co-(p-xylylene)) (blue) and were finally covalently grafted with poly(ethylene glycol) (red). The fiber was cut to remove insulation and expose the carbon fiber (gray). A recording site was prepared by electrochemically depositing PEDOT:PSS (green) on the exposed tip. C) Scanning electron micrograph of final neural probe. 7 μm diameter. D) Carbon fiber neural probes on top of a 10 mm silicon electrode. Scale bar, 50 μm . E) Carbon fibers (arrows) implanted 1.6 mm deep into the cortex of a rat brain. Scale bar, 100 μm . F) Simultaneous neural recordings with and without PEDOT:PSS. Single unit activities were only detected *in vivo* with PEDOT:PSS coating (SNRs of 12.7 and 4.71 and a noise floor of 23.4 μV). Adapted with permission.^[117] 2012, Macmillan Publishers Ltd.

Also towards conformable devices for more biocompatible neural probes, the microfabrication of PEDOT:PSS neural probes with parylene C has been recently developed (**Figure 7**).^[118–121] Conformability is especially important for measurements on the brain since

on the surface of the brain, the probe can follow its folds and while inside the brain, the probe can move and flex with micromotions associated with body movement, respiration, and blood flow. Using standard lithography procedures and spin coating of PEDOT:PSS, flexible probes were fabricated to be only 4 μm thick with micrometer-diameter, PEDOT:PSS-covered gold electrodes and OECTs. ECoG measurements on the surface of the brain were performed with these probes consisting of PEDOT:PSS OECTs. Compared to surface electrodes, PEDOT:PSS OECTs showed a superior signal-to-noise ratio than electrodes in measurements in rats as well as the detection of fast and low amplitude signals previously only obtainable with penetrating probes.^[121] In later work, the authors reported the unprecedented ability to detect single unit activity using PEDOT:PSS electrodes placed on the surface of the brain.^[119] These electrodes were also successfully used in humans to monitor brain activity in patients who were undergoing surgery for epilepsy treatment.^[119] These parylene-based probes have also been presented in a penetrating probe format with the aid of an insertion shuttle. When compared to the standard of silicon probes, parylene electronics showed minimal glial scarring in rats^[120]. Thicker parylene probes with electrochemically deposited PEDOT:PSS have also been demonstrated^[122], and these did not seem to require an insertion aid for brain penetration. Increasing the thickness, however, limits probe flexibility.

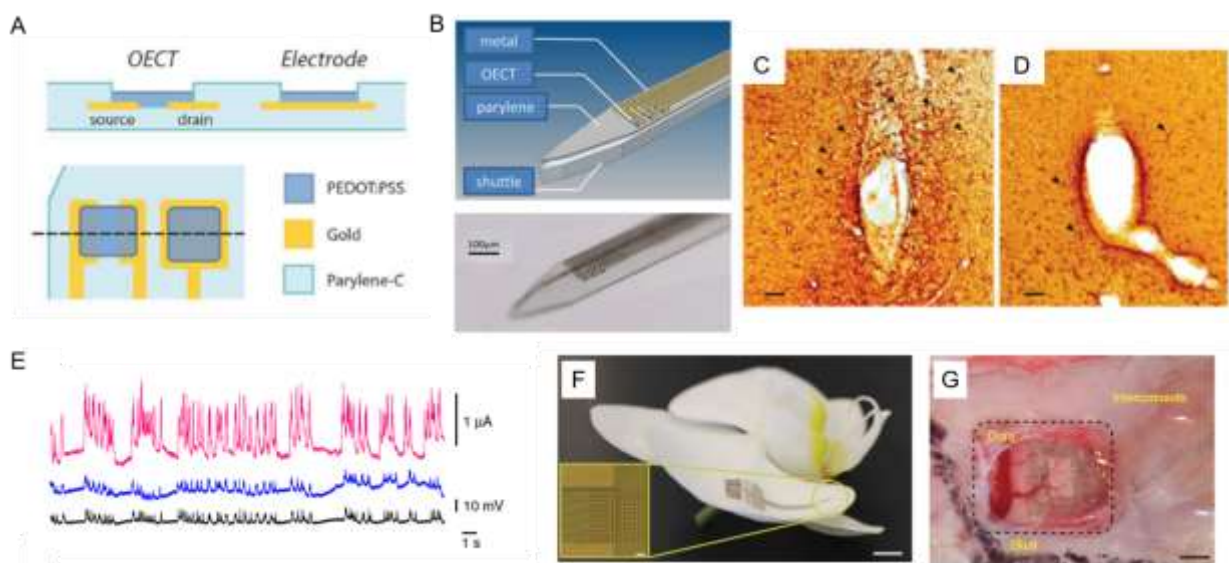


Figure 7. Flexible, parylene C neural probes with Au-PEDOT:PSS electrodes. A) Neural probes are microfabricated by photolithography. Recording sties can be in OEET or electrode configurations. B) Schematic (top) and optical micrograph (bottom) of neural probes for delaminating shuttle for insertion into the brain. C-D) Anti-glial fibrillary acidic protein staining of mouse brain after 1-month implantation of silicon (C) and parylene (D) probes. The glial scar is more evident silicon probes. Black arrows indicate example glial cell bodies. Scale bar, 50 μm . A-D) Adapted with permission^[120]. 2015, Wiley. E) Parylene ECoGs. When placed on the somatosensory cortex of rats PEDOT:PSS OEETs (pink) outperform PEDOT:PSS (blue) surface electrodes with a superior SNR. Measurements are also compared to penetrating Ir electrodes (black). Adapted with permission.^[121] 2013, Macmillan Publishers Ltd. F) A flexible, 256-electrode parylene ECoG (Neurogrid), laid onto an orchid petal. Scale bars 5 mm, 100 μm inset. G) Extracellular action potentials are detected from the surface of the cortex and hippocampus of rats. In another experiment, the probe detects LFPs and spiking activity in epilepsy patients. Adapted with permission.^[119] 2014, Macmillan Publishers Ltd.

Using replica molding with PDMS, an all-polymer microelectrode array was fabricated (**Figure 8**). Microchannels were made in the PDMS and were filled with PEDOT:PSS to create the electrode paths. Impedance ranged from 400 $\text{k}\Omega$ to 4 $\text{M}\Omega$ between 1 Hz and 1 kHz. The average impedance at 1 kHz, used for measuring action potentials, was approximately 40 times higher than metal electrodes; at 1 Hz, used for measuring local field potentials, impedance was 15 times lower. Interesting benefits to such a device include its support for cultured cells and optical transparency for subsequent biological imaging. Furthermore, the device is much more elastic than metal-based devices and this elasticity may be beneficial for some applications, especially those *in vivo*. The authors evaluated the utility of such devices *in vitro* and *in vivo* with various recordings, including cardiac activity from embryonic mice hearts, recordings of individual action potentials from stimulated retinal explants, spontaneous recording of cortico-hippocampal cells for 63 days, and the detection of LFPs in epidural and epicortical configurations on the primary visual cortex of rats.^[123]

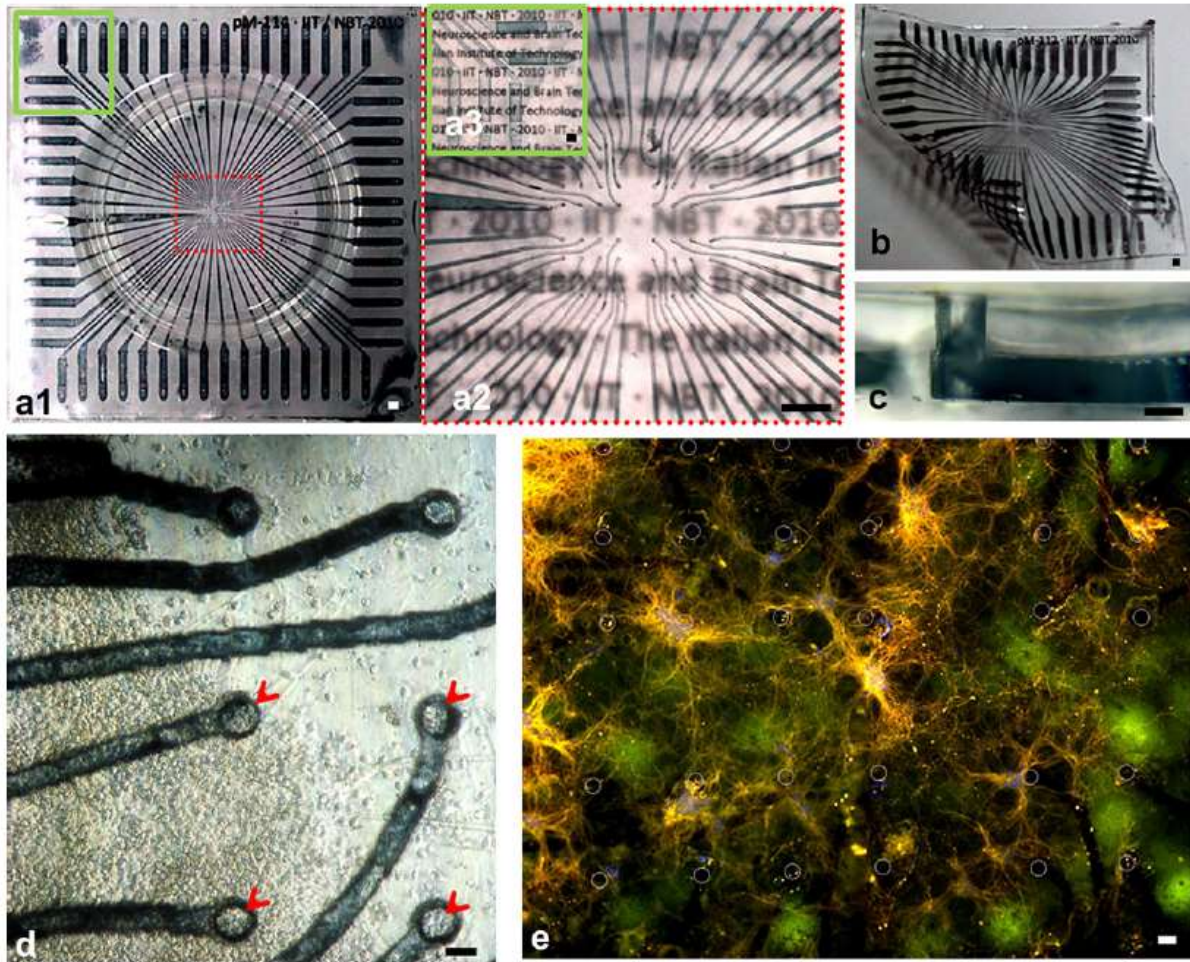


Figure 8. All-polymer microelectrode arrays composed of PEDOT:PSS within PDMS. A1) Transparent microelectrode array (60 electrodes, 49 x 49 mm²) with conductive PEDOT:PSS tracks (blue) comprising contact pads, channels, and recording sites. Fixed with well for cell culture. Scale bar, 1 mm. A2-A3) Higher magnification images of A1. Scale bars, 1 mm. Readable text of paper underneath array illustrates its transparency. B) Array is flexible (array with graphite-PDMS conductors) Scale bar, 1 mm. C) Cross-section of one PEDOT:PSS electrode. Scale bar, 100 mm. D) Cortico-hippocampal rat calls are supported on the device, 38 days *in vitro*. Optical imaging is facilitated by array transparency. PEDOT:PSS electrodes. Scale bar, 100 mm. E) Immunofluorescence staining of neural network. Beta-tubulin III, green, dendrites and axons. MAP2, red, dendrites. Hoechst stain, blue, nuclei. graphite-PDMS conductors. Scale bar, 100 mm. Adapted with permission.^[123] 2011, Elsevier.

In addition to recording, electrodes are also needed for stimulation in the central and peripheral nervous systems as well as in muscle. Stimulating electrodes can be used externally or internally. The applications discussed in this section are for implantable probes, while cutaneous applications are presented in the following section. Stimulation is used in cochlear implants^[124] and visual prostheses^[125], as well as for pain management^[126], Parkinson's

disease, depression, epilepsy and other neurological disorders^[127]. Stimulation can also assist recovery in neurorehabilitation after stroke and spinal cord injury.^[128–130]

Several years after the first reported neural recordings with PEDOT:PSS electrodes, the first stimulation was performed *in vivo* after implantation in the somatosensory cortex of rats.^[95,131] PEDOT:PSS significantly improved the charge injection limit over bare PtIr and IrOx, with the ability to deliver 15 times more charge and without causing electrolysis of water. Furthermore, significantly smaller voltage transients were obtained with constant current biphasic stimulation. Impedance at 1 kHz remained ~200 k Ω lower than bare electrodes and provided similar signal strength and lower noise power in recordings.

In addition to brain stimulation, auditory brainstem stimulation can help improve hearing in hearing loss patients who cannot benefit from cochlear implants.^[132] PEDOT:PSS devices were presented for such application with two main benefits: the increase in the charge injection properties over bare metal (especially towards small diameter electrode arrays) as well as the compatibility with flexible substrates, in this case polyimide (**Figure 9**). Not only are smaller and more flexible devices, in general, better for interfacing with tissue but also in this case, the confines of the implant site requires specific implant dimensions and specific bending configuration in order to reach the stimulation target (cochlear nucleus). In fact, after bending, there no observed significant differences in the impedance modulus at 1 kHz nor were there any visible cracks or delamination of the PEDOT:PSS. The device was successfully used in rats.^[132]

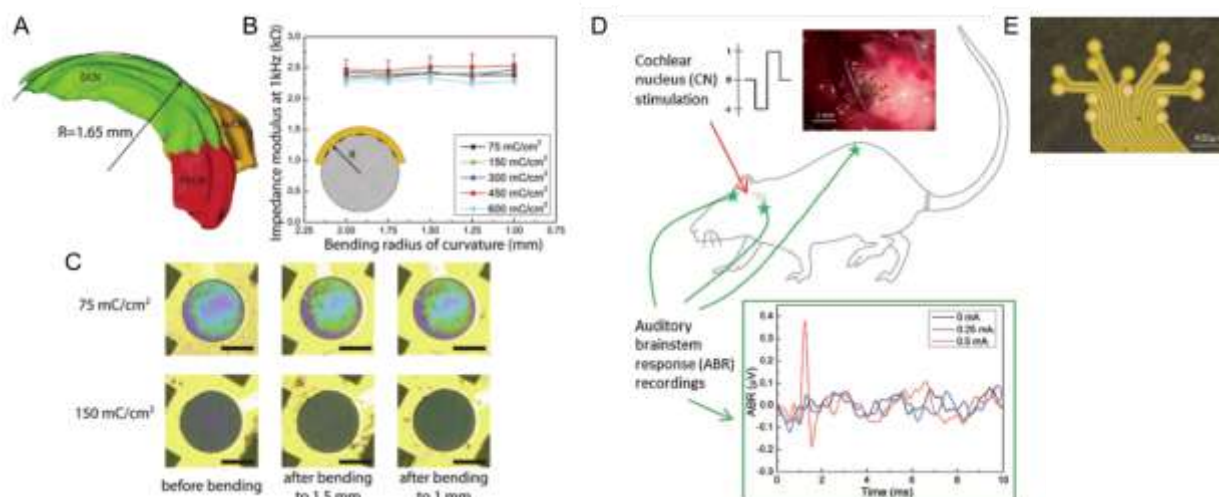


Figure 9. Auditory brainstem stimulation device consisting of Pt electrodes with electrochemically deposited PEDOT:PSS on flexible polyimide substrates. A) 3D reconstruction of a rat cochlear nucleus. The dorsal cochlear nucleus has a radius of 1.65 mm. DCN: dorsal cochlear nucleus, AVCN: anteroventral cochlear nucleus, PVCN: posteroventral cochlear nucleus. B) Impedance modulus at 1 kHz of PEDOT:PSS coated electrodes (diameter = 200 μm) after increasing compressive bending. C) Optical images of two electrode sites before bending, after bending to 1.5 mm radius and to 1 mm radius indicating the absence of cracks or delamination of the coating. Scale bars, 50 μm . D) Auditory brainstem responses (ABR) recorded following stimulation of the cochlear nucleus surface with the PEDOT:PSS coated electrode array. Photomicrograph shows the array in position on the exposed surface of the CN on the left side of the brainstem. Diagram shows the positions of the ABR recording electrodes. E) Picture of the electrode array fabricated on thin polyimide substrate with a finger-like shape to further increase conformability. Text reproduced with permission and figures adapted with permission.^[132] 2015, Royal Society of Chemistry.

For peripheral nerve applications, an implantable, miniaturized and wireless device for simultaneous stimulation and recording was reported using electrochemically deposited PEDOT:PSS on Pt. Similar to previous studies in the CNS, these probes have implications in both studying pathophysiology (e.g. chronic pain, diabetes, hormonal deregulation and epilepsy) and their treatment. Polyimide and PDMS were used to fabricate flexible devices, which is important for wrapping around the target peripheral nerve, and acute studies were successful in stimulating the aortic depressor nerve in rats.^[133]

1.4.1.2 Cutaneous

Non-invasive electrophysiology conducted on the surface of the skin has long been an asset to clinicians in healthcare monitoring. It includes surface electromyography EMG, electrocardiography ECG, and electroencephalography EEG (using scalp electrodes).

Desirable advancements of surface electrodes include improving long-term performance, patient comfort as well as developing low cost and environmentally-friendly fabrication methods.^[134] Another application of wearable electronics is for continuous daily monitoring of health and fitness as well as tracking disease onset and progression.^[135]

PEDOT:PSS OECTs fabricated on flexible PLGA for cutaneous interfacing were used for ECG (**Figure 10a-d**).^[136] Although not demonstrated in this study, PLGA is biodegradable and therefore, the device could be interesting for short-term uses in which the device dissolves away. OECTs have also been used for other electrophysiological measurements, including eye movement (electrooculography, EOG) and electroencephalography (EEG) covering a range of detectable signals, ~1 mV to ~10s μ V (Figure 10e,f).^[137]

Long-term cutaneous electrophysiology often requires the use of a gel electrolyte to decrease impedance between the electrode (often Ag/AgCl) and skin. Shortcomings of gel electrolytes include quick drying and increasing impedance, short circuiting with leaked liquid electrolytes between adjacent electrodes, and the tediousness of having to apply to each electrode by hand. To overcome the challenges of long-term cutaneous recordings (>1 day), the use of ionic liquids were proposed to interface PEDOT:PSS-coated gold electrodes.^[138] Ionic liquid gels are chemically and thermally stable as well as highly ionically conductive, but most importantly, these do not carry risks of drying out or leaking. These electrode/IL gel configurations quickly outperformed Ag/AgCl/gel over 12 hrs. Furthermore, the PEDOT:PSS/IL gel configurations demonstrated stable performance for over 72 hrs. and exhibited lower variations in impedance when compared to Au/IL gel electrodes.

As mentioned previously, PEDOT:PSS has been fabricated into devices by a variety of methods, including those that are compatible with flexible substrates. For example, PEDOT:PSS microelectrode arrays for surface EMG and ECG were inkjet printed on flexible polyimide foil.^[25] Flexible, printed temperature sensors have also been presented.^[139] Towards fabrication on cheaper and disposable substrates, PEDOT:PSS has been ink-printed onto

commercial paper. These printed devices for ECG were stable for at least 3 months and were functional with only one layer of printing.^[24] Another flexible substrate is textile, which is increasingly being explored for wearable electronics. PEDOT:PSS electrodes on textiles could detect EMG of voluntary and electrically evoked contractions.^[140] Furthermore, muscles were stimulated and these electrodes performed similarly to clinical Ag/AgCl electrodes.^[140] Such muscle-interfacing, wearable devices could be used for monitoring rehabilitation patients or providing electrotherapy. Textile ECG has also been conducted, both at rest and in motion, and were reusable and stable over time.^[37]

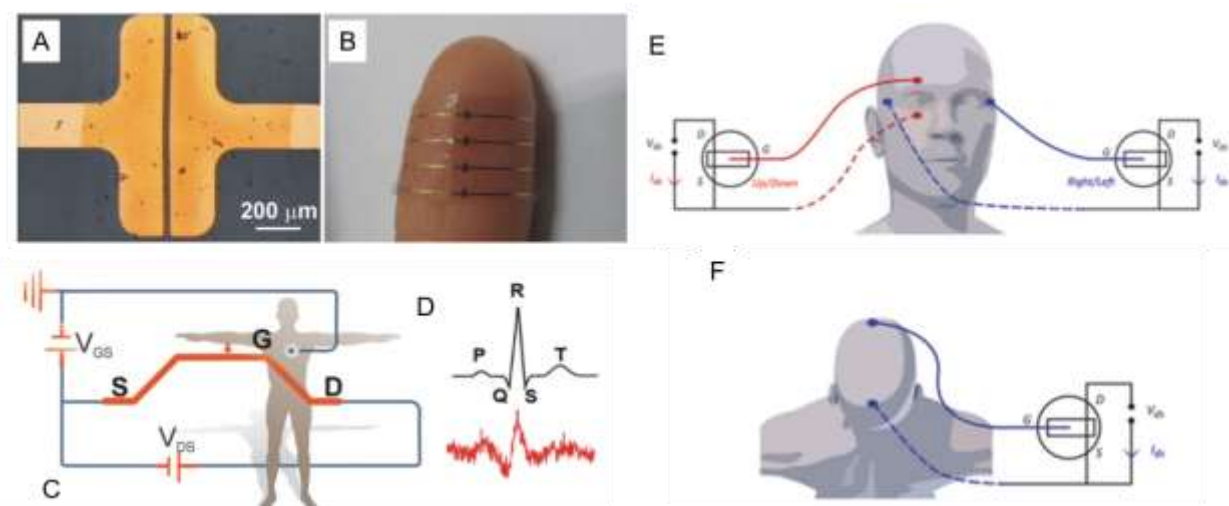


Figure 10. Cutaneous electrophysiology (ECG, EOG, EEG) with PEDOT:PSS OECTs. A) PEDOT:PSS-Au OECT. B) Device of OECTs fabricated on PLGA. Structure is flexible and transparent. C) OECT device was used for successful ECG. Wiring diagram. D) ECG trace (red), compared to textbook example, black. A-D) Adapted with permission.^[137] 2014, Wiley. PEDOT:PSS-Au OECTs fabricated into flexible, parylene-based devices. Wiring configurations for E) EOG and F) EEG. Adapted with permission.^[138] 2015, Wiley.

1.4.1.3 In Vitro

As in implantable devices, microelectrodes have been built into planar arrays for *in vitro* recording and stimulation of seeded cells and freshly extracted tissues. Although materials used should ideally be soft, this is not a firm requirement, and as well, only cytocompatibility, not biocompatibility, is needed; therefore, a wider range of materials and fabrication strategies can be implemented *in vitro* than *in vivo*. MEAs are critical tools for

studying physiological and pathophysiological conditions (especially neural) as well as for drug toxicology studies and screening.^[141–143]

Early work indicated that PEDOT:PSS was cytocompatible, proving that cells could adhere and survive on PEDOT:PSS coated electrodes.^[144] Later, PEDOT:PSS coated ITO microelectrode arrays showed success *in vitro* for recording and stimulation of dissociated cortical cells over the course of over one month.^[145]

Several ways of modulating the bioactivity of PEDOT:PSS have been presented. For example, peptides have been incorporated by co-depositing them as a counter ion, and this was aimed at improving cell adhesion.^[94,144] Other biological agents have also been incorporated. Nerve growth factor (NGF) was incorporated into electrochemically-polymerized PEDOT:PSS.^[146] Not only were the electrical properties unaltered, but also neurite extension in seeded rat pheochromacytoma (PC-12) was improved – proving the bioactivity of NGF was maintained through fabrication. Spermine and basic fibroblast growth factor (bFGF) were also shown to improve neurite extension as well as migration and proliferation of neurons and precursor cells.^[147]

In addition to improving bioactivity, others may seek to diminish it. Anti-adhesive coatings, for example, can be used to coax cells to adhere to certain domains (i.e. only to the electrode). Poly(L-lysine-graft-ethylene glycol) (PLL-g-PEG) was functionalized on PEDOT:PSS as an anti-adhesive coating.^[148] As well, self-assembling monolayers (either adhesive or anti-adhesive) on PEDOT:PSS combined with laser ablation can control cell patterning within the PEDOT:PSS region.^[149] PEDOT:PSS can be templated to be nanoporous^[150] or nanopillared^[150] with the goals of coaxing cell alignment and guiding neurite outgrowth as well as changing the stiffness, which is known to be an important biological signal that affects cell behavior. For chemical functionalization strategies of PEDOT, including for cell and tissue interfacing as well as biosensing discussed below, readers are directed to the following review.^[8]

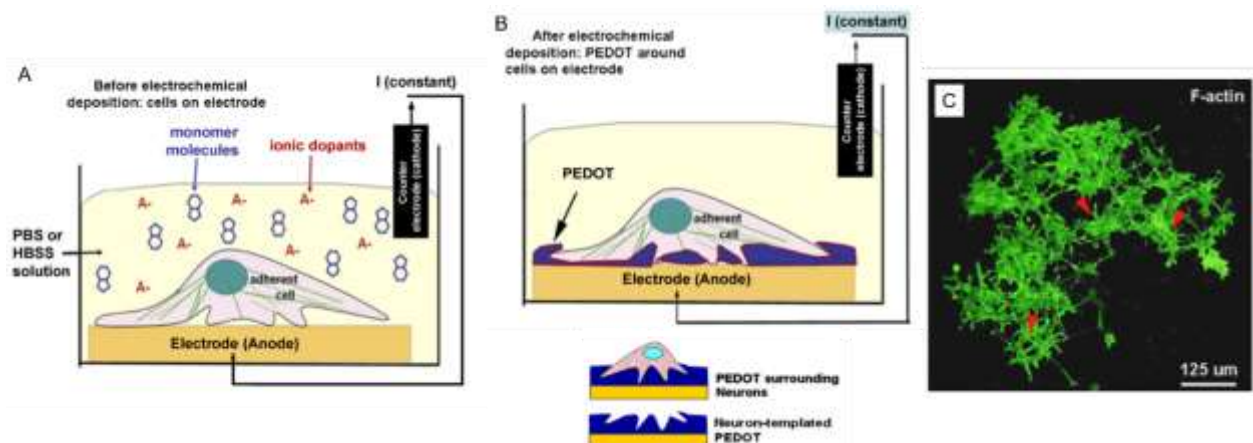


Figure 11. PEDOT:PSS electrochemically-polymerized around living cells. A) Cells are attached to the electrode and are submerged in a solution of EDOT monomers and ionic dopants B) PEDOT is electrochemically deposited around the seeded cells. Optionally, cells can be removed to create a templated electrode, one that has porosity and topography that can potentially coax axon infiltration into recording site. C) SY5Y cells cultured onto neuron-templated PEDOT:PSS. Green, F-actin. Adapted with permission.^[151] 2007, Elsevier.

Recording electrical activity of cells is ideally done when the cells are in direct contact with the electrode in order to have a specific and strong signal. The seeding of cells onto these devices is challenging and ideally one would like to localize the cells specifically on the electrodes. As an alternative to seeding cells directly on electrodes, electrochemical polymerization of PEDOT was conducted in the presence of cells (**Figure 11**).^[151] The PEDOT polymerizes around the cells to form intimate cell-electrode interactions. It was proposed that this may also help prevent migration of the cells away from the electrode surface. Although cells were viable initially, cells did begin to apoptose within a few days. More recently, nanopallets of PEDOT:PSS-silk fibroin lithographically patterned on SiO₂ have been reported (**Figure 12**).^[152] When seeded on the substrate, cells preferentially bound to the ECM-containing islands over the SiO₂. The nanopallets with attached cells could then be micromanipulated with capillaries and placed onto electrodes.

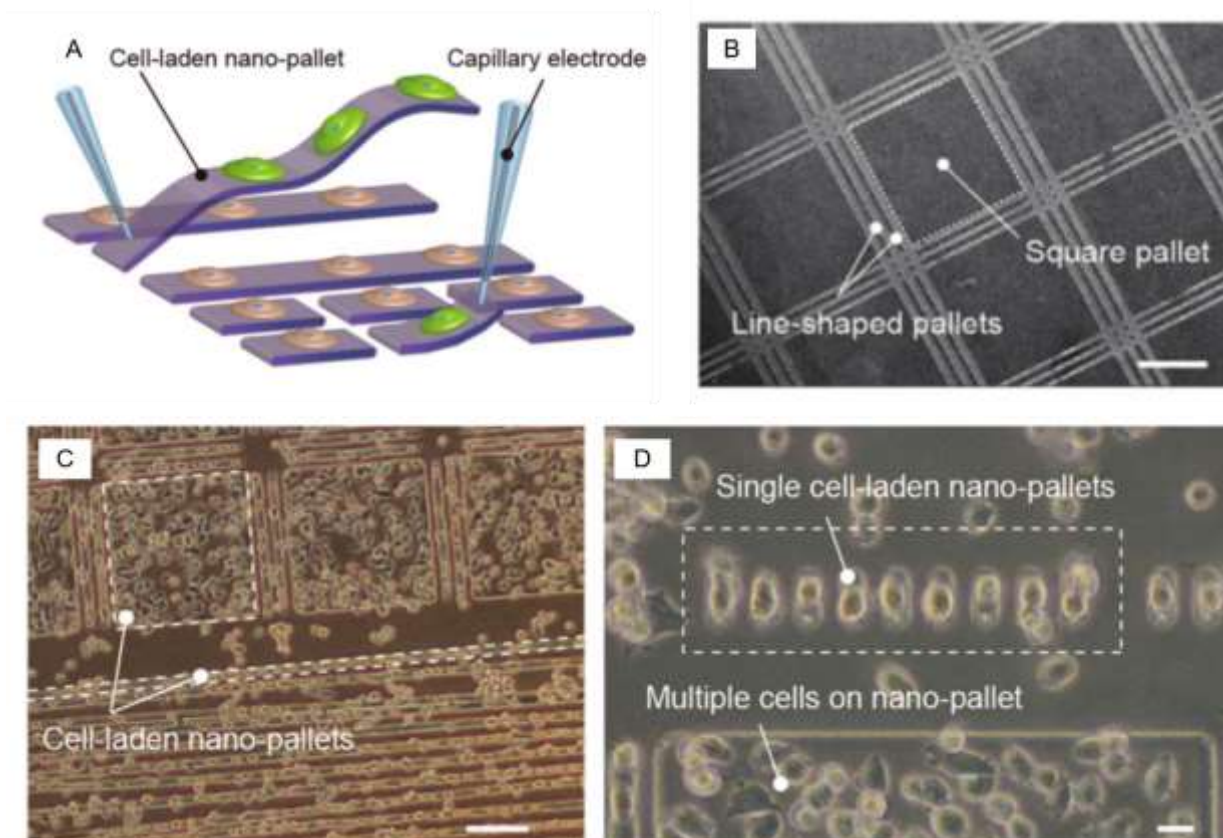


Figure 12. Cell-seeded nanopallets of PEDOT:PSS and silk fibroin for improving cell seeding on electrodes. A) Schematic image of manipulation of cell-laden nanopallets. B) SEM image of nanopallets with desired shapes of lines and squares. Scale bar, 10 μm . Phase-contrast images of cell-laden nanopallets. C) Multiple CHO cells. D) Single CHO cells. Scale bars, 100 μm . Text reproduced and figures adapted with permission.^[152] 2016, Wiley.

1.4.2 Tissue Engineering

Conducting polymers have many attractive uses in tissue engineering, especially for electroactive tissues and organs such as the heart, muscle, brain, and peripheral nerves.^[153–155]

Conducting polymers can be processed into forms that resemble the native extracellular matrix, such as 3D scaffolds and hydrogels. 3D conducting polymer substrates are useful for promoting communication and network formation of electrogenic cells as well as providing a means for electrical stimulation for tissue regeneration and repair (e.g. nerve, bone). These scaffold and hydrogel formats of conducting polymers might also be useful for creating softer and more tissue-like electrodes. The organic nature of conducting polymers also lends easy functionalization, especially compared to traditional inorganic electronic materials. Biological

molecules can be used as co-dopants or can be directly grafted for enhancing bioactivity. Finally, reversible oxidation states can “switch” the properties of the surface, creating the ability to control parameters such as cell adhesion.

GOPS cross-linked, spin coated PEDOT:PSS films have been used to culture and electrically stimulate neural stem cells. The PEDOT:PSS matrix led to more proliferation than the control glass substrate, supporting expansion before differentiation. Differentiation was induced with cell culture media and was further supported with electrical stimulation. Longer neurites and more cell elongation were observed with stimulation.^[156]

Towards 3D scaffolding, PEDOT:PSS has been electrochemically-polymerized in living^[157] and decellularized^[158] tissue. In living tissue, the EDOT monomer is injected at the electrode site and the polymerized PEDOT extends as a cloud from the implanted electrode. There is cytotoxicity associated with the monomer, but the exposure (only during active polymerization) is brief. The authors proposed this strategy as a potential to get past the “dead-zone” associated with electrode foreign body response. In contrast to the PEDOT grown in living tissue, PEDOT:PSS is grown throughout the tissue in decellularized matrix. These could be useful for electroactive tissue engineering scaffolds since decellularized extracellular matrix has potent bioactive cues, including tissue-specific extracellular matrix proteins as well as residual growth factors.^[159]

PEDOT:PSS scaffolds were first reported using a freeze-drying method.^[160] Freeze-dried gelatin and bioactive glass scaffolds loaded with PEDOT:PSS were proposed for bone tissue engineering and in which, bone cells would receive electrical stimulation to aid their growth (**Figure 13a-f**).^[161] The addition of PEDOT:PSS minimized degradation and led to scaffolds that were stable for at least 90 days in collagenase solution, which can degrade gelatin; scaffolds without PEDOT:PSS completely degraded within 10 days. These PEDOT:PSS-containing scaffolds also supported viable human mesenchymal cells, stem cells that can be differentiated into bone cells. Later, for more controlled freeze-drying,

PEDOT:PSS scaffolds were fabricated with ice-templating to control size, morphology, and distribution of porosity (Figure 13g-i).^[162] Additionally, extracellular matrix proteins were absorbed to the scaffold surface and using applied potentials (oxidized or reduced states). This was shown to change the conformation of the absorbed proteins and the behavior of cells that adhered to these scaffolds. The scaffolds were found to support cells throughout their volume.

Conducting polymer hydrogels can be synthesized by simply loading PEDOT:PSS dispersions into the precursor solution before gelation.^[163] The conductivity of the hydrogels can be increased with increasing volume fraction of PEDOT:PSS. Depending on the application, high conductivity might be desired and this can be achieved with a percolating network of PEDOT:PSS or with secondary dopants and treatments that improve PEDOT:PSS doping and/or morphology. The hydrogel “format” imparts very soft mechanical properties, nearly identical to surrounding tissue, and creates a heavily hydrated environment. The hydrogel network can also serve as backbone for attaching bioactive compounds.^[164] This can include interpenetrating networks of a hydrogel mesh alongside a network of conducting polymer. For example, a chemically synthesized PEDOT:PSS dispersion was added to polyvinyl alcohol methacrylate hydrogels and was then electropolymerized to induce growth of the PEDOT network from nucleation sites of the dispersed polymer chains in order to achieve a percolating network.^[165] The electroactivity of such hydrogels was lower than homogeneous conducting polymer; so although these might not yet be suitable for electrodes, these hydrogels are still very promising for tissue engineering – perhaps even including for cell encapsulation. Hydrogels composed solely of PEDOT:PSS have also been presented. Dispersed PEDOT:PSS was ionically cross-linked (via the PSS groups) with Mg^{2+} to form a hydrogel^[166] and were used as hydrogel electrodes in biosensing.^[167] Additionally, electrochemically-polymerized PEDOT:PSS has been cross-linked with Fe^{3+} to form hydrogels.^[168]

We would like to note that many have reported the use of PEDOT prepared with biomaterials, such as heparin, hyaluronic acid, fibrinogen^[169], gelatin^[170], alginate^[171], dextran sulfate^[171], chondroitin sulfate^[171], polyvinyl alcohol^[172], aimed at improving cell and tissue compatibility and interactions as we have discussed in the above examples. However, since these formulations are without PSS, they are beyond the scope of this paper.

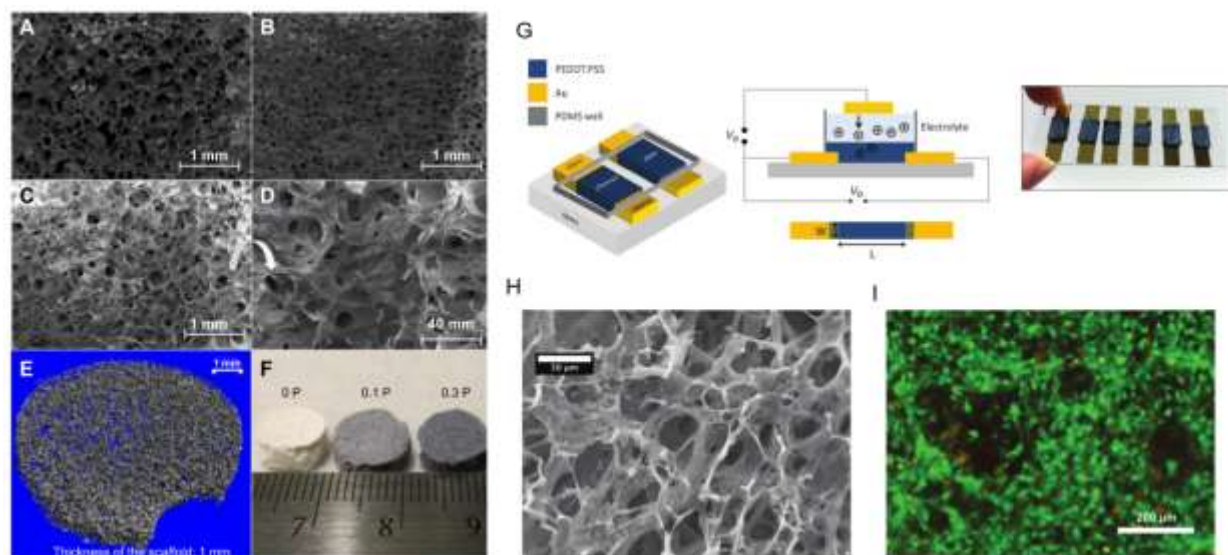


Figure 13. PEDOT:PSS-based scaffolds. Scaffolds of gelatin/bioactive glass loaded with PEDOT:PSS. A-C) Scanning electron micrographs of 0%, 0.1%, and 0.3% (w/w) PEDOT:PSS scaffolds with average pore sizes of 200, 110, 160 μm , respectively. D) Higher magnification of C. E) Micro-computed tomography of C. F) Image of scaffolds. A-F) Reproduced with permission^[161]. 2013, pending response from publisher. PEDOT:PSS scaffolds fabricated with ice-templated for OEETs and cell culture. G) Scaffolds were used in OEETs. 3D, cross sectional, and top view schematics of the OEET structure where $W = 6$ mm and $L = 6$ mm (figure not to scale). The photograph at right shows typical OEETs. The conductivity of the PEDOT:PSS scaffold interfacing the source and drain electrodes decreases by the injection of cations from the electrolyte, triggered by an applied bias through the second scaffold which acts as the gate electrode. H) SEM micrograph of PEDOT:PSS scaffold after 24 hours of cell culture, showing invasion of the scaffold by 3T3-L1s. I) Fluorescence micrograph of a PEDOT:PSS scaffold after 7 days of 3T3-L1 culture, showing very high cell viability. Live cells are stained with calcein (green), and dead cells are stained with propidium iodide (red). The pores of the scaffold are visible as large circular dark regions. Text reproduced and figures adapted with permission.^[162] 2015, The Royal Society of Chemistry.

1.4.3 Biosensing

Sensing of biological analytes is important for several different biomedical applications. *In vivo* sensing, both in implantable and cutaneous configurations, is of interest for continuous healthcare monitoring. Implantable *in vivo* sensors may be important to trigger drug delivery when the analyte falls below or rises above a certain threshold. Non-invasive cutaneous sensing is a key element in wearable electronics, which, for now, have many applications related to fitness monitoring but this may soon extend to patient monitoring. *In vitro* sensing can be incorporated in basic science studies as well as in drug screening and toxicology and models, "labs-on-a-chip" and other cell/tissue testing platforms. Both *in vitro* and *in vivo*, there are vast targets for sensing and these include ions, small molecules, and proteins.

Changes in both the concentrations as well as the compositions of ions have been detected with PEDOT:PSS OECTs.^[173] Reference-less pH sensing^[174] as well as ion-selective PEDOT:PSS OECT sensors (K^+ selective, Na^+ selective) have also been developed through the use of polymeric ion-selective membranes^[175,176] or lipid bilayers and ion pores^[177,178]. Biologically relevant ions (K^+ , Na^+ , Ca^{2+} , Cl^- , H^+ , etc.) can be important markers of gene expression and can be used to monitor cell activity. The ion sensing capabilities of the OECTs were used to measure the integrity of barrier tissue, which can include kidney and intestine epithelium as well as the endothelium and blood brain barrier (**Figure 14c**).^[51,179,180] Cells of the barrier tissue are tightly joined together by proteins, and in diseased states, these connections can become weaker and the tissue becomes more permeable. In the experiment, kidney cells were seeded onto the OECT. When healthy, these cells possess the tight junctions and disrupt ion transport to the OECT channel. When these cells are exposed to chemicals that disrupt the junctions, the cell layer becomes more permeable to ions and there is a change in the drain current. The principle has also been extended to monitoring cell monolayer formation and health in adherent cells that do not form barrier tissues.^[181] Such a platform

could be useful for *in vitro* toxicology and drug screening^[182], especially as part of “human-on-a-chip” technologies.

In addition to ions, many biological molecules have been detected with PEDOT:PSS OECTs. These are molecules that can undergo oxidation and are detected with OECTs that incorporate a Pt gate electrode which drives the oxidation reaction. A range of biomolecules have been detected including the neurotransmitters dopamine^[183] and adrenaline.^[184] PEDOT:PSS biosensors can be also used to detect analytes that are a part of known biological cascades/pathways, such as substrates for enzymes. Glucose has been detected with OECTs sensors coupled with glucose oxidase^[185–187] and lactate has been detected with lactate oxidase coupled OECTs^[188]. In the example of glucose detection, glucose oxidase catalyzes the conversion of glucose to gluconolactone and forms hydrogen peroxide (Figure 14a). Hydrogen peroxide transfers an electron to the gate electrode, leading to a decrease in the source-drain current. These OECTs have detected clinically relevant levels of glucose in biological fluids, including human saliva^[187] and sweat, and may find applications in wearable electronics, especially related to fitness monitoring.

In another method of biological molecule detection, PEDOT:PSS in OECTs can be functionalized with moieties that capture a target of interest. Antibody functionalization of the channel can serve to capture analytes through antibody-antigen interactions^[189,190]. Similarly, single stranded DNA has been functionalized to the gate and can hybridize with the complementary DNA target sequence^[191], which was used for determining the presence of a pathogenic strain of bacteria. Presence of the captured target can then be detected by a change in the effective gate voltage.

Similar to wearable electrophysiology devices mentioned previously, PEDOT:PSS biosensors have been incorporated onto textiles^[192] for wearable devices. Adrenaline (a stress hormone)^[184] and saline^[193] in human sweat have been detected with these textile devices

(Figure 14b). Silk fibroin has also been used as a platform for flexible and degradable sensing devices.^[194]

In addition to OECTs, other formats have been presented for biosensing, including nanowires^[195] and molecularly imprinted PEDOT:PSS.^[196] In molecularly imprinted polymers, PEDOT:PSS micro- and nanorods were electrochemically grown through track-etch membranes, which were previously adsorbed with the proteins to be templated (**Figure 15**).^[196] The membranes were then dissolved and the PEDOT:PSS rods capable of specific protein binding were left behind. In this work, researchers demonstrated recognition of avidin through fluorescence measurements. PEDOT:PSS is capable of hydrogen bonding, electrostatic interactions and π - π interactions, which can occur with the amino acid tryptophan; this great variety of possible interactions may be useful for creating specific protein-binding sites. Additional benefits of PEDOT:PSS include that there is little to no cross-reaction with proteins and its mild and aqueous synthesis can be conducted without harsh, harmful solvents that can denature proteins.

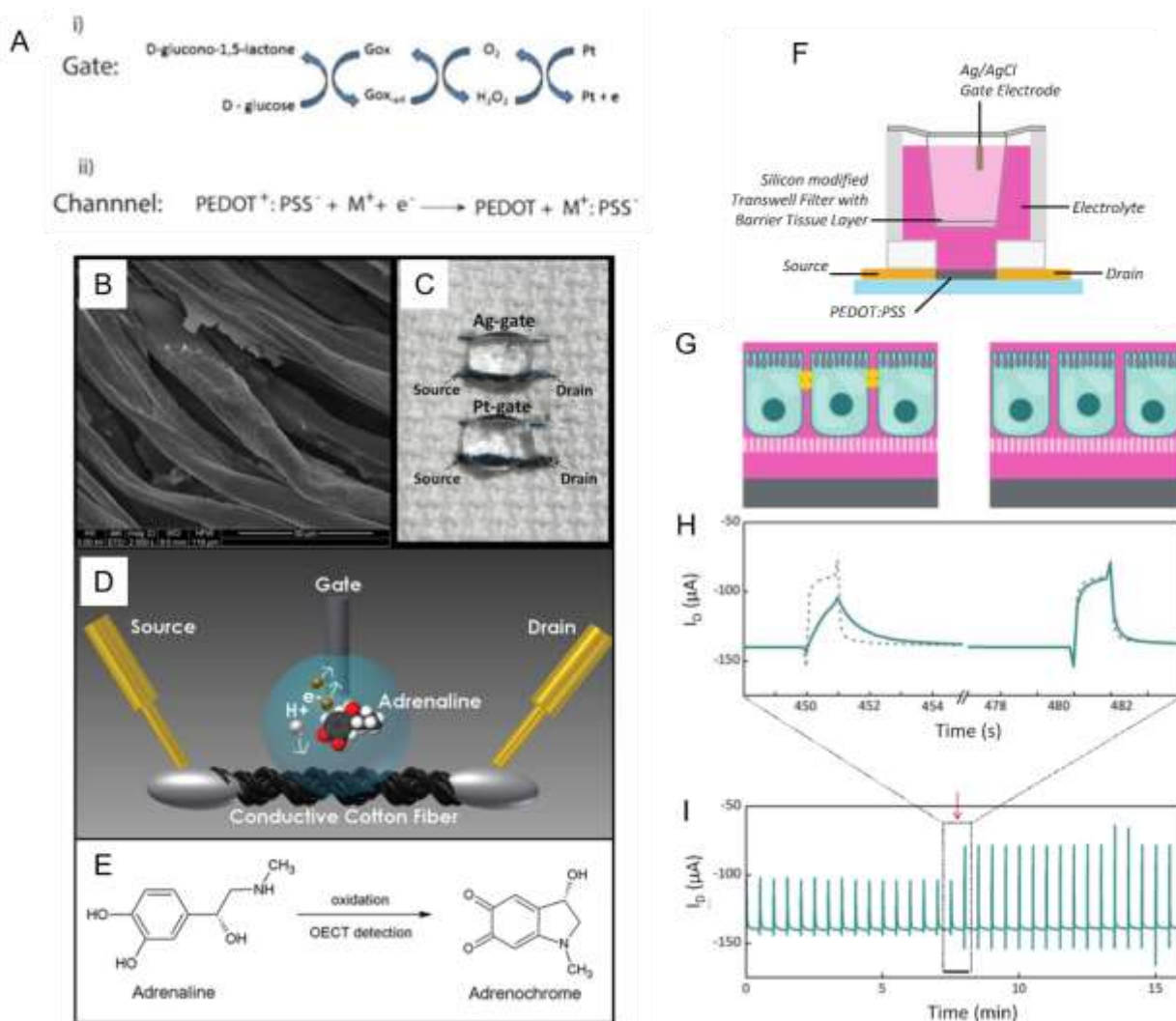


Figure 14. PEDOT:PSS OECTs for biosensing. A) Enzymatic glucose sensing. (i) transfer of electron from glucose to the gate through the biological reaction catalyzed by glucose oxidase and (ii) dedoping mechanism of PEDOT:PSS at the channel. Text and figure reproduced with permission.^[110] 2015, Wiley. Adrenaline sensing PEDOT:PSS OECTs on cotton fibers. B) Field emission SEM image of the cotton wire functionalized with PEDOT:PSS. Treats are uniformly covered. The PEDOT:PSS film thickness is randomly highlighted by some fringes at the treat borders; C) the cotton-OECT, directly integrated on cloth. On the top is shown an OECT device with an Ag-gate, while at the bottom the same device with a Pt-gate is shown. A drop of liquid electrolyte is placed in contact with the thread and the gate, the overlapping between the liquid electrolyte and the PEDOT:PSS wire defines the OECT channel. D) Schematic of the cotton-OECT device with a Pt gate and an adrenaline molecule in its sensing process. E) Adrenaline oxidation and adrenochrome formation simplified reaction. Text reproduced and figure adapted with permission^[184]. 2014, The Royal Society of Chemistry. Measurement of barrier tissue integrity with PEDOT:PSS OECTs. F) Device architecture. G) Cartoon showing polarized Caco-2 cells with tight junctions (left) and without (right), sitting on a porous cell culture membrane, above a PEDOT:PSS transistor channel. Tight junctions are shown in yellow. H) OECT I_D transient response with cells before (left) and after (right) the addition of 100 mM H_2O_2 , (solid lines). OECT I_D response in the absence of cells is overlaid (dashed lines). I) In situ OECT response to periodic square V_{GS} pulses. As indicated, data here correspond to the same measurement as shown in (H), but for an expanded time scale. The red arrow indicates the point of H_2O_2 introduction. The immediate change in

OECT response to the addition of H_2O_2 is evident by the drastic change in ΔI_D . Text reproduced and figure adapted with permission.^[180] 2012, Wiley.

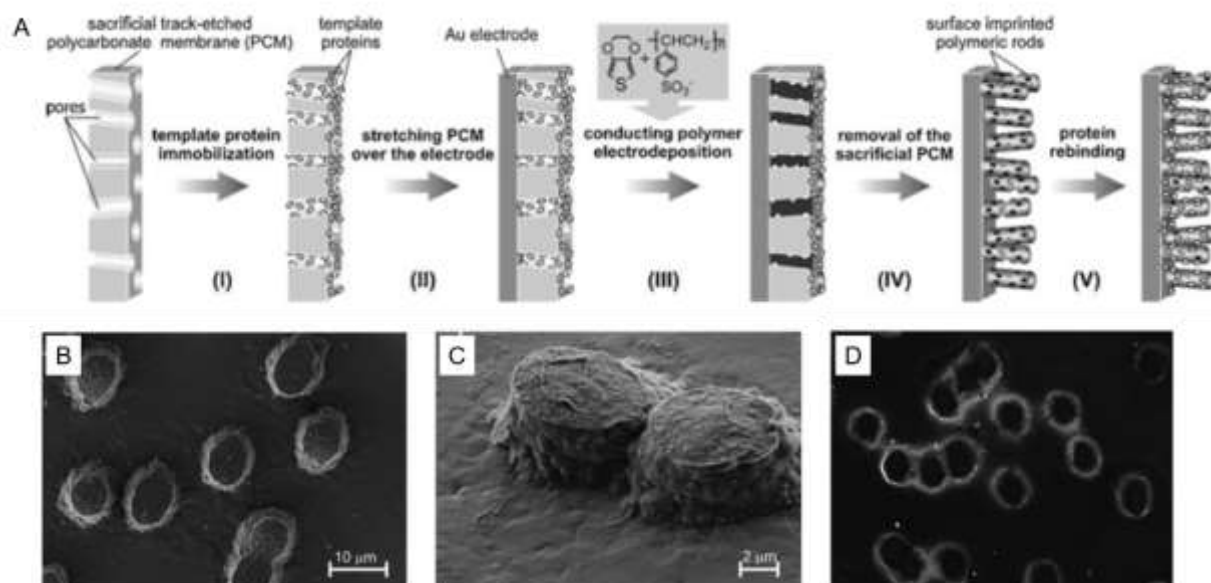


Figure 15. Molecularly imprinted PEDOT:PSS for biosensing. A) Schematic of fabrication of molecularly imprinted PEDOT:PSS for protein assays. B-C) Scanning electron micrograph of PEDOT:PSS microrods after membrane (PCM) removal. D) Fluorescence image of fluorescent avidin binding to microrods. Adapted with permission.^[196] 2009, Wiley.

1.4.4 Drug Delivery

Drug delivery is a very important field that seeks to improve patient compliance, increase drug efficacy, and diminish the harmful side effects of the administered pharmaceuticals. Advancements in drug delivery would have significant economic implications for a global industry (pharmaceuticals) that exceeds 1 trillion U.S. dollars annually.^[197] Most recent work on drug delivery has been on synthesizing micro- and nanoparticles for passive and active delivery when injected, most often intravenously. Alternatively, drug delivery incorporated with electronics brings several exciting avenues: to deliver drugs without the solvent ("dry" delivery), to locally deliver with implantable devices, to release upon receiving a stimulus (via a coupled electrode or sensor), and to electronically control release by adjustment outside the body.

As with other conducting polymers^[198], drugs have been directly incorporated into PEDOT:PSS during electropolymerization and after this, drugs can be released on-demand by electrical stimulation. Examples of incorporated drugs include dexamethasone 21-phosphate disodium salt (DEX) for inducing osteogenic differentiation as well as the neurotransmitter dopamine^[199], whose concentration can be disrupted in certain neurological diseases. In the case of PEDOT:DEX, the loaded material was covered with additional PEDOT:PSS to prevent passive diffusion of the drug from this reservoir. With electrical stimulation, 19 $\mu\text{g}/\text{cm}^2$ was released over 6 days *in vitro* (**Figure 16a-c**).^[148] Fabricated by wet spinning, conducting PEDOT:PSS:chitosan microfibers have also been used as a substrate onto which another conducting polymer and drug were co-deposited during electropolymerization (polypyrrole doped with the antibacterial drug ciprofloxacin). These fibers could then be electrically stimulated for drug release.^[200]

For the monitoring of drug payload carriers, PEDOT:PSS OECTs have been used for detecting micelle formation^[201] as well as determining the concentration and types of liposomes present^[202]. These sensors elements could be used *in vivo* to monitor drug dosing as well as *in vitro* in automated set-ups for drug carrier preparation (e.g. microfluidic platforms).

PEDOT:PSS particles have also been presented as therapeutic agents (**Figure 17**). Photothermal therapy for cancer treatment (tumor ablation) was conducted with PEGylated PEDOT:PSS nanoparticles.^[203] When intravenously injected, the particles are passively taken up by tumors (enhanced permeability and retention effect). Near-IR irradiation is applied to the tumor site where the particles absorb light and generate heat to locally kill cancer cells. PEDOT:PSS nanoparticles in conjunction with laser treatment increased the survival of tumor-bearing mice for at least 45 days (versus 16-18 days for control groups), and no apparent toxicity was observed in major organ and blood analyses. The motivation for using PEDOT:PSS is to explore organic nanoparticles for such therapies, since the majority of photothermal agents investigated to date have been inorganic. Organics are generally more

biocompatible, can be engineered to be biodegradable, and allow more manipulation of material properties. These particles were also used for drug delivery of three different drug molecules for combination therapy.^[204] PEDOT:PSS particles were found to increase the solubility of water-insoluble chemotherapeutics and provide local delivery upon photothermal trigger. Another drug, a photodynamic agent, was loaded to enhance photothermal therapy. As stated previously in the example of molecularly imprinting, PEDOT:PSS provides multiple types of interactions to capture drugs of interest; in particular, aromatic drugs through π - π stacking and hydrophobic interactions.

Finally, the mixed conductivity of PEDOT:PSS has been exploited for ion delivery through electrophoretic ion pumps. These devices can provide spatially and temporally controlled drug delivery through device dimensions created by microfabrication and the application of a voltage (pulsed or continuous), respectively.^[205] First reported in 2007, the on/off delivery of the cations K^+ and Ca^{2+} was demonstrated, even against concentration gradients (Figure 16d-f).^[206] These electronically controlled ion fluxes can influence intercellular communications as well as intracellular processes. Improvements on this work include making smaller channels comparable to the size of a single cell (10 μ m) and speeding the time of delivery to seconds (rather than minutes).^[207] In addition to resolution, ion pumps have the advantage of dispersing the ions without flow or additional fluid volume, which can be disruptive to surrounding tissue. Extending this work, the same group demonstrated the electronic control of positively-charged neurotransmitter delivery, including excitatory glutamate and aspartate and inhibitory gamma-amino butyric acid (GABA).^[206] Although diffusion will eventually carry ions away from the delivery site, physiologically relevant concentrations can be obtained with these devices, corresponding to those at the synaptic cleft. By using a specific neurotransmitter, the researchers were able to effectively target a single population of cells. Later, a neuron-mimetic electronic alongside H^+ and acetylcholine delivery in response.^[208] Devices that combined ion pumps with PEDOT:PSS electrodes were

able to achieving chemical delivery and electrical recording at the same site, leveraging the ionic and electric conduction of PEDOT:PSS. Delivery of GABA was conducted after abnormal electrical activity was recorded from a tissue slice.^[209]

In an *in vivo* syringe-like configuration of the ion pump device, excess glutamate was delivered to induce an excitotoxic effect on only the inner hair cells of a Guinea pig cochlea in a proof-of-principle experiment (Figure 16g-k).^[210] Later work would demonstrate the use GABA-delivering ion pumps for the treatment of neuropathic pain in a more clinically relevant example.^[211] As well, epileptiform activity was stopped with GABA delivery in a tissue slice model.^[212] A notable improvement for this *in vivo* device was the development of a fabrication method to incorporate microfluidic channels.^[213] Microfluidic channels decreased the distance for electrophoretic transport of the drug and hence decreased the applied voltage for delivery to levels that are safe for the body. Channels can also provide an inexhaustible drug reservoir.

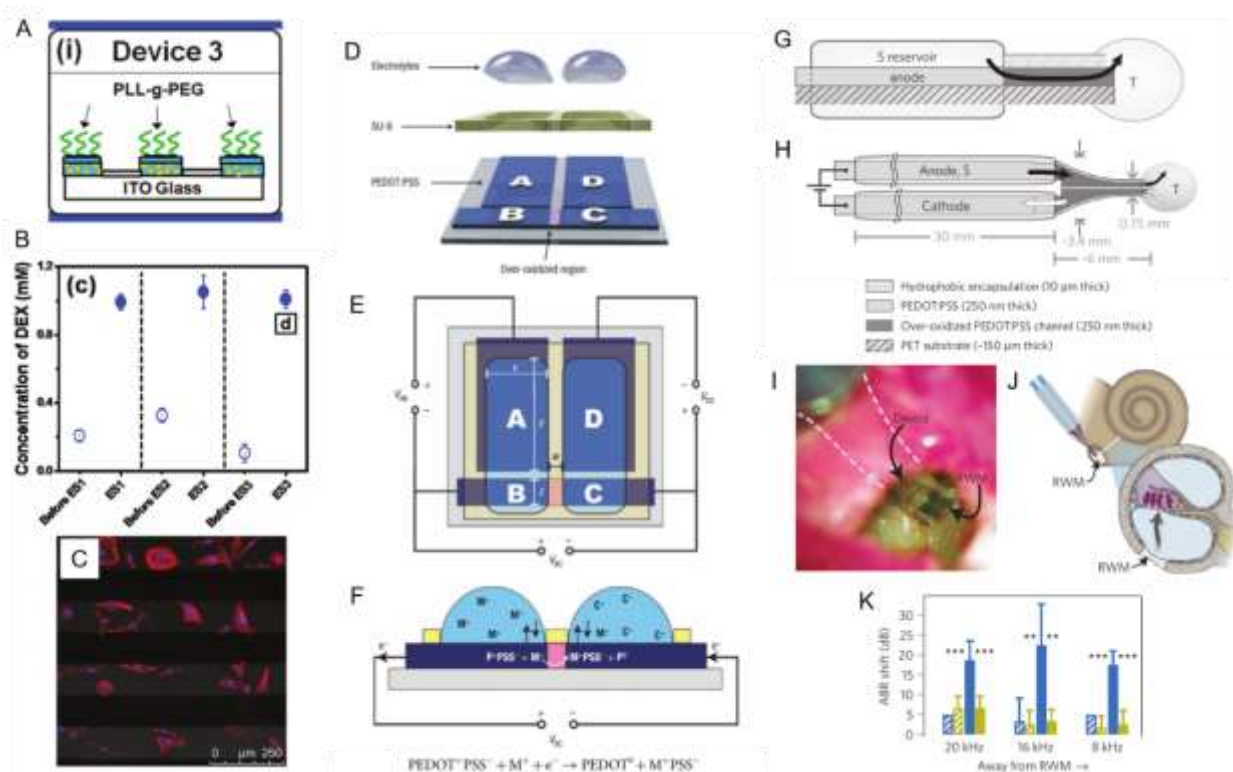


Figure 16. Drug delivery with PEDOT:PSS. A) Devices consisting dexamethasone 21-phosphate (DEX)-loaded PEDOT:PSS. PEDOT:PSS islands were PEGylated to prevent cell adhesion. B) electrically stimulated (ES) release of DEX. C) Fluorescent image of human

mesenchymal stem cells (F-actin, red; DAPI, blue) seeded on the devices and after 3 electrical stimulation cycles and one day of culture. Adapted with permission.^[148] 2013, Wiley.

PEDOT:PSS ion pump. D) The architecture of the ion pump shown as separated layers. The four PEDOT:PSS electrodes are labelled A to D. PEDOT:PSS in the over-oxidized region (pink) between B and C conducts ions but not electrons. E) Schematic top view of the device with voltages applied. $x=7$ mm, $y=12$ mm, $z=4$ mm or 50 μm and $w=2$ mm. V_{BC} drives the ion transport, whereas V_{AB} and V_{CD} regenerate the B and C electrodes. F) Schematic cross-section of the B and C electrodes. The cation M^+ is present in a relatively high concentration in the AB electrolyte (left) and binds to PSS in the polymer film. When V_{BC} is applied, PEDOT (denoted P) in the B electrode (left) is oxidized. The positive charge on the polymer chain is neutralized with PSS, thereby releasing one M^+ . Simultaneously, electrode C (right) receives an electron and PEDOT:PSS on this side is consequently reduced. There is a net flow of M^+ from the left to the right and every transported (monovalent) ion ideally corresponds to one charge measured between B and C. As the polymer film is very thin (200 nm), ion exchange will immediately occur between the C electrode and the CD electrolyte, which also contains other cations (C^+). Hence, the concentration of M^+ increases in the CD electrolyte as soon as voltage is applied and as long as B and C can be oxidized and reduced, respectively. Text reproduced and figure adapted with permission.^[206] 2007, Macmillan Publishers Ltd.

G-H) Encapsulated, syringe-like configuration of implantable ion pump. G) Side-view. Black arrow, ion flow. H) Top-view. T, target system. White arrow, flow of positively charged species to from target to cathodic electrolyte. I) Photograph of ion pump on round window membrane (RWM) in Guinea pig. J) Ions/drugs can diffuse from RWM to cochlea. K) Glutamate and H^+ pumping led to auditory brainstem response (ABR) shifts. Mean ABR shift for varying recording frequency after 15 min (hatched bars) and 60 min (filled bars) of Glu (blue) and H^+ (yellow) delivery. Adapted with permission.^[210] 2009, Macmillan Publishers Ltd.

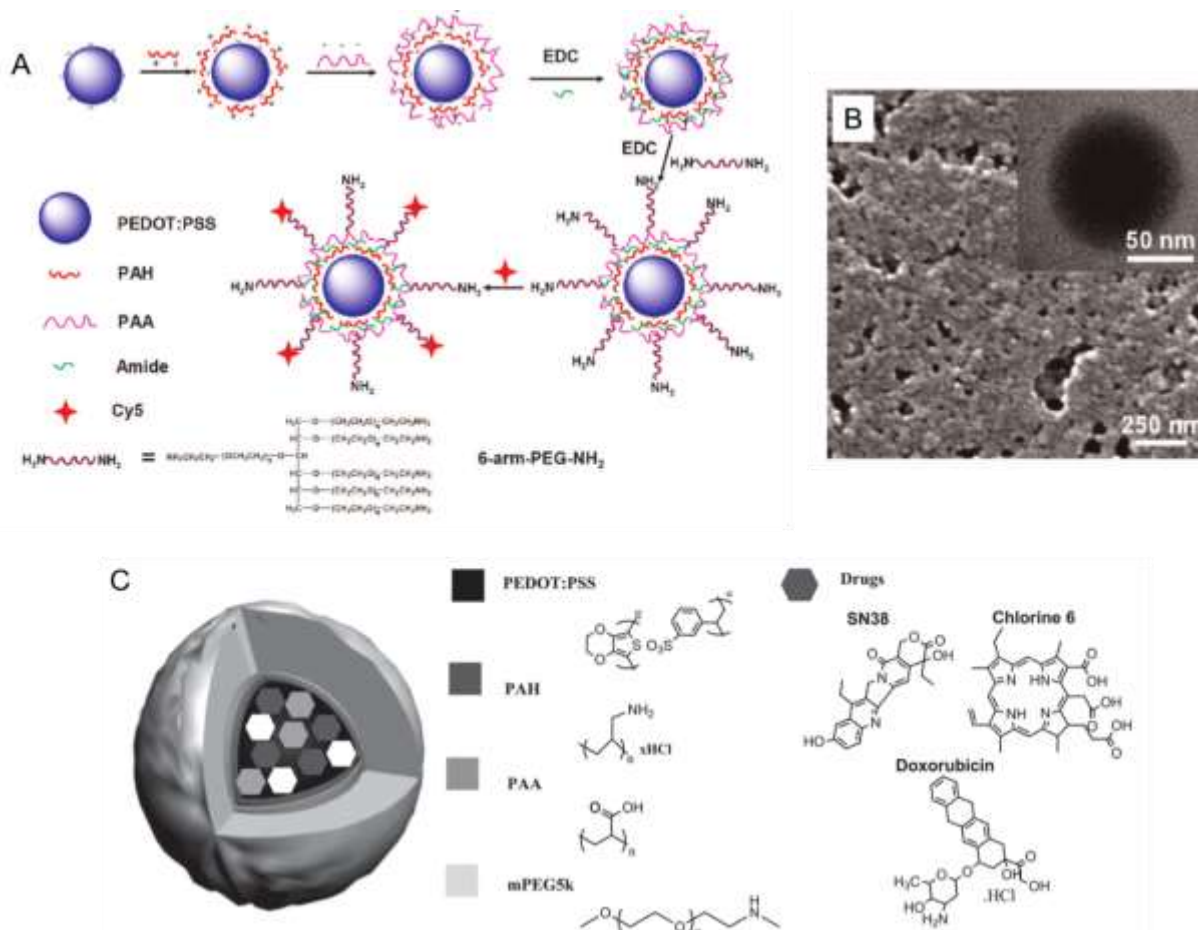


Figure 17. PEGylated PEDOT:PSS nanoparticles for cancer photothermal therapy. A) Scheme showing the fabrication process of PEDOT:PSS-PEG. Note that a linear structure is drawn for simplification purposes to represent the branched six-arm-PEG-amine. B) SEM image of PEDOT:PSS-PEG nanoparticles deposited on a silicon substrate. Inset: TEM image of a single PEDOT:PSS-PEG nanoparticle. Text reproduced and figure adapted with permission.^[203] 2012, American Chemical Society. C) A schematic drawing showing DOX, Ce6, and SN38 loaded on PEDOT:PSS-PEG. Text reproduced and figure adapted with permission.^[204] 2013, Wiley.

1.5. Conclusions and Future Directions

PEDOT:PSS is a prototypical example of a conducting polymer due to its ease of synthesis and processing as well as its exceptional mechanical and electrical properties. In the last 20 years, much research has been conducted on PEDOT:PSS to construct structure vs. properties relationships. By using advanced imaging and spectroscopic methods, important information on the structure and morphology of PEDOT:PSS films has been uncovered. Mechanical and electrical properties were tailored and enhanced with additives that cause changes in film structure and morphology. By using PEDOT:PSS in devices, connections between properties and device performance are being elaborated.

A variety of techniques have enabled PEDOT:PSS to be processed into many forms and showing different properties. Applications of PEDOT:PSS in photovoltaics have led to its integration with advanced fabrication techniques, such as roll-to-roll printing and flexographic printing. These techniques will also prove useful for biomedical applications in the future, as emphasis on metrics such as production cost and yield become important.

PEDOT:PSS has proven to be a model system for demonstrating how the application of conducting polymers in bioelectronics will impact the future of medicine. Already, many promising applications have been shown in electrophysiology, biosensing, tissue engineering and drug delivery. Supercapacitors and batteries for powering wireless and/or autonomous/self-powered implantable medical devices are also becoming a reality, and PEDOT:PSS can play a major role in their development. PEDOT:PSS devices will be used in continuous disease monitoring and treatment, especially through wearable, non-invasive formats. Additional uses in soft robotics, microsurgical robots and assistive care robotics are envisioned. PEDOT:PSS has often been used as the first example of these applications, and in the future, its use will continue to facilitate both proof-of-principle and optimized devices for biology and medicine.

References

- [1] J. Rivnay, R. M. Owens, G. G. Malliaras, *Chem. Mater.* **2014**, *26*, 679.
- [2] T. Someya, Z. Bao, G. G. Malliaras, *Nature* **2016**, *540*, 379.
- [3] T. A. Skotheim, J. Reynolds, Eds. , *Handbook of Conducting Polymers*, CRC Press, **2007**.
- [4] N. K. Guimard, N. Gomez, C. E. Schmidt, *Prog. Polym. Sci.* **2007**, *32*, 876.
- [5] J. Rivnay, S. Inal, B. A. Collins, M. Sessolo, E. Stavrinidou, X. Strakosas, C. Tassone, D. M. Delongchamp, G. G. Malliaras, *Nat. Commun.* **2016**, *7*, 11287.
- [6] X. Cui, D. C. Martin, *Sens. Actuat B-Chem* **2003**, *89*, 92.
- [7] J. L. H. and D. C. M. D.-H. Kim, S. Richardson-Burns, L. Povlich, M. R. Abidian, S. Spanninga, *CRC Press. Durham, North Carolina* **2008**, part IV, n.
- [8] X. Strakosas, B. Wei, D. C. Martin, R. M. Owens, *J. Mater. Chem. B* **2016**, *4*, 4952.
- [9] V. Castagnola, C. Bayon, E. Descamps, C. Bergaud, *Synth. Met.* **2014**, *189*, 7.
- [10] L. Groenendaal, F. Jonas, D. Freitag, H. Pielartzik, J. R. Reynolds, *Adv. Mater.* **2000**, *12*, 481.
- [11] M. Lefebvre, Z. Qi, D. Rana, P. G. Pickup, *Chem. Mater.* **1999**, *11*, 262.
- [12] K. R. Andreas Elschner, Stephan Kirchmeyer, Wilfried Lovenich, Udo Merker, CRC Press, **2011**, pp. 113–165.
- [13] G. Zotti, S. Zecchin, G. Schiavon, F. Louwet, L. Groenendaal, X. Crispin, W. Osikowicz, W. Salaneck, M. Fahlman, *Macromolecules* **2003**, *36*, 3337.
- [14] J. Hwang, D. B. Tanner, I. Schwendeman, J. R. Reynolds, *Phys. Rev. B* **2003**, *67*, 115205.
- [15] N. Karibyants, H. Dautzenberg, *Macromolecules* **1997**, *9297*, 7803.
- [16] F. Greco, A. Zucca, S. Taccola, A. Menciassi, T. Fujie, H. Haniuda, S. Takeoka, P. Dario, V. Mattoli, *Soft Matter* **2011**, *7*, 10642.
- [17] M. Elmahmoudy, S. Inal, A. Charrier, I. Uguz, G. G. Malliaras, S. Sanaur, *Macromol. Mater. Eng.* **2017**, DOI 10.1002/mame.201600497.
- [18] A. Elschner, S. Kirchmeyer, *{PEDOT}-Type Materials in Organic Solar Cells*, **2008**.
- [19] K. Norrman, A. Ghanbari-Siahkali, N. B. Larsen, *Annu. Reports Sect. "C" (Physical Chem.* **2005**, *101*, 174.
- [20] H. A. Becerril, M. E. Roberts, Z. Liu, J. Locklin, Z. Bao, *Adv. Mater.* **2008**, *20*, 2588.
- [21] G. Giri, E. Verploegen, S. C. B. Mannsfeld, S. Atahan-Evrenk, D. H. Kim, S. Y. Lee, H. A. Becerril, A. Aspuru-Guzik, M. F. Toney, Z. Bao, *Nature* **2011**, *480*, 504.
- [22] Y. Diao, B. C.-K. Tee, G. Giri, J. Xu, D. H. Kim, H. A. Becerril, R. M. Stoltenberg, T. H. Lee, G. Xue, S. C. B. Mannsfeld, Z. Bao, *Nat. Mater.* **2013**, *12*, 665.
- [23] B. J. Worfolk, S. C. Andrews, S. Park, J. Reinspach, N. Liu, M. F. Toney, S. C. B. Mannsfeld, Z. Bao, *Proc. Natl. Acad. Sci.* **2015**, *112*, 14138.
- [24] E. Bihar, T. Roberts, M. Saadaoui, T. Hervé, J. B. De Graaf, G. G. Malliaras, *Adv. Healthc. Mater.* **2017**, *6*, DOI 10.1002/adhm.201601167.
- [25] T. Roberts, J. B. De Graaf, C. Nicol, T. Hervé, M. Fiocchi, S. Sanaur, *Adv. Healthc. Mater.* **2016**, *5*, 1462.
- [26] E. Bihar, Y. Deng, T. Miyake, M. Saadaoui, G. G. Malliaras, M. Rolandi, *Sci. Rep.* **2016**, *6*, 27582.
- [27] E. Bihar, T. Roberts, E. Ismailova, M. Saadaoui, M. Isik, A. Sanchez-Sanchez, D. Mecerreyes, T. Hervé, J. B. De Graaf, G. G. Malliaras, *Adv. Mater. Technol.* **2017**, 1600251.
- [28] Y. Li, R. Torah, S. Beeby, J. Tudor, *Proc. IEEE Sensors* **2012**, 5.
- [29] Y. F. Lim, S. Lee, D. J. Herman, M. T. Lloyd, J. E. Anthony, G. G. Malliaras, *Appl. Phys. Lett.* **2008**, *93*, 85.

- [30] F. Ely, A. Matsumoto, B. Zoetebier, V. S. Peressinotto, M. K. Hirata, D. A. De Sousa, R. Maciel, *Org. Electron. physics, Mater. Appl.* **2014**, *15*, 1062.
- [31] K. J. Kim, Y. S. Kim, W. S. Kang, B. H. Kang, S. H. Yeom, D. E. Kim, J. H. Kim, S. W. Kang, *Sol. Energy Mater. Sol. Cells* **2010**, *94*, 1303.
- [32] Y. Kim, J. Lee, H. Kang, G. Kim, N. Kim, K. Lee, *Sol. Energy Mater. Sol. Cells* **2012**, *98*, 39.
- [33] J. G. Tait, B. J. Worfolk, S. A. Maloney, T. C. Hauger, A. L. Elias, J. M. Buriak, K. D. Harris, *Sol. Energy Mater. Sol. Cells* **2013**, *110*, 98.
- [34] J. Weickert, H. Sun, C. Palumbiny, H. C. Hesse, L. Schmidt-Mende, *Sol. Energy Mater. Sol. Cells* **2010**, *94*, 2371.
- [35] H. Okuzaki, M. Ishihara, *Macromol. Rapid Commun.* **2003**, *24*, 261.
- [36] H. Okuzaki, Y. Harashina, H. Yan, *Eur. Polym. J.* **2009**, *45*, 256.
- [37] S. Takamatsu, T. Lonjaret, D. Crisp, J.-M. Badier, G. G. Malliaras, E. Ismailova, *Sci. Rep.* **2015**, *5*, 15003.
- [38] A. M.-D. Wan, S. Inal, T. Williams, K. Wang, P. Leleux, L. Estevez, E. P. Giannelis, C. Fischbach, G. G. Malliaras, D. Gourdon, *J. Mater. Chem. B* **2015**, *3*, 5040.
- [39] U. Lang, N. Naujoks, J. Dual, *Synth. Met.* **2009**, *159*, 473.
- [40] U. Lang, E. Muller, N. Naujoks, J. Dual, *Adv. Funct. Mater.* **2009**, *19*, 1215.
- [41] A. M. Nardes, M. Kemerink, R. A. J. Janssen, J. A. M. Bastiaansen, N. M. M. Kiggen, B. M. W. Langeveld, A. J. J. M. Van Breemen, M. M. De Kok, *Adv. Mater.* **2007**, *19*, 1196.
- [42] and F. J. T. M. Kemerink, S. Timpanaro, M. M. de Kok, E. A. Meulenkaamp, *J. Phys. Chem. B* **2004**, *108*, 18820.
- [43] G. Greczynski, T. Kugler, W. . Salaneck, *Thin Solid Films* **1999**, *354*, 129.
- [44] G. Greczynski, T. Kugler, M. Keil, W. Osikowicz, M. Fahlman, W. . Salaneck, *J. Electron Spectros. Relat. Phenomena* **2001**, *121*, 1.
- [45] M. Vosgueritchian, D. J. Lipomi, Z. Bao, *Adv. Funct. Mater.* **2012**, *22*, 421.
- [46] E. Stavrinidou, P. Leleux, H. Rajaona, D. Khodagholy, J. Rivnay, M. Lindau, S. Sanaur, G. G. Malliaras, *Adv. Mater.* **2013**, *25*, 4488.
- [47] C. Duc, A. Vlandas, G. G. Malliaras, V. Senez, *Soft Matter* **2016**, *12*, 5146.
- [48] J. D. U. Lang, in (Ed.: I.I.C. on P. and A. in M. and Photonics), NewYork, **n.d.**
- [49] J. Qu, L. Ouyang, C. C. Kuo, D. C. Martin, *Acta Biomater.* **2016**, *31*, 114.
- [50] D. Khodagholy, J. N. Gelinas, T. Thesen, W. Doyle, O. Devinsky, G. G. Malliaras, G. Buzsáki, *Nat. Neurosci.* **2014**, *18*, 310.
- [51] J. Rivnay, P. Leleux, A. Hama, M. Ramuz, M. Huerta, G. G. Malliaras, R. M. Owens, *Sci. Rep.* **2015**, *5*, 11613.
- [52] D. Khodagholy, T. Doublet, P. Quilichini, M. Gurfinkel, P. Leleux, A. Ghestem, E. Ismailova, T. Hervé, S. Sanaur, C. Bernard, G. G. Malliaras, *Nat. Commun.* **2013**, *4*, 1575.
- [53] A. H??kansson, S. Han, S. Wang, J. Lu, S. Braun, M. Fahlman, M. Berggren, X. Crispin, S. Fabiano, *J. Polym. Sci. Part B Polym. Phys.* **2017**, *55*, 814.
- [54] D. Mantione, I. del Agua, W. Schaafsma, M. ElMahmoudy, I. Uguz, A. Sanchez-Sanchez, H. Sardon, B. Castro, G. G. Malliaras, D. Mecerreyes, *ACS Appl. Mater. Interfaces* **2017**, acsami.7b02296.
- [55] C. Chen, A. Kine, R. D. Nelson, J. C. LaRue, *Synth. Met.* **2015**, *206*, 106.
- [56] J. I. Jones, *Br. Polym. J.* **1973**, *5*, 493.
- [57] N. Liu, G. Fang, J. Wan, H. Zhou, H. Long, X. Zhao, *J. Mater. Chem.* **2011**, *21*, 18962.
- [58] C. H. Chen, A. Torrents, L. Kulinsky, R. D. Nelson, M. J. Madou, L. Valdevit, J. C. Larue, *Synth. Met.* **2011**, *161*, 2259.
- [59] C. H. Chen, A. Torrents, L. Kulinsky, R. D. Nelson, M. J. Madou, L. Valdevit, J. C. Larue, *Synth. Met.* **2011**, *161*, 2259.

- [60] D. Tank, H. H. Lee, D. Y. Khang, *Macromolecules* **2009**, *42*, 7079.
- [61] S. Baek, R. A. Green, L. A. Poole-Warren, *J. Biomed. Mater. Res. - Part A* **2014**, *102*, 2743.
- [62] L. Giraudet, S. Fauveaux, O. Simonetti, C. Petit, K. Blary, T. Maurel, A. Belkhir, *Synth. Met.* **2006**, *156*, 838.
- [63] H. Shi, C. Liu, Q. Jiang, J. Xu, *Adv. Electron. Mater.* **2015**, *1*, 1.
- [64] J. Feng-Xing, X. Jing-Kun, L. Bao-Yang, X. Yu, H. Rong-Jin, L. Lai-Feng, *Chinese Phys. Lett.* **2008**, *25*, 2202.
- [65] S.-I. Na, G. Wang, S.-S. Kim, T.-W. Kim, S.-H. Oh, B.-K. Yu, T. Lee, D.-Y. Kim, *J. Mater. Chem.* **2009**, *19*, 9045.
- [66] O. P. Dimitriev, D. A. Grinko, Y. V. Noskov, N. A. Ogurtsov, A. A. Pud, *Synth. Met.* **2009**, *159*, 2237.
- [67] I. Cruz-Cruz, M. Reyes-Reyes, M. A. Aguilar-Frutis, A. G. Rodriguez, R. Lopez-Sandoval, *Synth. Met.* **2010**, *160*, 1501.
- [68] C. Liu, B. Lu, J. Yan, J. Xu, R. Yue, Z. Zhu, S. Zhou, X. Hu, Z. Zhang, P. Chen, *Synth. Met.* **2010**, *160*, 2481.
- [69] G. Wang, S.-I. Na, T.-W. Kim, Y. Kim, S. Park, T. Lee, *Org. Electron.* **2012**, *13*, 771.
- [70] P. Wilson, C. Lekakou, J. F. Watts, *Org. Electron.* **2012**, *13*, 409.
- [71] K. Lim, S. Jung, S. Lee, J. Heo, J. Park, J. W. Kang, Y. C. Kang, D. G. Kim, *Org. Electron. physics, Mater. Appl.* **2014**, *15*, 1849.
- [72] S. Zhang, P. Kumar, A. S. Nouas, L. Fontaine, H. Tang, F. Cicoira, *APL Mater.* **2015**, *3*, DOI 10.1063/1.4905154.
- [73] J. Y. Kim, J. H. Jung, D. E. Lee, J. Joo, *Synth. Met.* **2002**, *126*, 311.
- [74] S. L. Lai, M. Y. Chan, M. K. Fung, C. S. Lee, S. T. Lee, *Mater. Sci. Eng. B* **2003**, *104*, 26.
- [75] S. Timpanaro, M. Kemerink, F. J. Touwslager, M. M. De Kok, S. Schrader, *Chem. Phys. Lett.* **2004**, *394*, 339.
- [76] J. Ouyang, C. W. Chu, F. C. Chen, Q. Xu, Y. Yang, *Adv. Funct. Mater.* **2005**, *15*, 203.
- [77] P. Wilson, C. Lekakou, J. F. Watts, *Org. Electron. physics, Mater. Appl.* **2013**, *14*, 3277.
- [78] H. Yan, T. Jo, H. Okuzaki, *Polym. J.* **2009**, *41*, 1028.
- [79] J. Ouyang, Q. Xu, C. W. Chu, Y. Yang, G. Li, J. Shinar, *Polymer (Guildf)*. **2004**, *45*, 8443.
- [80] J. P. Thomas, L. Zhao, D. McGillivray, K. T. Leung, *J. Mater. Chem. A* **2014**, *2*, 2383.
- [81] A. M. Nardes, R. A. J. Janssen, M. Kemerink, *Adv. Funct. Mater.* **2008**, *18*, 865.
- [82] A. M. Nardes, M. Kemerink, M. M. de Kok, E. Vinken, K. Maturova, R. A. J. Janssen, *Org. Electron.* **2008**, *9*, 727.
- [83] T. F. Otero, J. G. Martinez, K. Hosaka, H. Okuzaki, *J. Electroanal. Chem.* **2011**, *657*, 23.
- [84] A. Onorato, M. A. Invernale, I. D. Berghorn, C. Pavlik, G. A. Sotzing, M. B. Smith, *Synth. Met.* **2010**, *160*, 2284.
- [85] J. Ouyang, Y. Yang, *Adv. Mater.* **2006**, *18*, 2141.
- [86] J. Rivnay, P. Leleux, M. Ferro, M. Sessolo, A. Williamson, D. A. Koutsouras, D. Khodagholy, M. Ramuz, X. Strakosas, R. M. Owens, C. Benar, J.-M. Badier, C. Bernard, G. G. Malliaras, *Sci. Adv.* **2015**, *1*, e1400251.
- [87] D. A. Koutsouras, P. Gkoupidenis, C. Stolz, G. G. Malliaras, V. Subramanian, D. C. Martin, *ChemElectroChem* **2017**, DOI 10.1002/celc.201700297.
- [88] J. Rivnay, P. Leleux, M. Ferro, M. Sessolo, A. Williamson, D. A. Koutsouras, D. Khodagholy, M. Ramuz, X. Strakosas, R. M. Owens, C. Benar, J.-M. Badier, C. Bernard, G. G. Malliaras, *Sci. Adv.* **2015**, *1*, e1400251.
- [89] D. C. Martin, G. G. Malliaras, *ChemElectroChem* **2016**, *3*, 686.

- [90] C. M. Proctor, J. Rivnay, G. G. Malliaras, *J. Polym. Sci. Part B Polym. Phys.* **2016**, *54*, 1433.
- [91] I. Uguz, M. Ganji, A. Hama, A. Tanaka, S. Inal, A. Youssef, R. M. Owens, P. P. Quilichini, A. Ghestem, C. Bernard, S. A. Dayeh, G. G. Malliaras, *Adv. Healthc. Mater.* **2016**, *1*.
- [92] H. Yamato, M. Ohwa, W. Wernet, *J. Electroanal. Chem.* **1995**, *397*, 163.
- [93] E. M. Thaning, M. L. M. Asplund, T. A. Nyberg, O. W. Inganäs, H. Von Holst, *J. Biomed. Mater. Res. - Part B Appl. Biomater.* **2010**, *93*, 407.
- [94] X. Cui, D. C. Martin, *Sensors Actuators B Chem.* **2003**, *89*, 92.
- [95] S. Venkatraman, J. Hendricks, Z. A. King, A. J. Sereno, S. Richardson-Burns, D. Martin, J. M. Carmena, *IEEE Trans. Neural Syst. Rehabil. Eng.* **2011**, *19*, 307.
- [96] A. Kros, N. A. J. M. Sommerdijk, R. J. M. Nolte, *Sensors Actuators B Chem.* **2005**, *106*, 289.
- [97] X. T. Cui, D. D. Zhou, *IEEE Trans. Neural Syst. Rehabil. Eng.* **2007**, *15*, 502.
- [98] D. W. L. Hukins, A. Mahomed, S. N. Kukureka, *Med. Eng. Phys.* **2008**, *30*, 1270.
- [99] A. Schander, T. Tesmann, S. Strovkov, H. Stemmann, A. K. Kreiter, W. Lang, in *2016 38th Annu. Int. Conf. IEEE Eng. Med. Biol. Soc.*, IEEE, **2016**, pp. 6174–6177.
- [100] P.-A. Mouthuy, S. J. Snelling, S. G. Dakin, L. Milković, A. Č. Gašparović, A. J. Carr, N. Žarković, *Biomaterials* **2016**, *109*, 55.
- [101] A. Lecomte, A. Degache, E. Descamps, L. Dahan, C. Bergaud, *Procedia Eng.* **2016**, *168*, 189.
- [102] P. R. Patel, H. Zhang, M. T. Robbins, J. B. Nofar, S. P. Marshall, M. J. Kobylarek, T. D. Y. Kozai, N. A. Kotov, C. A. Chestek, *J. Neural Eng.* **2016**, *13*, 66002.
- [103] T. D. Y. Kozai, K. Catt, Z. Du, K. Na, O. Srivannavit, R. U. M. Haque, J. Seymour, K. D. Wise, E. Yoon, X. T. Cui, *IEEE Trans. Biomed. Eng.* **2016**, *63*, 111.
- [104] A. Schander, H. Stemmann, E. Tolstosheeva, R. Roesse, V. Biefeld, L. Kempen, A. K. Kreiter, W. Lang, *Sensors Actuators, A Phys.* **2016**, *247*, 125.
- [105] M. Vomero, E. Castagnola, F. Ciarpella, E. Maggiolini, N. Goshi, E. Zucchini, S. Carli, L. Fadiga, S. Kassegne, D. Ricci, *Sci. Rep.* **2017**, *7*, 40332.
- [106] Y. Lu, Y. Li, J. Pan, P. Wei, N. Liu, B. Wu, J. Cheng, C. Lu, L. Wang, *Biomaterials* **2012**, *33*, 378.
- [107] L. Ouyang, B. Wei, C. Kuo, S. Pathak, B. Farrell, D. C. Martin, *Sci. Adv.* **2017**, *3*, e1600448.
- [108] C. Boehler, F. Oberueber, S. Schlabach, T. Stieglitz, M. Asplund, *ACS Appl. Mater. Interfaces* **2016**, DOI 10.1021/acsami.6b13468.
- [109] H. S. White, G. P. Kittlesen, M. S. Wrighton, *J. Am. Chem. Soc.* **1984**, *106*, 5375.
- [110] X. Strakosas, M. Bongo, R. M. Owens, *J. Appl. Polym. Sci.* **2015**, *132*, 1.
- [111] J. D. Morris, S. B. Thourson, K. R. Panta, B. N. Flanders, C. K. Payne, *J. Phys. D. Appl. Phys.* **2017**, *50*, 174003.
- [112] N. G. Hatsopoulos, J. P. Donoghue, *Annu. Rev. Neurosci.* **2009**, *32*, 249.
- [113] M. A. Lebedev, M. A. L. Nicolelis, *Physiol. Rev.* **2017**, *97*, 767.
- [114] S. P. Lacour, G. Courtine, J. Guck, *Nat. Rev. Mater.* **2016**, *1*, 16063.
- [115] V. S. Polikov, P. A. Tresco, W. M. Reichert, *J. Neurosci. Methods* **2005**, *148*, 1.
- [116] M. Jorfi, J. L. Skousen, C. Weder, J. R. Capadona, *J. Neural Eng.* **2015**, *12*, 11001.
- [117] T. D. Yoshida Kozai, N. B. Langhals, P. R. Patel, X. Deng, H. Zhang, K. L. Smith, J. Lahann, N. A. Kotov, D. R. Kipke, *Nat. Mater.* **2012**, *11*, 1065.
- [118] D. Khodagholy, T. Doublet, M. Gurfinkel, P. Quilichini, E. Ismailova, P. Leleux, T. Herve, S. Sanaur, C. Bernard, G. G. Malliaras, *Adv. Mater.* **2011**, *23*, 268.
- [119] D. Khodagholy, J. N. Gelinas, T. Thesen, W. Doyle, O. Devinsky, G. G. Malliaras, G. Buzsáki, *Nat. Neurosci.* **2014**, *18*, 310.
- [120] A. Williamson, M. Ferro, P. Leleux, E. Ismailova, A. Kaszas, T. Doublet, P. Quilichini,

- J. Rivnay, B. Rózsa, G. Katona, C. Bernard, G. G. Malliaras, *Adv. Mater.* **2015**, *27*, 4405.
- [121] D. Khodagholy, T. Doublet, P. Quilichini, M. Gurfinkel, P. Leleux, A. Ghestem, E. Ismailova, T. Hervé, S. Sanaur, C. Bernard, G. G. Malliaras, *Nat. Commun.* **2013**, *4*, 1575.
- [122] V. Castagnola, E. Descamps, A. Lecestre, L. Dahan, J. Remaud, L. G. Nowak, C. Bergaud, *Biosens. Bioelectron.* **2015**, *67*, 450.
- [123] A. Blau, A. Murr, S. Wolff, E. Sernagor, P. Medini, G. Iurilli, C. Ziegler, F. Benfenati, *Biomaterials* **2011**, *32*, 1778.
- [124] G. S. G. Geleoc, J. R. Holt, *Science (80-)*. **2014**, *344*, 1241062.
- [125] R. K. Shepherd, M. N. Shivdasani, D. A. X. Nayagam, C. E. Williams, P. J. Blamey, *Trends Biotechnol.* **2013**, *31*, 562.
- [126] T. R. Deer, N. Mekhail, D. Provenzano, J. Pope, E. Krames, M. Leong, R. M. Levy, D. Abejon, E. Buchser, A. Burton, A. Buvanendran, K. Candido, D. Caraway, M. Cousins, M. Dejongste, S. Diwan, S. Eldabe, K. Gatzinsky, R. D. Foreman, S. Hayek, P. Kim, T. Kinfe, D. Kloth, K. Kumar, S. Rizvi, S. P. Lad, L. Liem, B. Linderoth, S. Mackey, G. McDowell, P. McRoberts, L. Poree, J. Prager, L. Raso, R. Rauck, M. Russo, B. Simpson, K. Slavin, P. Staats, M. Stanton-Hicks, P. Verrills, J. Wellington, K. Williams, R. North, *Neuromodulation* **2014**, *17*, 515.
- [127] A. M. Lozano, N. Lipsman, *Neuron* **2013**, *77*, 406.
- [128] G. Di Pino, G. Pellegrino, G. Assenza, F. Capone, F. Ferreri, D. Formica, F. Ranieri, M. Tombini, U. Ziemann, J. C. Rothwell, V. Di Lazzaro, *Nat. Rev. Neurol.* **2014**, *10*, 597.
- [129] K. T. Ragnarsson, *Spinal Cord* **2008**, *46*, 255.
- [130] L. R. Sheffler, J. Chae, *Muscle Nerve* **2007**, *35*, 562.
- [131] S. Venkatraman, J. Hendricks, S. Richardson-Burns, E. Jan, D. Martin, J. M. Carmena, *2009 4th Int. IEEE/EMBS Conf. Neural Eng. NER '09* **2009**, *4*, 383.
- [132] A. Lie, A. Guex, N. Vachicouras, A. E. Hight, M. C. Brown, D. J. Lee, S. Phanie, P. Lacour, *J. Mater. Chem. B* **2015**, *3*, 5021.
- [133] P. Schonle, F. Michoud, N. Brun, A. Guex, S. P. Lacour, Q. Wang, Q. Huang, *Proc. Annu. Int. Conf. IEEE Eng. Med. Biol. Soc. EMBS* **2016**, *2016–Octob*, 4439.
- [134] W. Zeng, L. Shu, Q. Li, S. Chen, F. Wang, X. M. Tao, *Adv. Mater.* **2014**, *26*, 5310.
- [135] M. Stoppa, A. Chiolerio, *Sensors (Switzerland)* **2014**, *14*, 11957.
- [136] A. Campana, T. Cramer, D. T. Simon, M. Berggren, F. Biscarini, *Adv. Mater.* **2014**, *26*, 3874.
- [137] P. Leleux, J. Rivnay, T. Lonjaret, J. M. Badier, C. Bénar, T. Hervé, P. Chauvel, G. G. Malliaras, *Adv. Healthc. Mater.* **2015**, *4*, 142.
- [138] P. Leleux, C. Johnson, X. Strakosas, J. Rivnay, T. Hervé, R. M. Owens, G. G. Malliaras, *Adv. Healthc. Mater.* **2014**, *3*, 1377.
- [139] W. Honda, S. Harada, T. Arie, S. Akita, K. Takei, *Adv. Funct. Mater.* **2014**, *24*, 3299.
- [140] M. Papiordanidou, S. Takamatsu, S. Rezaei-Mazinani, T. Lonjaret, A. Martin, E. Ismailova, *Adv. Healthc. Mater.* **2016**, *5*, 2001.
- [141] A. F. M. Johnstone, G. W. Gross, D. G. Weiss, O. H. U. Schroeder, A. Gramowski, T. J. Shafer, *Neurotoxicology* **2010**, *31*, 331.
- [142] A. Stett, U. Egert, E. Guenther, F. Hofmann, T. Meyer, W. Nisch, H. Haemmerle, *Anal. Bioanal. Chem.* **2003**, *377*, 486.
- [143] M. E. Spira, A. Hai, *Nat. Nanotechnol.* **2013**, *8*, 83.
- [144] Y. Xiao, D. C. Martin, X. Cui, M. Shenai, *Appl. Biochem. Biotechnol.* **2006**, *128*, 117.
- [145] T. Nyberg, A. Shimada, K. Torimitsu, *J. Neurosci. Methods* **2007**, *160*, 16.
- [146] D.-H. Kim, S. M. Richardson-Burns, J. L. Hendricks, C. Sequera, D. C. Martin, *Adv. Funct. Mater.* **2007**, *17*, 79.

- [147] J. E. Collazos-Castro, J. L. Polo, G. R. Hernández-Labrado, V. Padiál-Cañete, C. García-Rama, *Biomaterials* **2010**, *31*, 9244.
- [148] Y.-S. Hsiao, C.-W. Kuo, P. Chen, *Adv. Funct. Mater.* **2013**, *23*, n/a.
- [149] D. Ohayon, C. Pitsalidis, A.-M. Pappa, A. Hama, Y. Zhang, L. Gallais, R. M. Owens, *Adv. Mater. Interfaces* **2017**, *1700191*, 1700191.
- [150] E. Moyon, A. Hama, E. Ismailova, L. Assaud, G. Malliaras, M. Hanbucken, R. M. Owens, *Nanotechnology* **2016**, *27*, 74001.
- [151] S. M. Richardson-Burns, J. L. Hendricks, B. Foster, L. K. Povlich, D. H. Kim, D. C. Martin, *Biomaterials* **2007**, *28*, 1539.
- [152] T. Teshima, H. Nakashima, N. Kasai, S. Sasaki, A. Tanaka, S. Tsukada, K. Sumitomo, *Adv. Funct. Mater.* **2016**, *26*, 8185.
- [153] A.-D. Bendrea, L. Cianga, I. Cianga, *J. Biomater. Appl.* **2011**, *26*, 3.
- [154] R. Balint, N. J. Cassidy, S. H. Cartmell, *Acta Biomater.* **2014**, *10*, 2341.
- [155] L. Ghasemi-Mobarakeh, M. P. Prabhakaran, M. Morshed, M. H. Nasr-Esfahani, H. Baharvand, S. Kiani, S. S. Al-Deyab, S. Ramakrishna, *J. Tissue Eng. Regen. Med.* **2011**, *5*, e17.
- [156] F. Pires, Q. Ferreira, C. A. V Rodrigues, J. Morgado, F. C. Ferreira, *Biochim. Biophys. Acta - Gen. Subj.* **2015**, *1850*, 1158.
- [157] S. M. Richardson-Burns, J. L. Hendricks, D. C. Martin, *J. Neural Eng.* **2007**, *4*, L6.
- [158] A. Peramo, M. G. Urbanek, S. A. Spanninga, L. K. Povlich, P. Cederna, D. C. Martin, *Tissue Eng. Part A* **2008**, *14*, 423.
- [159] S. Krishnan, N. Wang, C. K. Ober, J. A. Finlay, M. E. Callow, J. A. Callow, A. Hexemer, K. E. Sohn, E. J. Kramer, D. A. Fischer, *Biomacromolecules* **2006**, *7*, 1449.
- [160] X. Zhang, C. Li, Y. Luo, *Langmuir* **2011**, *27*, 1915.
- [161] Tayebi, A. Shahini, M. Yazdimamaghani, K. J. Walker, M. Eastman, H. Hatami-Marbini, B. Smith, J. L. Ricci, S. Madihally, D. Vashae, *Int. J. Nanomedicine* **2013**, *9*, 167.
- [162] A. M.-D. Wan, S. Inal, T. Williams, K. Wang, P. Leleux, L. Estevez, E. P. Giannelis, C. Fischbach, G. G. Malliaras, D. Gourdon, *J. Mater. Chem. B* **2015**, *3*, 5040.
- [163] H. Warren, M. in het Panhuis, *MRS Proc.* **2013**, *1569*, mrs13.
- [164] R. A. Green, R. T. Hassarati, J. A. Goding, S. Baek, N. H. Lovell, P. J. Martens, L. A. Poole-Warren, *Macromol. Biosci.* **2012**, *12*, 494.
- [165] A. J. Patton, R. A. Green, L. A. Poole-Warren, *APL Mater.* **2015**, *3*, DOI 10.1063/1.4904820.
- [166] S. Ghosh, O. Ingan's, *Adv. Mater.* **1999**, *11*, 1214.
- [167] P. Åsberg, O. Inganäs, *Biosens. Bioelectron.* **2003**, *19*, 199.
- [168] T. Dai, X. Jiang, S. Hua, X. Wang, Y. Lu, *Chem. Commun.* **2008**, 4279.
- [169] M. Asplund, H. von Holst, O. Inganäs, *Biointerphases* **2008**, *3*, 83.
- [170] M. Bongo, O. Winther-Jensen, S. Himmelberger, X. Strakosas, M. Ramuz, A. Hama, E. Stavrinidou, G. G. Malliaras, A. Salleo, B. Winther-Jensen, R. M. Owens, *J. Mater. Chem. B* **2013**, *1*, 3860.
- [171] P. J. Molino, Z. Yue, B. Zhang, A. Tibbens, X. Liu, R. M. I. Kapsa, M. J. Higgins, G. G. Wallace, *Adv. Mater. Interfaces* **2014**, *1*, 1.
- [172] J. Goding, A. Gilmour, P. Martens, L. Poole-Warren, R. Green, *Adv. Healthc. Mater.* **2017**, *6*, 1601177.
- [173] P. Lin, F. Yan, H. L. W. Chan, *ACS Appl. Mater. Interfaces* **2010**, *2*, 1637.
- [174] G. Scheiblin, R. Coppard, R. M. Owens, P. Mailley, G. G. Malliaras, *Adv. Mater. Technol.* **2017**, *2*, 1600141.
- [175] M. Sessolo, J. Rivnay, E. Bandiello, G. G. Malliaras, H. J. Bolink, *Adv. Mater.* **2014**, *26*, 4803.
- [176] Z. Mousavi, A. Ekholm, J. Bobacka, A. Ivaska, *Electroanalysis* **2009**, *21*, 472.

- [177] D. A. Bernards, G. G. Malliaras, G. E. S. Toombes, S. M. Gruner, *Appl. Phys. Lett.* **2006**, *89*, 53505.
- [178] Y. Zhang, S. Inal, C. Y. Hsia, M. Ferro, M. Ferro, S. Daniel, R. M. Owens, *Adv. Funct. Mater.* **2016**, *26*, 7304.
- [179] S. Tria, L. H. Jimison, A. Hama, M. Bongo, R. M. Owens, *Biosensors* **2013**, *3*, 44.
- [180] L. H. Jimison, S. A. Tria, D. Khodagholy, M. Gurfinkel, E. Lanzarini, A. Hama, G. G. Malliaras, R. M. Owens, *Adv. Mater.* **2012**, *24*, 5919.
- [181] M. Ramuz, A. Hama, J. Rivnay, P. Leleux, R. M. Owens, *J. Mater. Chem. B* **2015**, *3*, 5971.
- [182] C. Yao, C. Xie, P. Lin, F. Yan, P. Huang, I. M. Hsing, *Adv. Mater.* **2013**, *25*, 6575.
- [183] H. Tang, P. Lin, H. L. W. Chan, F. Yan, *Biosens. Bioelectron.* **2011**, *26*, 4559.
- [184] N. Coppedè, G. Tarabella, M. Villani, D. Calestani, S. Iannotta, A. Zappettini, *J. Mater. Chem. B* **2014**, *2*, 5620.
- [185] Z.-T. Zhu, J. T. Mabeck, C. Zhu, N. C. Cady, C. A. Batt, G. G. Malliaras, *Chem. Commun.* **2004**, *123*, 1556.
- [186] D. A. Bernards, D. J. Macaya, M. Nikolou, J. A. DeFranco, S. Takamatsu, G. G. Malliaras, *J. Mater. Chem.* **2008**, *18*, 116.
- [187] D. J. Macaya, M. Nikolou, S. Takamatsu, J. T. Mabeck, R. M. Owens, G. G. Malliaras, *Sensors Actuators, B Chem.* **2007**, *123*, 374.
- [188] M. Braendlein, A.-M. Pappa, M. Ferro, A. Lopresti, C. Acquaviva, E. Mamessier, G. G. Malliaras, R. M. Owens, *Adv. Mater.* **2017**, 1605744.
- [189] R.-X. He, M. Zhang, F. Tan, P. H. M. Leung, X.-Z. Zhao, H. L. W. Chan, M. Yang, F. Yan, *J. Mater. Chem.* **2012**, *22*, 22072.
- [190] D.-J. Kim, N.-E. Lee, J.-S. Park, I.-J. Park, J.-G. Kim, H. J. Cho, *Biosens. Bioelectron.* **2010**, *25*, 2477.
- [191] P. Lin, X. Luo, I. M. Hsing, F. Yan, *Adv. Mater.* **2011**, *23*, 4035.
- [192] G. Mattana, P. Cosseddu, B. Fraboni, G. G. Malliaras, J. P. Hinstroza, A. Bonfiglio, *Org. Electron. physics, Mater. Appl.* **2011**, *12*, 2033.
- [193] G. Tarabella, M. Villani, D. Calestani, R. Mosca, S. Iannotta, A. Zappettini, N. Coppedè, *J. Mater. Chem.* **2012**, *22*, 23830.
- [194] R. K. Pal, A. A. Farghaly, C. Wang, M. M. Collinson, S. C. Kundu, V. K. Yadavalli, *Biosens. Bioelectron.* **2016**, *81*, 294.
- [195] J. A. Arter, D. K. Taggart, T. M. McIntire, R. M. Penner, G. A. Weiss, *Nano Lett.* **2010**, *10*, 4858.
- [196] A. Menaker, V. Syritski, J. Reut, A. Öpik, V. Horváth, R. E. Gyurcsányi, *Adv. Mater.* **2009**, *21*, 2271.
- [197] “Worldwide pharmaceutical market,” **n.d.**
- [198] D. Svirskis, J. Travas-Sejdic, A. Rodgers, S. Garg, *J. Control. Release* **2010**, *146*, 6.
- [199] L. Sui, X. J. Song, J. Ren, W. J. Cai, L. H. Ju, Y. Wang, L. Y. Wang, M. Chen, *J. Biomed. Mater. Res. - Part A* **2014**, *102*, 1681.
- [200] D. Esrafilzadeh, J. M. Razal, S. E. Moulton, E. M. Stewart, G. G. Wallace, *J. Control. Release* **2013**, *169*, 313.
- [201] G. Tarabella, G. Nanda, M. Villani, N. Coppedè, R. Mosca, G. G. Malliaras, C. Santato, S. Iannotta, F. Cicoira, *Chem. Sci.* **2012**, *3*, 3432.
- [202] G. Tarabella, A. G. Balducci, N. Coppedè, S. Marasso, P. D’Angelo, S. Barbieri, M. Cocuzza, P. Colombo, F. Sonvico, R. Mosca, S. Iannotta, *Biochim. Biophys. Acta - Gen. Subj.* **2013**, *1830*, 4374.
- [203] L. Cheng, K. Yang, Q. Chen, Z. Liu, *ACS Nano* **2012**, *6*, 5605.
- [204] H. Gong, L. Cheng, J. Xiang, H. Xu, L. Feng, X. Shi, Z. Liu, *Adv. Funct. Mater.* **2013**, *23*, 6059.
- [205] A. Jonsson, T. A. Sjöström, K. Tybrandt, M. Berggren, D. T. Simon, *Sci. Adv.* **2016**,

- 2, e1601340.
- [206] J. Isaksson, P. Kjäll, D. Nilsson, N. Robinson, M. Berggren, A. Richter-Dahlfors, *Nat. Mater.* **2007**, *6*, 673.
 - [207] K. Tybrandt, K. C. Larsson, S. Kurup, D. T. Simon, P. Kjäll, J. Isaksson, M. Sandberg, E. W. H. Jager, A. Richter-Dahlfors, M. Berggren, *Adv. Mater.* **2009**, *21*, 4442.
 - [208] D. T. Simon, K. C. Larsson, D. Nilsson, G. Burström, D. Galter, M. Berggren, A. Richter-Dahlfors, *Biosens. Bioelectron.* **2015**, *71*, 359.
 - [209] A. Jonsson, S. Inal, Ilke Uguz, A. J. Williamson, L. Kergoat, J. Rivnay, D. Khodagholy, M. Berggren, C. Bernard, G. G. Malliaras, D. T. Simon, *Proc. Natl. Acad. Sci.* **2016**, *113*, 9440.
 - [210] D. T. Simon, S. Kurup, K. C. Larsson, R. Hori, K. Tybrandt, M. Goiny, E. W. H. Jager, M. Berggren, B. Canlon, A. Richter-Dahlfors, *Nat. Mater.* **2009**, *8*, 742.
 - [211] A. Jonsson, Z. Song, D. Nilsson, B. A. Meyerson, D. T. Simon, B. Linderoth, M. Berggren, *Sci. Adv.* **2015**, *1*, e1500039.
 - [212] A. Williamson, J. Rivnay, L. Kergoat, A. Jonsson, S. Inal, I. Uguz, M. Ferro, A. Ivanov, T. A. Sjöström, D. T. Simon, M. Berggren, G. G. Malliaras, C. Bernard, *Adv. Mater.* **2015**, *27*, 3138.
 - [213] I. Uguz, C. M. Proctor, V. F. Curto, A.-M. Pappa, M. J. Donahue, M. Ferro, R. M. Owens, D. Khodagholy, S. Inal, G. G. Malliaras, *Adv. Mater.* **2017**, *1701217*, 1701217.

Chapter 2

Tailoring the Electrochemical and Mechanical Properties of PEDOT:PSS Films for Bioelectronics

2.1 Introduction

Bioelectronics uses electrical signals to interact with biological systems. Sensors that allow for electrical read-out of important disease markers, and implants/stimulators used for the detection and treatment of pathological cellular activity are only a few examples of what this technology can offer^[1-2]. In the last few decades, due to their intriguing electroactive and mechanical properties, organic electronics or π -conjugated materials have been extensively explored regarding their use in bioelectronics applications^[3-8]. Historically, the interest in organic electronic materials stemmed from their soft and flexible nature which dampens the mechanical properties mismatch with tissue^[7]. This less “foreign” surface enhances the signal transfer to/from cells *in vitro*^[9]. It also elicits a small foreign body response when used *in vivo*, improving the performance as well as the lifetime of the implanted device. The other attractive feature of π -conjugated materials and more particularly of conducting polymers for bioelectronics is their mixed electronic/ionic conductivity^[10-12]. Mixed conductivity enables coupling between the electronic charges in the bulk of the organic films with ion fluxes in biological medium. This translates into low electrochemical impedance at the biotic interface and therefore efficient transduction as well as stimulation of biological signals. As a matter of

fact, the materials research for bioelectronics strives for soft materials that exhibit low impedance.

The prototypical material of organic bioelectronics is the conducting polymer poly(3,4-ethylenedioxythiophene) (PEDOT) doped with polystyrene sulfonate (PSS). PEDOT:PSS is commercially available, water-dispersible conjugated polymer complex that can be cast into films of high hole and cation conductivity, good charge storage capacity, biocompatibility, and chemical stability. In PEDOT:PSS films, PEDOT chains accumulate in a pancake-like morphology surrounded by a PSS network^[11]. While hole transport is facilitated within/among the PEDOT aggregates, the PSS phase attracts a considerable amount of water, enabling penetration and transport of ions in the film. Ion transport, and consequently electrochemical activity, benefits from such hydrated pathways. This, however, brings together the challenge of maintaining the integrity of films when exposed to an aqueous environment such as the biological tissue for *in vivo* applications and the cell culture media for *in vitro* studies.

In order to avoid delamination/disintegration of the films in aqueous environment, PEDOT:PSS dispersions are typically mixed with other chemical compounds. Some studies have reported blending the dispersion with water soluble polymers such as the polyvinyl alcohol (PVA)^[13-16]. The main problem with these blends is the dramatic drop in the conductivity. For instance, when mixed with PVA at a weight ratio of 20 and 60 %, the electrical conductivity of films dropped by 1 and 5 orders of magnitude, respectively^[13]. The silane based crosslinking agent, 3-glycidoxypropyltrimethoxysilane (GOPS), on the other hand, was reported to make relatively stable PEDOT:PSS films (with conductivities up to 800 S cm⁻¹) for a large variety of bioelectronic devices^[17-24], when used at a particular concentration in the dispersion (0.1 wt%). The epoxy group in GOPS (see the inset of Figure

1 for the chemical structure of GOPS) can react with amines, thiols, and acids, as well as interacting with itself and covalently with SiO₂ substrates^[25]. Although the interaction mechanism between GOPS and PEDOT:PSS is yet unclear, XPS studies suggested that the cross-linker can polymerize in water to form a multilayered structure^[26]. However, depending on its concentration in the film, GOPS might change electronic and ionic transports as well as mechanical properties of PEDOT:PSS, presumably due to alterations on the structure and morphology of films. Only a few reports have touched upon the effect of GOPS concentration on the electrical properties of the resulting films^[27]. Nevertheless, it is essential to maintain the electrical performance and softness of PEDOT:PSS while improving the thin film stability in aqueous media using a stabilizer such as GOPS. This is particularly crucial for long term use of bioelectronic devices, a direct example being the organic electrochemical transistors (OECTs) which are chronically implanted into cortex to record neural activities. Balancing these needs requires a systematic synthetic work or processing related interventions which aim to improve the electrochemical properties while not impeding mechanical properties. Moreover, materials with high performance electronic properties and physical characteristics matched to those of the tissue have great potential to bring forth applications for soft electronics. Here, post-processing can provide alternative modification routes as crystalline materials exhibiting high charge mobility typically have low mechanical resilience.

In this work, we investigate the effect of GOPS content in PEDOT:PSS dispersions on the properties of films spun cast from these formulations. We find out that the concentration of GOPS has a tremendous, yet gradual impact on the electrical, electrochemical, and mechanical properties of the PEDOT:PSS/GOPS films and that there is an optimum concentration which maximizes a particular feature of the film such as its water uptake or elasticity. The benefits of aqueous stability and mechanical strength with GOPS are to be compensated by an increase in the electrochemical impedance. Our findings suggest that a

trade-off cross-linker concentration exists, which enables sufficient electrical conductivity with mechanical robustness and stability in aqueous environment.

2.2 Results and Discussion

2.2.1 Effect of the cross-linker on electrical properties

To gain insight into the effect of the cross-linker on the electrical properties of dry PEDOT:PSS films, we casted films from dispersions containing a variety of GOPS concentration (0.05, 1, 2.5, 3.5 and 5 wt%) in addition to a constant concentration of the conductivity enhancer, ethylene glycol (EG, 5 vol%) and the surfactant, dodecyl benzene sulfonic acid (DBSA, 0.002 vol%). The films were spin-cast at the same speed on four sets of substrates: Au-coated polyimide films (Au thickness: 100 μm , surface area: 96.7 mm^2 and 24 mm^2) and glass substrates of different geometries (25 x 25 mm^2 , 75 x 25 mm^2). **Figure 1** shows that GOPS content in the film affects the bulk conductivity significantly: the highest conductivity (ca. 460 $\text{S}\cdot\text{cm}^{-1}$) is observed for the film containing the least amount of GOPS (0.05 wt%), whereas the conductivity dropped by 4 times (120 $\text{S}\cdot\text{cm}^{-1}$) with a GOPS concentration of 5 wt%. These results are in agreement with those of Zhang et al who reported a gradual decrease in the conductivity of PEDOT:PSS film (cast from a dispersion with 5 vol% glycerol and 0.5 vol% of DBSA) with an increase in GOPS concentration^[27]. The Clevios PH1000 PEDOT:PSS dispersion has a polymer content of 1.15 wt%, with a PEDOT to PSS ratio of 1:2.5 (ca. 0.3 wt% PEDOT and ca. 0.8 wt% PSS). It is intriguing that although PEDOT:PSS comprises only 18.5 wt% in the presence of 5 wt% GOPS, the conductivity of the film exceeds 100 $\text{S}\cdot\text{cm}^{-1}$.

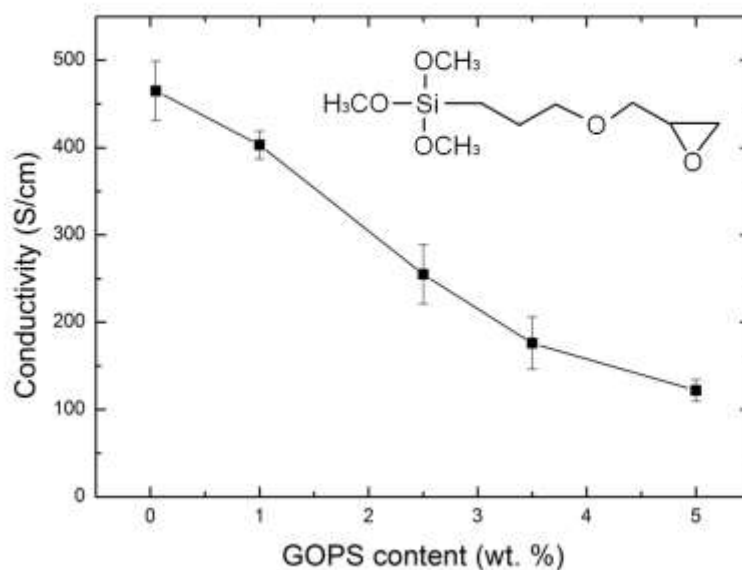


Figure 1. Electrical conductivity of PEDOT:PSS films cast from dispersions with GOPS concentration of 0.05, 1, 2.5, 3.5, and 5 wt%. Error bars result from error propagation taking into account 9 measurements, and the standard deviation in film thickness determination. The chemical structure of GOPS is given in the inset to the figure.

Moreover, the films processed from dispersions that contained more GOPS are thicker than the ones that had less of the cross-linker (ca. 3x difference between 0.05 wt% and 5 wt% of GOPS, **Figure S1**). We attribute this to an increase in the viscosity of the dispersions in the presence of GOPS. On the other hand, interactions of the cross-linker with the non-volatile additives in the dispersion might lead to an increased material content since the amount of cross-linked network in the film with respect to the PEDOT:PSS increases with GOPS content^[27]. This can as well account for the observed decrease in the conductivity as a larger content of non-evaporating and non-conducting species would be present in the film^[27]. However, for our case, i.e., dispersions containing EG, X-ray studies showed no evidence for EG remaining in the films^[11]. We therefore attribute the decrease in electrical conductivity to a dilution effect of the conducting phase by the cross-linker. Indeed, hole mobility also decreases ca. 4 times in the range of cross-linker concentrations investigated. The mobilities were estimated by measuring OECTs prepared from PEDOT:PSS formulations of different

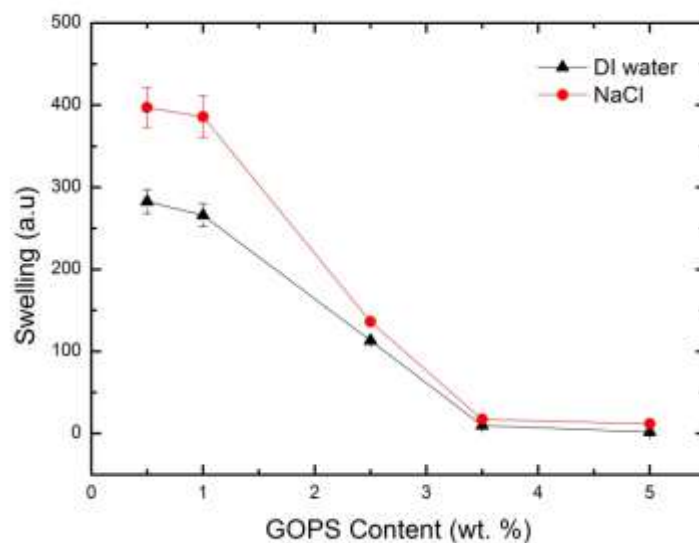
GOPS concentrations (**Figure S2a** and experimental section). For instance, while the hole mobility of the 0.05 wt% GOPS-cast film is $6.4 \text{ cm}^2 \text{ V}^{-1} \text{ s}^{-1}$, this value drops to $1.7 \text{ cm}^2 \text{ V}^{-1} \text{ s}^{-1}$ for the 5 wt% GOPS-cast film. It is likely that GOPS limits the extent of aggregation of PEDOT chains by introducing crosslinks into the system. In an OECT, upon application of a positive gate voltage (V_G), cations from the electrolyte are injected into the channel, compensate the sulfonate groups of the PSS and deplete the holes of the PEDOT (See Figure S2a for a schematic of an OECT). This mechanism is measured as a decrease in the drain current (I_D). The performance of an OECT is therefore evaluated as its transconductance ($g_m = \frac{\partial I_D}{\partial V_G}$), i.e., the extent of the modulation of the drain current with a change in gate voltage. As the GOPS content in the channel increases, not only the channel becomes less conductive, we also measure a gradual decrease in the transconductance of OECTs (Figure S2b).

2.2.2 Cross-linked PEDOT:PSS properties in aqueous environment

Since applications in bioelectronics necessitate an aqueous environment, it is critical to characterize the properties of the polymer film in aqueous working conditions. Using the quartz crystal microbalance dissipation (QCM-D), we quantify the swelling capability of the PEDOT:PSS/GOPS films cast on quartz crystals when exposed to DI water or an aqueous solution of NaCl. In these measurements, a decrease in the frequency (f) accompanied with an increase in dissipation (D) with the inflow of water indicates an increase in the mass of the film, i.e. swelling due to uptake of molecules. Here, the inflow of NaCl induces a further decrease in f for all samples, attributed to penetration of solvated ions in addition to the trapped water molecules. In order to quantify the swelling of the films casted from different GOPS concentrations, we treated our data both with Sauerbrey model which directly correlates the change in f to coupled mass (more appropriate for rigid films) and with Kelvin-Voigt model which is considered typically for soft films (see Experimental section). The

swelling percentages estimated from these two models are summarized in Table S1. The results suggest a reduction in the swelling capacity of films with an increase in GOPS content (**Figure 2a**). The ability of PEDOT:PSS film to uptake water drops from 397% to 12% when GOPS concentration increases from 0.05 to 5 wt%. Using AFM to estimate the thickness of PEDOT:PSS films before and after exposure to DI water, Duc et al. reported a swelling ratio of a $40 \pm 1\%$ for a PEDOT:PSS film that contained 1 wt% of GOPS^[28]. This value is well below our estimations (ca. 266%) for the same formulation. These authors also reported $660 \pm 90\%$ swelling for a PEDOT:PSS film that does not contain GOPS. Using the same technique, Stavrinidou et al. reported $155 \pm 53\%$ of swelling for the film prepared in the absence of GOPS and $35 \pm 4\%$ in the presence of 1 wt% of GOPS^[19]. These variations in the reported values could be due to the characterization techniques, the film/dispersion preparation, and the measurement conditions. The latter is particularly challenging to control since PEDOT:PSS films change their volume rather rapidly due to the humidity in the environment. Our results are rather meant to demonstrate only the relative decrease in swelling with changing the GOPS content in PEDOT:PSS/GOPS films. For our measurements, we dried the films under vacuum over night to ensure that the film has minimal water trapped prior to its interactions with water molecules. Notably, we observed that such a dry film requires ca. two hours under constant water flow to reach a steady-state change in frequency, i.e., fully hydrated state. (Table S1). Interestingly, although the film that contained a higher GOPS content was thicker than the one that had less GOPS, its stabilization time was shorter: 30 min for 5 wt% GOPS-cast film in comparison to ca. 103 min for 1 wt% GOPS-cast film. Taken together, the trend of stabilization time and GOPS content is consistent throughout the whole formulation series.

a)



b)

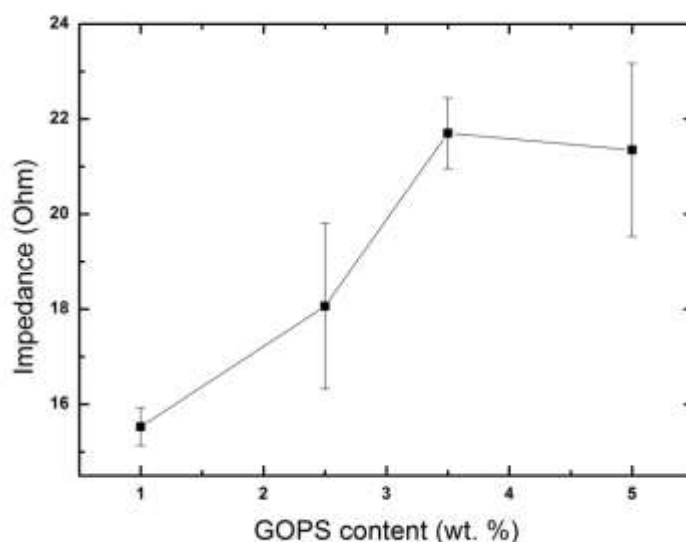


Figure 2. a) The relative effect of GOPS concentration in the PEDOT:PSS dispersion on the swelling capacity of the spin cast films: swelling in DI water (triangle) and aqueous NaCl solution (circles). Error bars are due to different models used to estimate the water/electrolyte uptake and the standard deviation in film thickness determination. **b)** The effect of GOPS concentration in the PEDOT:PSS dispersion on the electrochemical impedance measured at 1 kHz of PEDOT:PSS/GOPS films (100 nm). Error bars result from error propagation taking into account 2 measurements.

It is absolutely mandatory to investigate the impedance characteristics of conducting materials dedicated to bioelectronics applications. Figure 2b shows the electrochemical impedance (Z) of PEDOT:PSS/GOPS films measured at 1 kHz as a function of the cross-linker concentration. Here, since the films had different thicknesses due to variations in GOPS

content (Figure S1), we normalized Z values measured at 1 kHz for a 100nm-thick film. First, the Bode plots (log Z vs log frequency) were fit to an equivalent circuit model (RC) to extract the resistance (R) and capacitance (C) values. Then, the capacitance was estimated for a 100 nm thick film using $C' = \frac{C \times 100}{d}$, where C' is the normalized impedance and d (in nm) is the film thickness. Finally, C' was substituted in the impedance formula ($|Z'| = \sqrt{R^2 + \frac{1}{\omega^2 C'^2}}$) to estimate the normalized impedance (Z'), knowing that the change in R is negligible. Our results show that 1 kHz impedance increases indistinctly as the film contains more GOPS. This is in fact consistent with the trend in swelling. At low GOPS concentrations, the film uptakes more water (Figure 2a), suggesting that the ions of the electrolyte can more readily penetrate and travel inside the polymer film without significant accumulation at the polymer/electrolyte interface, leading to low impedance values. Likewise, less swelling at high GOPS content impedes ionic mobility in the film, resulting in higher impedance.

Finally, we studied the effect of GOPS on the mechanical properties of PEDOT: PSS films in solution via Nano-indentation experiment using the tip of an atomic force microscope (**Figure 3a**). During the course of the experiment, the tip-sample distance is modulated and the subsequent interaction between the tip and the sample is monitored through the vertical displacement of the cantilever probe. Young's modulus can be extracted from such force-distance curves using the appropriate model. In this experiment, we used a derived model of the Sneddon contact mechanics assuming a conical tip with a non-negligible radius of curvature at its apex in contact with a flat surface^[29]. The applied force (F) and the indentation (h) are related with the Young modulus (E), the Poisson ratio ($\nu \sim 0.5$), the radius of curvature of the tip apex (R), and the half opening angle of the tip (θ) as in the following:

$$F = \frac{2E}{\pi \cdot (1-\nu^2)} \{2Rh[1 - \tan(\theta)] + h^2 \tan(\theta)\} \quad (1)$$

For each sample prepared, a series of 50 measurements was performed at different locations of the film. A typical challenge encountered for thin films is that the deformation of the film under the tip goes through continuous change by the presence of the hard substrate underlying the sample. This results in an overestimation of the Young moduli. In our case, the thickness of the films varies from 60 nm for the 0.05 wt% GOPS-cast film to 180 nm for the 5 wt% GOPS. In order to overcome challenges related to thin films, we performed the measurements at varying indentation depths.

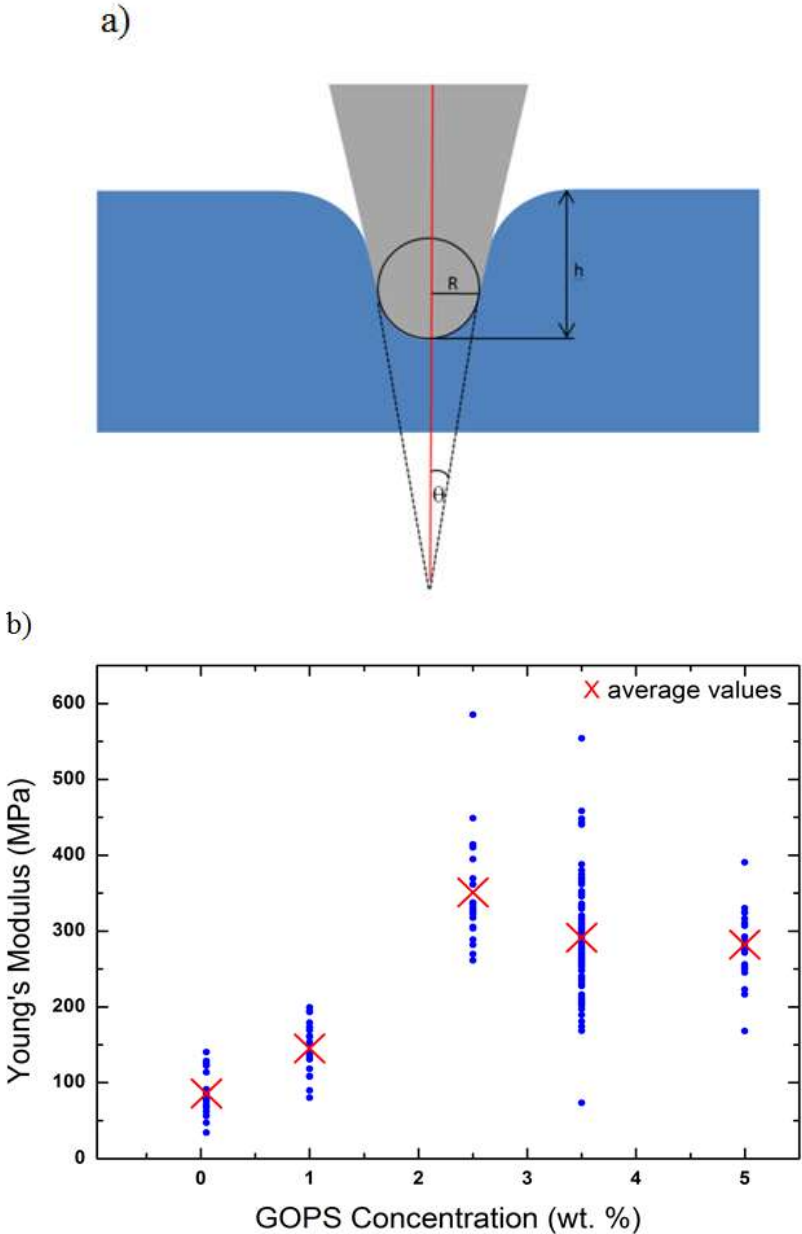


Figure 3. a) Schematic of the AFM tip indenting PEDOT:PSS thin film **b)** The change in Young's modulus of PEDOT:PSS films determined in DI water as a function of GOPS content in the film.

We found the Young's modulus to drastically increase with the indentation depth, reflecting the substrate effect and that it can therefore be minimized with low indentation depth experiments (**Figure S3**). Therefore, we limited the indentations to 10 nm. The roughness of the PEDOT:PSS/GOPS thin films was also estimated from the AFM images taken in water (**Figure S4**). Samples containing 0.05 and 3.5 wt.% GOPS showed average surface roughness of 1.46 and 1.43 nm (root mean square= 1.98 and 1.81 nm) respectively. These roughness values are much smaller than the chosen indentation depth (10nm). Figure 3b shows that the Young modulus of the films increases from 90 MPa for the 0.05 wt% of GOPS to 150 MPa for the 1 wt% of GOPS. Above 2.5 wt%, the cross-linker doesn't seem to influence the elasticity of the films (ca. 350 MPa). Moreover, we observe that the mechanical stiffness of PEDOT:PSS films decreases dramatically (by ca. 25x) in aqueous environment compared to air (**Figure S5**). The decrease in film stiffness in DI water is directly related to the swelling of the polymer. Our results are in agreement with those reported by Okuzaki et al (1.4 ± 0.6 GPa), and Lang et al. (1.3 ± 0.6 GPa), and by Qu et al. (2.6 ± 1.4 GPa)^[30–32]. These results suggest that GOPS is a versatile additive that can be used not only to improve the aqueous stability of films but also to modify their elasticity.

As par these results, considering the use of PEDOT:PSS based OECTs for long term implantations in the brain^[22], we intended to evaluate the performance of devices over several days. The OECT that was selected for this test had GOPS content that led to films with optimal water uptake, softness and conductivity: 1 wt%. **Figure 4** depicts the change in the transconductance of an OECT comprising 1 wt% GOPS in the channel over 21 days, within sub-chronic period, measured in PBS. In order to obtain stable current values at day 0 (prior to the performance evaluation experiments), the devices were incubated in water overnight

followed by multiple current-voltage cycles. This enabled the dissolution/diffusion of low molecular components in the film into the solution. In fact, another study reported that when gold electrodes coated with electropolymerized EDOT were soaked in a buffer for several days, the impedance of some of these electrodes raised steadily associated with decreases in charge storage capacity. This decrease was attributed to partial delamination of the PEDOT coating in PBS [33]. Nevertheless, our devices (width = 10 μm , length = 5 μm , thickness = 275 ± 25 nm) showed stable transconductance values ($g_m = 7.3 \pm 0.2$ mS) over the course of this study. In a separate study, we found that the devices that contain even higher (3.5 wt%) GOPS in the channel had similar performance in stability, tested over 4 days in aqueous environment (Figure S6). Overall, the results obtained from 5 different OECTs suggest that the films cast with 1% wt of GOPS maintain their structural integrity in aqueous media and but also exhibit adequate long-term electrical performance.

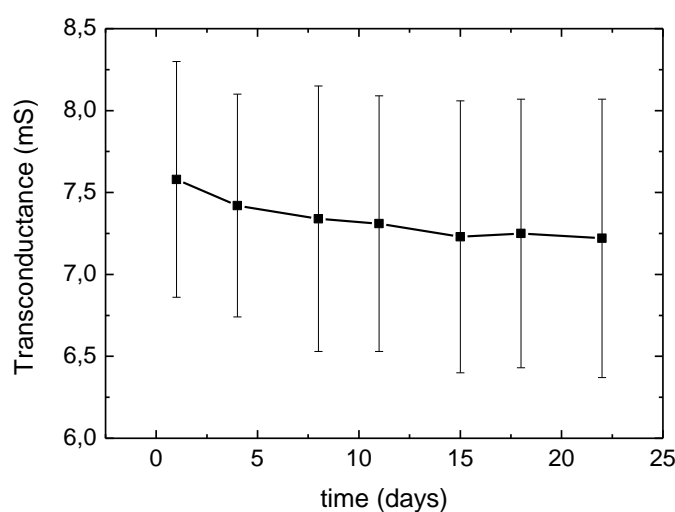


Figure 4. The performance of an OECT (channel: PEDOT:PSS with 1 wt% GOPS) chronically submerged in sterile PBS over 21 days. The transconductance was measured at $V_G = 0\text{V}$. The error bars are deduced from the measurements performed with 5 different OECTs. At day 0, each device has been cycled several times until the current values were stable, i.e., multiple current-voltage measurements were performed. Once the measurement was complete, the devices were kept in 4 $^{\circ}\text{C}$ to prevent the effects of water evaporation in the buffer on the device performance. The devices had a width of 10 μm , length of 5 μm , and a thickness of 275 ± 25 nm.

2.3 Conclusion

In this work we investigated the electrical, swelling, electrochemical, and mechanical properties of PEDOT:PSS films modified with varying amounts of the silane based cross-linker, GOPS. As the cross-linker content increases from 0.05 to 5 wt%, we observed a drop in the bulk conductivity from ca. 530 to 120 S.cm⁻¹, a decrease in the swelling from ca. 397% to 12%, and a relative increase in the electrochemical impedance (from ca. 15 to 20 Ohm at 1 kHz for films of 100 nm with a surface area of 96.7 mm²). The benefits of aqueous stability with GOPS are therefore to be compensated by losses in electronic transport and increase in the electrochemical impedance. Nevertheless, the presence of the cross-linker led to an increase in the mechanical strength of the films when they are hydrated (ca. 90 to 300 MPa in DI water for 0.05 and 5 wt% of GOPS in the dispersion, respectively), as these films uptake significantly less amount of water. We also emphasize the tolerance of PEDOT:PSS films to a large quantity of the cross-linker (only 18.5 wt% of PEDOT:PSS in the solution can lead to conductivity up to 100 S.cm⁻¹). GOPS aids obtaining highly conductive films with excellent mechanical integrity in aqueous media. Moreover, devices that contain 1 wt% GOPS, which is a concentration that leads to film with high electrical conductivity with sufficient mechanical stability, exhibit steady performance over 3 weeks. These results suggest that variations in the concentration of such a dispersion additive like GOPS can enable facile co-optimization of electrical and mechanical properties of a conducting polymer film.

2.4 Experimental Section

Sample Preparation: PEDOT:PSS (Clevios PH-1000 from Heraeus Holding GmbH.), dodecyl benzene sulfonic acid (DBSA; 0.002 vol%), ethylene glycol (EG; 5 vol%) and GOPS (ranging from 0.05 to 5 wt%) were mixed, sonicated for 30 minutes at room temperature and

then filtered using 1.2 μm hydrophilic syringe filters (Minisart, from Sartorius Stedim Biotech). The substrates were cleaned and exposed to plasma oxygen for 2 minutes at 100 Watts for surface activation and further cleaning. All films were spin cast at 2500 rpm for 40 sec. The films were then baked at 140°C for 1 hour. The thickness of PEDOT:PSS films was determined using a Dektak mechanical profilometer.

Electrical and Electrochemical Characterization: We measured the sheet resistance (R_s in $\Omega.\text{sq}^{-1}$) of PEDOT:PSS/ GOPS films cast on glass substrates using a four-point probe (Jandel RM3-AR). Given the film thickness (d), we could calculate the resistivity ($\rho = R_s \times d$, where ρ is resistivity in $\Omega.\text{cm}$) from which the conductivity ($1/\rho$ in $\text{S}.\text{cm}^{-1}$) was obtained. Electrochemical impedance spectroscopy (EIS) was performed in NaCl solution (0.1M) via an impedance spectrometer (potentiostat/galvanostat, Metrohm Autolab B.V.) with a three-electrode configuration, where the polymer-coated substrate is the working electrode, a Pt mesh is the counter electrode, and Ag/AgCl is used as a standard reference electrode. EIS was performed over a range of 10 kHz to 1Hz with an AC 10 mV sine wave, and a DC offset of 0 V. In order to extract capacitance (C), and the resistance, R , the spectra of films were fit to an (RC) equivalent circuit using NOVA software.

OECT fabrication and characterization: OECTs were fabricated using photolithography, as previously described ^[34]. Briefly, 150 nm thick gold lines were patterned on a glass slide with S1813 photoresist, exposed to UV light using a SUSS MBJ4 contact aligner, and developed using MF-26 developer. Upon the deposition, a standard metal lift-off process in acetone was employed and gold interconnects and pads were insulated from the electrolyte by a 1.5 μm parylene C film deposited using a SCS Labcoater 2. A second sacrificial layer of parylene C was coated, patterned with AZ9260 photoresist, developed, and selectively etched by an

CF6/O₂ plasma using an Oxford 80 plus to define the transistor channel. Finally, PEDOT:PSS dispersion was cast and the sacrificial layer of parylene C was peeled, and the devices were baked at 110 °C for 1 hour.

The PEDOT:PSS channel had a width/length (W/L) of 50 μm/50 μm. The transistors were operated in the common source configuration with a Ag/AgCl pellet electrode (Warner Instruments) immersed in NaCl solution (0.1M). The characterization was performed using a National Instruments PXIe-1062Q system. The gate bias was applied and controlled using a NI PXI-6289 modular instrument, and current recorded with either the NI PXI-4145 SMU or a NI PXI-4071 digital multimeter. The recorded signals were saved and analyzed using customized LabVIEW and MATLAB software. Hole mobilities were extracted using impedance matching method reported for OECTs^[21].

Swelling Measurements: The swelling of the thin polymer films was investigated by quartz crystal microbalance with dissipation set-up (QCM-D) (Q-Sense, from Biolin Scientific). PEDOT:PSS dispersions at a given GOPS concentration were spun-cast on cleaned gold-coated Q-sensors. They were then kept under vacuum overnight to ensure complete drying of the film. Filtered DI water or aqueous NaCl solution (0.1 M) were flown over the samples at 24 °C at a flow rate of 50 - 100 μL.min⁻¹ controlled by a peristaltic pump. The adsorbed mass (Δm) can be approximately estimated from Δf using the Sauerbrey equation:

$$\Delta m = -C \frac{\Delta f_n}{n} \quad (2)$$

where C is the mass sensitivity constant (17.7 ng.cm⁻² Hz at $f = 5$ MHz) and Δf_n is the change in resonance frequency at n th overtone^[35]. We used the 5th overtone for our calculations. Given the initial thickness of the films, we could estimate the water uptake. Kelvin-Voigt viscoelastic model was also used (equations 3, 4, and 5) where G^* is the

complex shear modulus, ρ is the density (kg m^{-3}), η is the viscosity (G''/ω) (kg ms^{-1}), μ is the elasticity (G') (Pa), and δ is the thickness (m)^[36].

$$G^* = G' + jG'' = \mu + j2\pi f \eta \quad (3)$$

$$\Delta f = f_1 (n, h_f, \rho_f, \mu_f, \delta_f) \quad (4)$$

$$\Delta D = f_2 (n, h_f, \rho_f, \mu_f, \delta_f) \quad (5)$$

Mechanical Characterization: Young's modulus was obtained from the force-curve measurements that were realized by using an NTEGRA AFM system (from NT-MDT). In all experiments AFM tips (NSC35 from Mikromash) were used with typical resonant frequency of 150 kHz, spring constants ranging from 5 to 12 N.m^{-1} and apex radius of 8 nm as verified by scanning electronic microscopy. For each tip, the spring constant was determined using the thermal noise method after obtaining the deflection sensitivity of the cantilever by pressing the AFM tip against a hard reference silicon surface. The measurements were all performed in water after allowing the samples to hydrate for 2 hours.

References

- [1] Karunakaran, C., Bhargava, K. and Benjamin, R., *Biosensors and bioelectronics*, Elsevier, 2015, Ch 1.
- [2] P. Lin, C.-W. Lin, R. Mansour, F. Gu, *Biosens. Bioelectron.* 2013, *47*, 451.
- [3] G. G. Malliaras, *Biochim. Biophys. Acta BBA - Gen. Subj.* 2013, *1830*, 4286.
- [4] S. Löffler, B. Libberton, A. Richter-Dahlfors, *Electronics* 2015, *4*, 879.
- [5] M. Berggren, A. Richter-Dahlfors, *Adv. Mater.* 2007, *19*, 3201.
- [6] J. Rivnay, R. M. Owens, G. G. Malliaras, *Chem. Mater.* 2014, *26*, 679.
- [7] D. T. Simon, E. O. Gabrielsson, K. Tybrandt, M. Berggren, *Chem. Rev.* 2016, *10.1021*.
- [8] C. Liao, M. Zhang, M. Y. Yao, T. Hua, L. Li, F. Yan, *Adv. Mater.* 2015, *27*, 7493.
- [9] N. K. Guimard, N. Gomez, C. E. Schmidt, *Progr. Polym. Sci.* 2007, *32*, 876.
- [10] E. Stavrinidou, O. Winther-Jensen, B. S. Shekibi, V. Armel, J. Rivnay, E. Ismailova, S. Sanaur, G. G. Malliaras and B. Winther-Jensen, *Phys. Chem. Chem. Phys.*, 2014, *16*, 2275-2279.
- [11] J. Rivnay, S. Inal, B. A. Collins, M. Sessolo, E. Stavrinidou, X. Strakosas, C. Tassone, D. M. DeLongchamp, G. G. Malliaras, *Nat. Commun.* 2016, *7*, 11287.
- [12] D.C. Martin and G. G. Malliaras, *ChemElectroChem*, 2016, *3*, 686.
- [13] A. R. Hopkins, J. R. Reynolds, *Macromolecules* 2000, *33*, 5221.
- [14] C. Chen, A. Kine, R. D. Nelson, J. C. LaRue, *Synth. Met.* 2015, *206*, 106.
- [15] N. Liu, G. Fang, J. Wan, H. Zhou, H. Long, X. Zhao, *J. Mater. Chem.* 2011, *21*, 18962.
- [16] C. Chen, J. C. LaRue, R. D. Nelson, L. Kulinsky, M. J. Madou, *J. Appl. Polym. Sci.* 2012, *125*, 3134.
- [17] D. Khodagholy, J. N. Gelinas, T. Thesen, W. Doyle, O. Devinsky, G. G. Malliaras, G. Buzsáki, *Nat. Neurosci.* 2015, *18*, 310.
- [18] D. Khodagholy, T. Doublet, M. Gurfinkel, P. Quilichini, E. Ismailova, P. Leleux, T. Herve, S. Sanaur, C. Bernard, G. G. Malliaras, *Adv. Mater.* 2011, *23*, H268.
- [19] E. Stavrinidou, P. Leleux, H. Rajaona, D. Khodagholy, J. Rivnay, M. Lindau, S. Sanaur, G. G. Malliaras, *Adv. Mater.* 2013, *25*, 4488.
- [20] J. Rivnay, P. Leleux, A. Hama, M. Ramuz, M. Huerta, G. G. Malliaras, R. M. Owens, *Sci. Rep.* 2015, *5*, 11613.
- [21] J. Rivnay, M. Ramuz, P. Leleux, A. Hama, M. Huerta, R. M. Owens, *Appl. Phys. Lett.* 2015, *106*, 043301.

- [22] D. Khodagholy, T. Doublet, P. Quilichini, M. Gurfinkel, P. Leleux, A. Ghestem, E. Ismailova, T. Hervé, S. Sanaur, C. Bernard, G. G. Malliaras, *Nat. Commun.* 2013, 4, 1575.
- [23] A. Williamson, J. Rivnay, L. Kergoat, A. Jonsson, S. Inal, I. Uguz, M. Ferro, A. Ivanov, T. A. Sjöström, D. T. Simon, M. Berggren, G. G. Malliaras, C. Bernard, *Adv. Mater.* 2015, 27, 3138.
- [24] A. Williamson, M. Ferro, P. Leleux, E. Ismailova, A. Kaszas, T. Doublet, P. Quilichini, J. Rivnay, B. Rózsa, G. Katona, C. Bernard, G. G. Malliaras, *Adv. Mater.* 2015, 27, 4405.
- [25] A. K. Y. Wong, U. J. Krull, *Anal. Bioanal. Chem.* 2005, 383, 187.
- [26] U. Maskos, E. M. Southern, *Nucleic Acids Res.* 1992, 20, 1679.
- [27] S. Zhang, P. Kumar, A. S. Nouas, L. Fontaine, H. Tang, F. Cicoira, *APL Mater.* 2015, 3, 014911.
- [28] C. Duc, A. Vlandas, G. G. Malliaras, V. Senez, *Soft Matter* 2016, 12, 5146-5153.
- [29] I. N. Sneddon, *Int. J. Eng. Sci.* 1965, 3, 47.
- [30] H. Okuzaki, M. Ishihara, *Macromol. Rapid Commun.* 2003, 24, 261.
- [31] U. Lang, N. Naujoks, *J. Dual, Synth. Met.* 2009, 159, 473.
- [32] J. Qu, L. Ouyang, C. Kuo, D. C. Martin, *Acta Biomater.* 2016, 31, 114.
- [33] T. D. Y Kozai, K. Catt, Z. Du, K. Na, O. Srivannavit, R. M. Haque, J. Seymour, K. D Wise, E. Yoon, X. T. Cui, *IEEE Trans Biomed Eng.*, 2016, 63, 111.
- [34] S. Inal, J. Rivnay, P. Leleux, M. Ferro, M. Ramuz, J. C. Brendel, M. M. Schmidt, M. Thelakkat, G. G. Malliaras, *Adv. Mater.* 2014, 26, 7450.
- [35] R. Schumacher, G. Borges, K. K. Kanazawa, *Surf. Sci.* 1985, 163, L621.
- [36] M.V. Voinova, M. Rodahl, M. Jonson, B. Kasemo, *Phys. Scr.* 1991, 59, 391.

Supporting Information

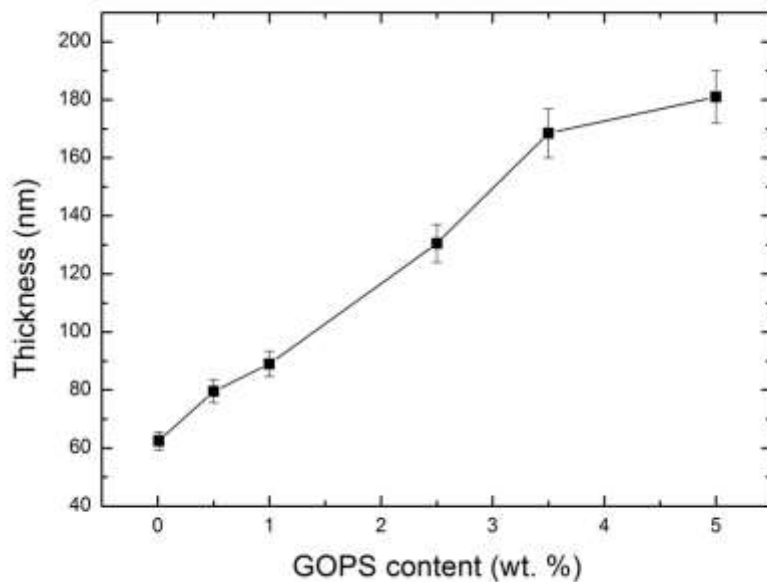
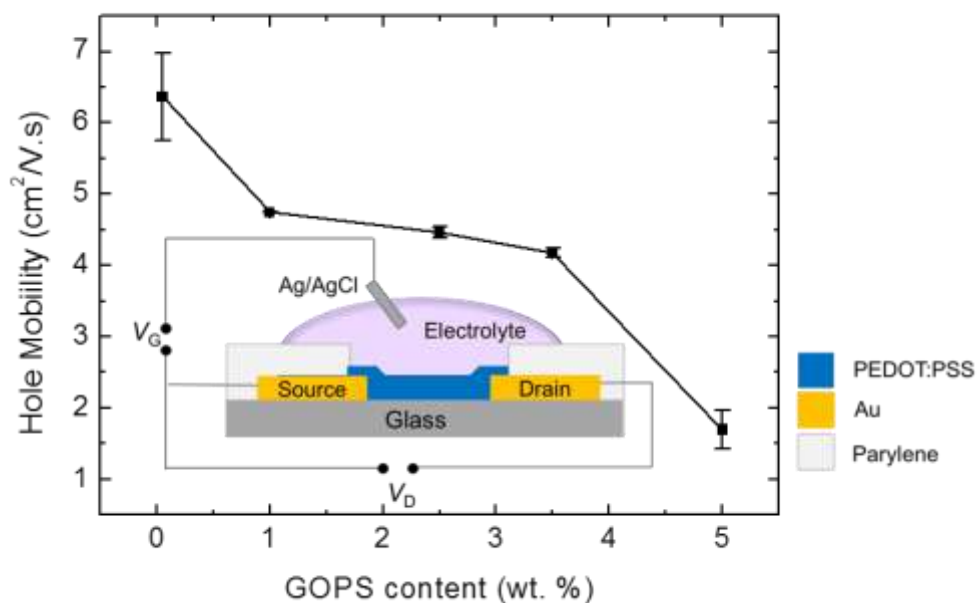


Figure S1. Thickness of PEDOT:PSS films at a given spin-coating conditions (2500 rpm, 40 s) as a function of GOPS concentration in the dispersion. The error bars stand for standard deviation estimated from 3 measurements.

a)



b)

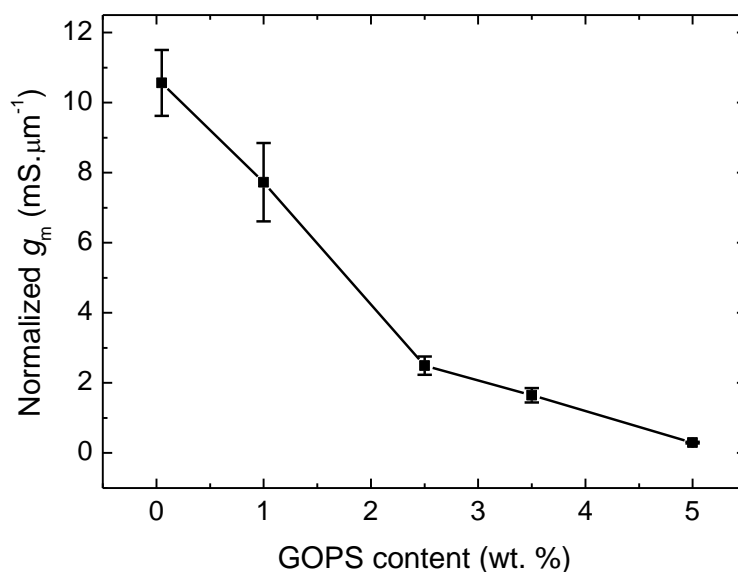


Figure S2. a) Hole mobility of PEDOT:PSS films, extracted from working OECTs, as a function of GOPS concentration in the PEDOT:PSS dispersion. The channel dimensions were 50*50 μm . Also shown is a schematic of the OECT. Cations of the electrolyte enter the channel between two gold source and drain electrodes upon application of a positive gate voltage (V_G) through Ag/AgCl. This leads to a change in drain current measured at a specific drain voltage (V_D). b) The transconductance ($(g_m = \frac{\partial I_D}{\partial V_G})$) of OECTs comprising PEDOT:PSS channels of varying GOPS concentration. The transconductance (at $V_G = 0$ V) was normalized with respect to film thickness in the channel. The error bars are deduced from measurements of two identical channels (50*50 μm in length*width).

Table S1. Swelling ratios of PEDOT:PSS films in DI water and in NaCl solution (0.1 M) with varying GOPS content (using Sauerbrey and Kelvin-Voigt models). Standard deviation is calculated according to the swelling capacity estimated via different models.

GOPS (wt %)	Swelling using Sauerbrey model (%)		Swelling using Voigt model (%)		Standard deviation		Time to stabilize (min)
	DI	NaCl	DI	NaCl	DI	NaCl	
0.05	283	397	364	480	58	57	66
1.0	266	386	387	497	78	86	103
2.5	113	136	224	248	79	78	61
3.5	10	17	128	130	80	83	38
5.0	2	12	127	138	89	88	31

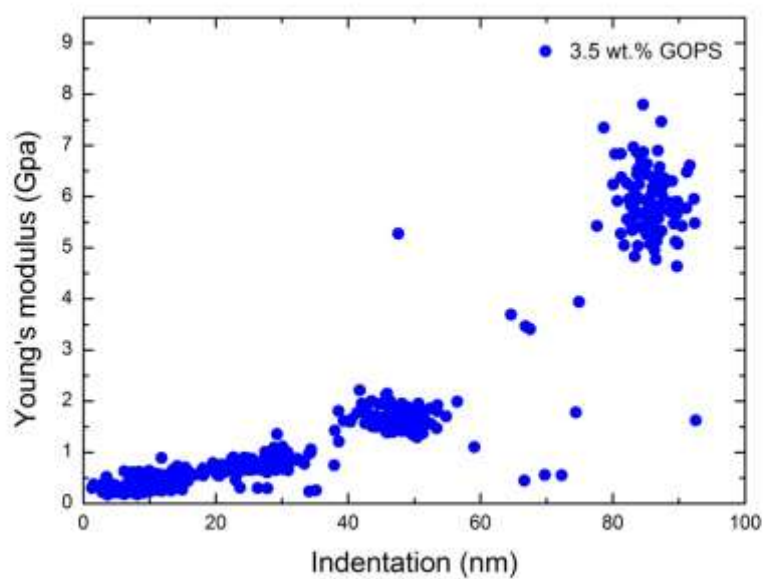
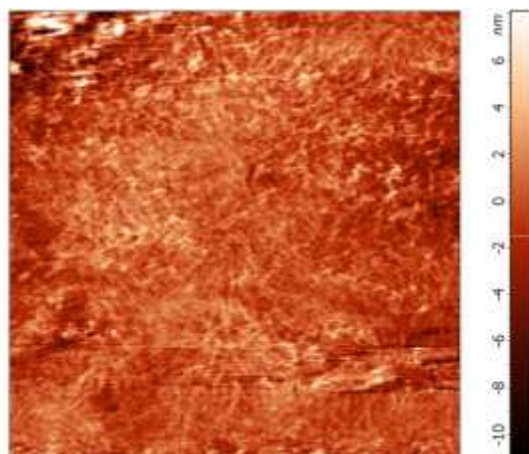


Figure S3. Young's modulus diverging with the indentation depth of a PEDOT:PSS film with 3.5 wt% of GOPS in the formulation. The values stabilize at indentation depth < 20 nm, which is consistent for the samples cast from dispersions with different GOPS concentrations.

a)



b)

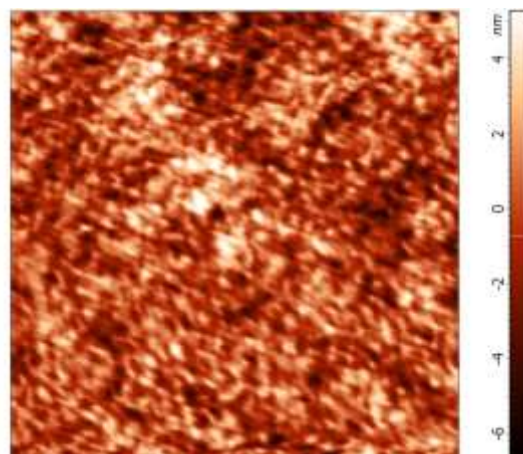


Figure S4. AFM topographical images of PEDOT:PSS/GOPS thin films comprising a) 0.05 wt. % GOPS b) 3.5 wt. % GOPS.

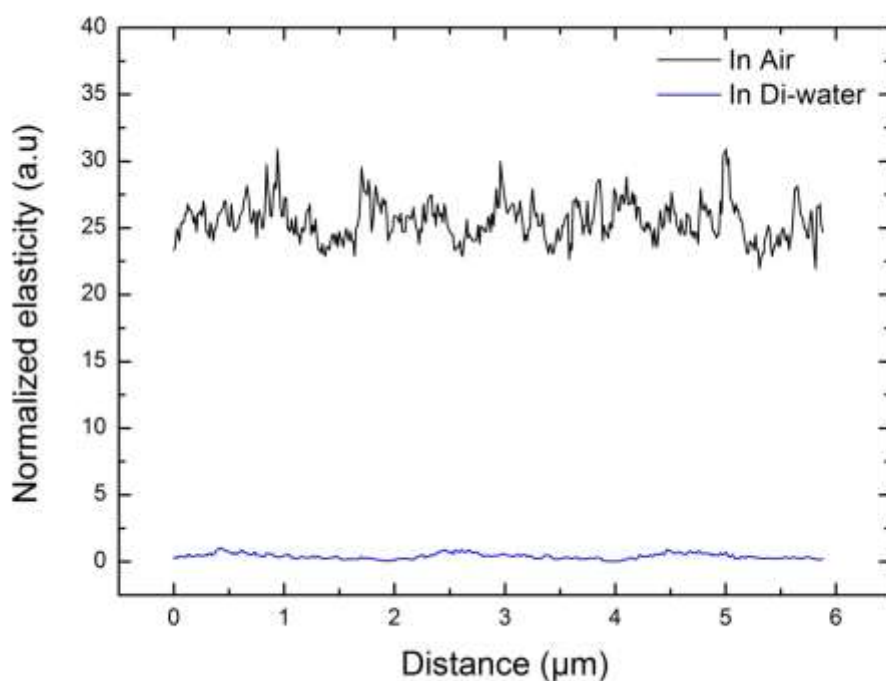


Figure S5. Mechanical elasticity of PEDOT:PSS (5 wt% GOPS) in air (black) and in DI water (blue) using AFM peak force tapping mode using Derjaguin– Muller–Toporov (DMT) model.

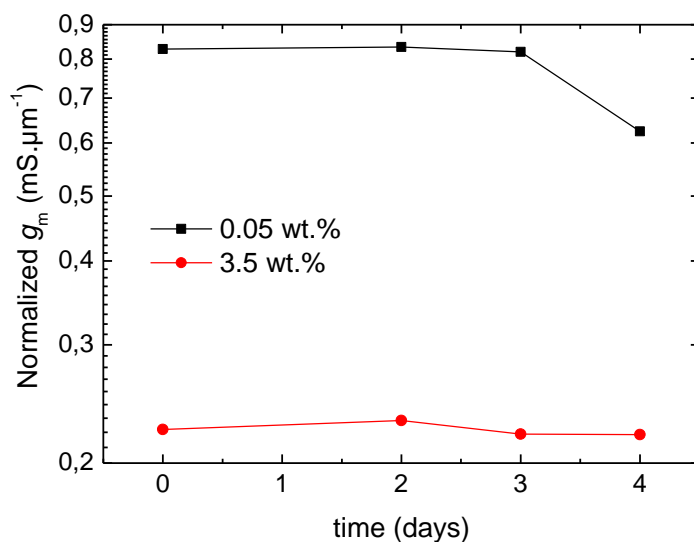


Figure S6. The transconductance (g_m) of OECTs with channels cast from either a low (0.05 wt.% , squares) or a high (3.5 wt.% , circles) GOPS content PEDOT:PSS formulation, measured over 4 days in NaCl solution (0.1 M). The devices had a width and length of 50 μm. The transconductance was measured at $V_G = 0V$ and normalized with the thickness of the film in the channel. These devices were cycled multiple times over 10 months.

Chapter 3

Facile Nano-Patterning of PEDOT:PSS Thin Films

3.1 Introduction

Conducting polymers (CPs) are widely used in the field of optoelectronics and bioelectronics for a wide range of applications.^[1,2] PEDOT:PSS is considered as the prototypical material for conducting polymers due to its processing adaptability, tunability, biocompatibility, and commercial availability as well as its outstanding electrical and mechanical properties. PEDOT:PSS has been used in organic electronic devices such as photovoltaic devices and light emitting diodes as a hole injection/collection anode thanks to its transparency and high work function.^[3-5] In comparison with inorganic oxide anodes, PEDOT:PSS shows a more stable work function, hence more reliable characteristics.^[6] PEDOT:PSS can be used as a charge injection bi-layer on indium tin oxide ITO electrode, or by its own as an anode. However when PEDOT:PSS is used as anode, enhancing its conductivity becomes critical. PEDOT:PSS has also been used widely in biomedical devices due to its soft nature that provides a better contact with biology.^[7-9] For instance, it is critical for the electrodes used in bio-sensing, and electrophysiological recording or stimulation, whether in *in-vitro* or *in-vivo* systems, to have low impedance contacts to allow high signal to noise ratio (SNR) recording, or improved transduction. By coating the metallic electrodes with thin film CPs such as PEDOT:PSS, their electrochemical impedance decreases dramatically, which is demonstrated to be in the range of 2 orders of magnitude (in the low frequency range).^[10-12] The mixed ionic and electronic conductivity of PEDOT:PSS causes this dramatic drop in impedance. The

PSS allows the PEDOT:PSS film to swell the liquid electrolyte which permits ionic diffusion, while the PEDOT particles allow higher chances for electronic/ionic charge exchange.^[13]

Nano-patterned PEDOT:PSS was reported a few times to be used in organic photovoltaic applications as a hole transport layer and to improve light-scattering and absorption, and in organic light emitting diodes (OLED) applications to improve light extraction and control the spectral tunability.^[14] Kwon et al. reported using patterned PEDOT as a counter electrode in a solar cell setup.^[15] They obtained the patterned electrode simply by spin-coating PEDOT oligomer solution on a nano-patterned (nano-holes) polystyrene (PS) layer, followed by thermal polymerization step. In this method the PEDOT followed the nano-patterns on the PS substrate. As a result, they have found a higher current density and lower charge transfer resistance, compared to the flat PEDOT, due to the increased surface area. Petti et al. have used a high resolution electron beam lithography to pattern PEDOT:PSS for organic optoelectronic applications.^[16] In this approach they patterned a resist layer (styrene methyl acrylate based polymer) spin-coated over PEDOT:PSS thin film, and after developing the resist, they etch through using plasma etching to transfer the patterns to the PEDOT:PSS layer. Finally they remove resist by a strong solvent (NMP; N-methyl-2-pyrrolidone) to obtain the nano-patterned PEDOT:PSS film. Using this method they created a high density PEDOT:PSS photonic crystal. Direct nano-patterning of PEDOT:PSS is another approach to increase the effective surface area of an electrode without having to increase the electrode size or to use a patterned substrate. Choi et al. have used a polyurethane acrylate (PUA) mold to pattern PEDOT:PSS film to use it in solar cells applications as a hole transport layer.^[14] They applied the mold on a spin-coated layer of PEDOT:PSS with pressure to obtain maximum replication at the room temperature, then followed this by a heating step before demolding before demolding to obtain the nano-patterned PEDOT:PSS. This method can be described as soft thermal-nanoimprint lithography (soft T-NIL). Yang et al. adapted a similar approach by using a silicon (Si) master mold directly as a stamp to nano-pattern PEDOT:PSS by applying

pressure and heat, a method that is called T-NIL.^[17] They used the nano-patterned PEDOT:PSS film as a hole transport and electron blocking layer in organic photovoltaic devices. Emah et al. have patterned PEDOT:PSS film by placing PDMS stamp on it top with applying temperature and without any pressure, except for the pressure introduced by the weight of the stamp, then after baking, they demold the stamp to obtain the nano-patterned PEDOT:PSS.^[18] The disadvantage of this method is the low replication yield (PDMS feature depth = 27 nm, and imprinted PEDOT:PSS feature depth = 10 nm). This method can be called capillary force lithography (CFL).^[19]

For reducing the electrochemical impedance of an electrode at a given size for biomedical application, Sanetra et al. have used a nano-patterned (nano-pillars) gold electrode and covered it with a thin film of PEDOT:PSS in order to follow the surface roughness.^[20] This structuring has led to an increase in the surface area of the PEDOT:PSS film. In effect, they have reported a reduction in the impedance of these films compared to the PEDOT:PSS films that are spin-coated on a planar gold electrode. Abidian et al. have demonstrated the use of nano-structured (nano-tubes) PEDOT electrochemically polymerized on the surface of neural micro-electrodes. They have found a dramatic decrease (by 2 orders of magnitude) in the electrochemical impedance. This reduction is due to the increased surface area introduced by using the nanotubes. These studies suggest an impact of the effective surface area of nano-patterned or nano-structured conducting polymers on the ion diffusion and the impedance of coated electrodes.^[21]

In this work we present a facile fabrication technique for nano-patterning PEDOT:PSS thin films over large areas. This technique includes using a UV-curable epoxy as a supporting layer for lifting off the patterned polymer layer and/or gold layer from a nano-pattered mold and sticking it to a substrate; whether it's rigid such as glass or flexible such as polyimide films (kapton). We have also investigated the electrochemical impedance of the obtained nano-patterned films with different dimensions and compared it to the impedance obtained

from a flat PEDOT:PSS film keeping the same electrode size. The results showed a decrease in the impedance when patterning the film surface due to increasing the effective surface area. These results pave the way for incorporating nano-patterned conducting polymers in biomedical devices for better recordings or for higher spatial resolution while keeping the impedance low.

3.2 Results and Discussion

The fabrication scheme of nano-patterning PEDOT:PSS and PEDOT:PSS/Au is shown in **Figure 1**. This technique starts with making a PDMS replica of a Si master mold. For replicating features less than a 100 nm, a double-layer PDMS was used (hard-PDMS/PDMS).^[22] Figure 1 (b-e) demonstrates the transfer of the nano-patterns from the PDMS replica to a PEDOT:PSS thin film and how to stick it to a polyimide substrate by using a UV-curable epoxy layer. This strategy includes spin coating PEDOT:PSS solution and epoxy respectively on the nano-patterned PDMS replica. And by using a supporting substrate (kapton) it was possible to demold the two layers stack from PDMS after curing the epoxy layer by UV light. The epoxy layer plays a double-role. First, it acts as a sticking layer between the PEDOT:PSS layer and the applied substrate. Second, when demolding, the epoxy layer peels off the PEDOT:PSS from the PDMS replica. This later is due to the affinity of PEDOT:PSS to the layer with higher surface energy knowing that the PDMS has inherently a low surface energy. The GOPS content (which has the epoxy group) in the PEDOT:PSS mixture can be also helping adhering to the epoxy layer stronger. Interestingly, gold can be incorporated in this fabrication method as an interlayer between the PEDOT:PSS and epoxy layers (figure 1 (c'-f')). In this case the epoxy layer peels the PEDOT:PSS/Au off the PDMS replica thanks to the strong adhesion between epoxy and gold, and between gold and PEDOT:PSS, and the weak adhesion between the PEDOT:PSS and PDMS as mentioned. After demolding, the final electrode structure using this fabrication strategy is a stack of nano-

patterned PEDOT:PSS on Au/epoxy/kapton. This strategy makes it possible to fabricate highly conducting nano-patterned electrodes that can be used in several biomedical applications as discussed in the introduction section. The fabrication steps are described in details in the experimental section.

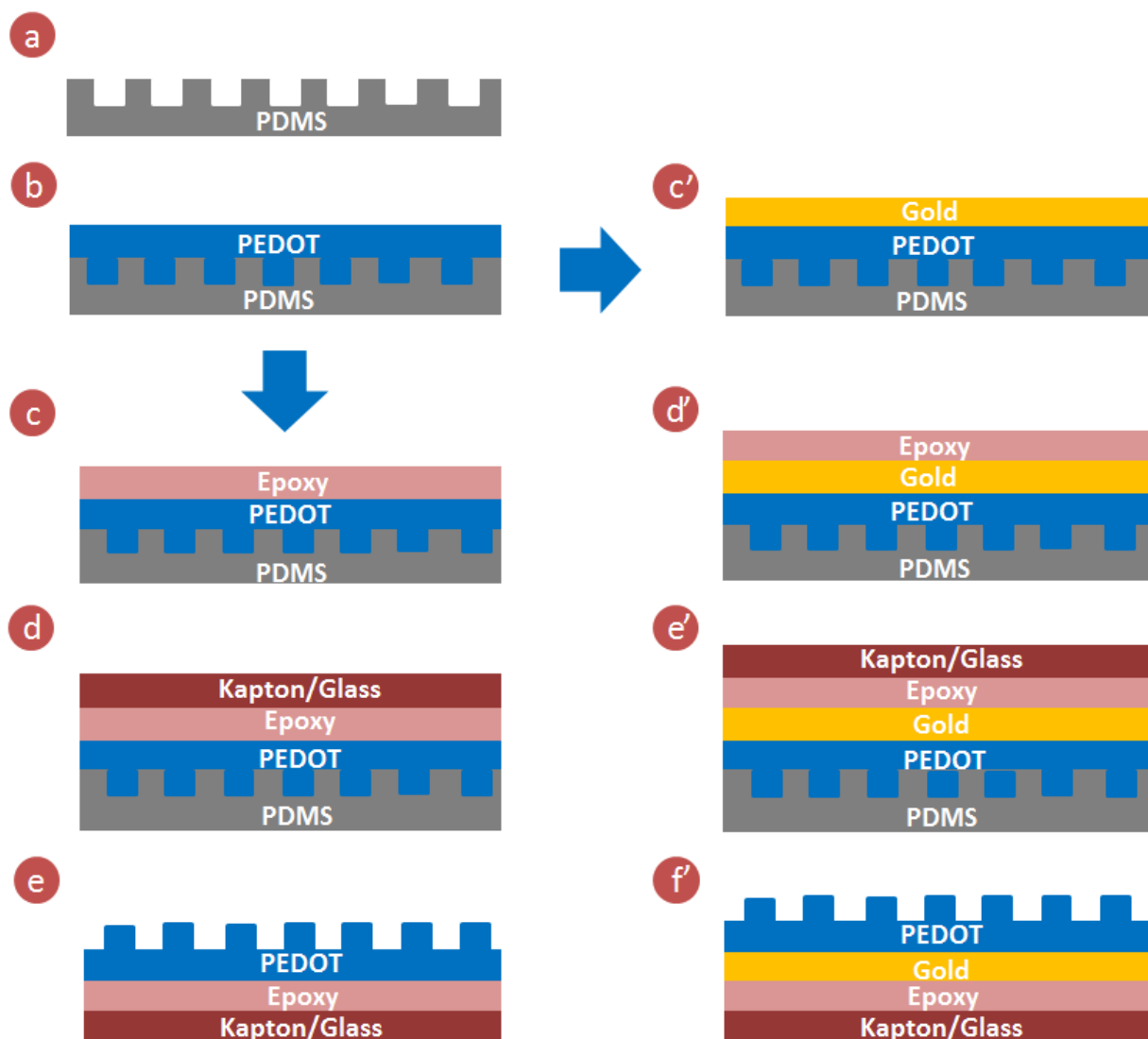


Figure 1. Schematic of the fabrication process of nano-patterned PEDOT:PSS (a) PDMS replica of the nano-patterned Si master mold. (b) Spin-coating and baking PEDOT:PSS thin film. (c') Evaporating a thin layer of gold. (c) & (d') Spin-coating a layer of epoxy. (d) & (e') Placing the substrate and exposing to UV-light. (e) & (f') Demolding the layers from the PDMS.

Alternatively and in the same fashion, a nano-patterned Au layer can be obtained as shown in the fabrication scheme in **Figure S1**. In this strategy a thin layer of gold is directly evaporated on a nano-patterned PDMS replica. Then an epoxy layer is spin-coated on the gold and sandwiched between the Au layer and the carrier substrate. Because of the strong surface

affinity of the gold layer towards the epoxy vs the gold to the PDMS layer, it is possible to nicely peel off the gold layer from the PDMS. The obtained nano-patterned gold electrode can be then electrochemically coated by PEDOT:PSS as shown in **figure S2**. This method makes it easy to nano-pattern gold instead of using photo-lithography or electron beam lithography, and it can save money, time and effort as one PDMS replica can make as many electrodes as needed. More details on this fabrication strategy are mentioned in the experimental section.

For the rest of this article we will be only discussing the results obtained from the fabrication approach demonstrated in figure 1 as it is the focus of this study as discussed in the introduction section. **Figure 2** shows images of the electrodes obtained using our fabrication technique (described in figure 1). Figure 2 (a) shows the nano-patterned PEDOT:PSS/epoxy electrodes after demolding on kapton, and the PDMS replica covered with PEDOT:PSS except where the kapton was applied. The carrier substrate can be flexible as shown in figure 2 (b-c) (kapton; 125 μm and 25 μm in thickness) without causing damages to the gold or nano-patterned PEDOT:PSS layers when folded. The epoxy layer can be obtained very thin by spin-coating at high speeds which facilitates the folding of the electrode. Figure 2 (d-f) shows the nano-patterned PEDOT:PSS/Au electrodes after demolding. We have also tried glass substrates and they worked as efficient as the kapton (Figure S3). Different shapes and electrode sizes can be applied as carrier substrates. In our study the smallest electrode size we tried was 1x1 mm due to limitations having a clean laser cut on the kapton film.

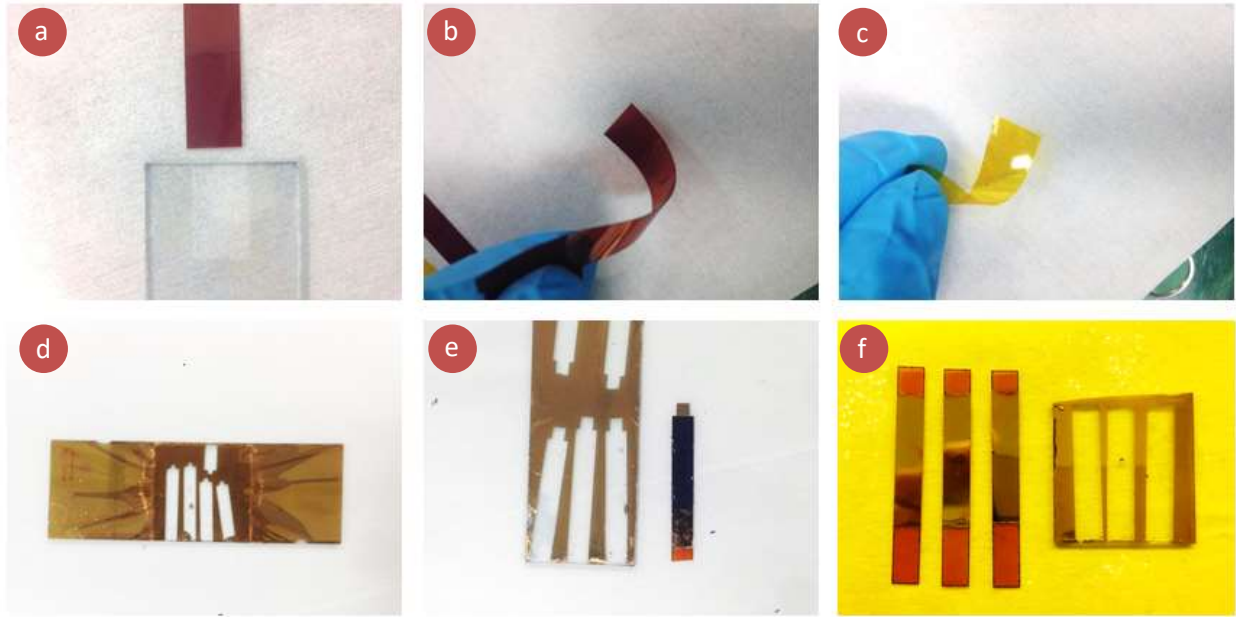


Figure 2. Macroscopic images of the nano-patterned PEDOT:PSS electrodes (a-c) Nano-patterned PEDOT:PSS film transferred from PDMS replica to polyimide films (thickness; 125 μm , and 50 μm). (d-f) Nano-patterned PEDOT:PSS/Au films transferred from PDMS replica to polyimide films of different surface areas of interest; 1x1 mm, 5x5 mm, and 7x25 mm respectively from (d) to (f).

Figure 3 shows scanning electron microscopy (SEM) images of the PDMS replica and PEDOT:PSS films obtained using our epoxy-supported nano-patterning technique. The images include different dimensions of the nano-patterns (based on Si master mold with dimensions; 70 nm, 140 nm, and 250 nm linewidth, 140 nm, 280 nm, 455nm period respectively). These images prove the transfer of nano-patterns on the PEDOT:PSS/Au electrodes and validate the fabrication technique. **Figure 4** shows atomic force microscopy (AFM) images of the PDMS replica (a-c) of the smallest feature size Si master mold (70 nm linewidth and 50 nm depth), and the patterned PEDOT:PSS (d-f). The PDMS replica features measured 87 nm line width 42 nm depth, while the PEDOT:PSS features were 87 nm width and 30 nm depth. The increase in the feature size of the PDMS and PEDOT:PSS can be due to swelling in humid environment.^[23]

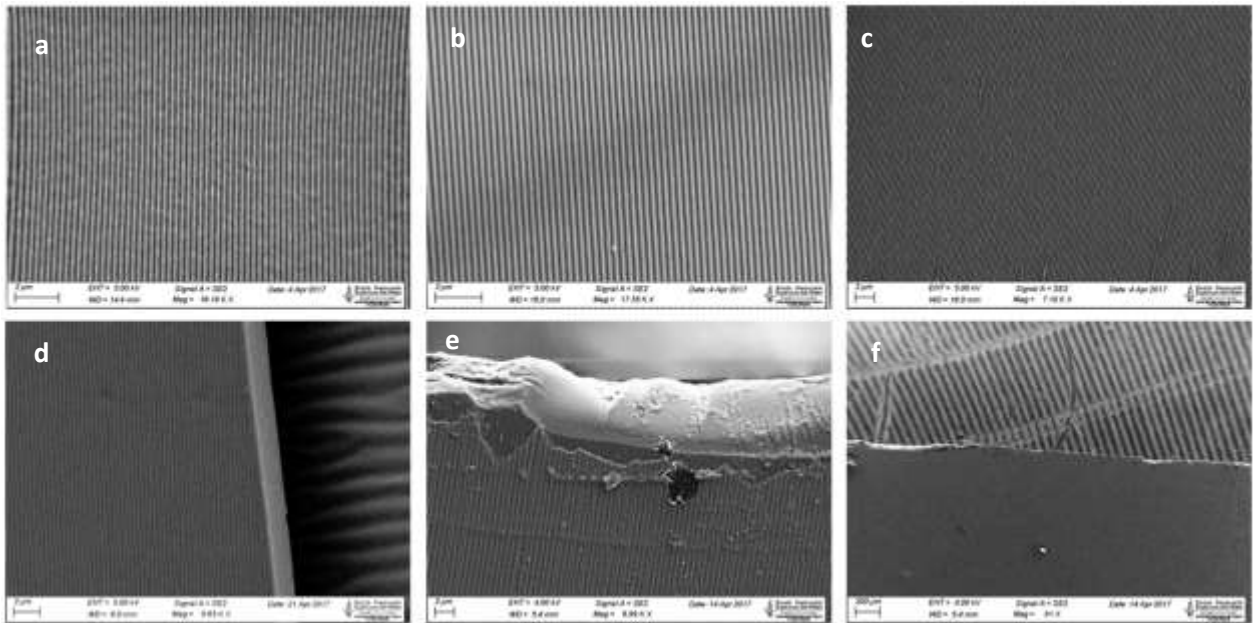


Figure 3. SEM images. (a) PDMS replica (~ 455 nm pitch, 165 nm groove depth, and ~ 250 nm linewidth). (b-f) PEDOT:PSS top layer after demolding. (b) & (c) Same dimensions as (a). (d) Based on Si mold; 140 nm period, and 70 nm linewidth. (e) Based on Si mold; 280 nm period, and 140 nm linewidth. (f) Flat film.

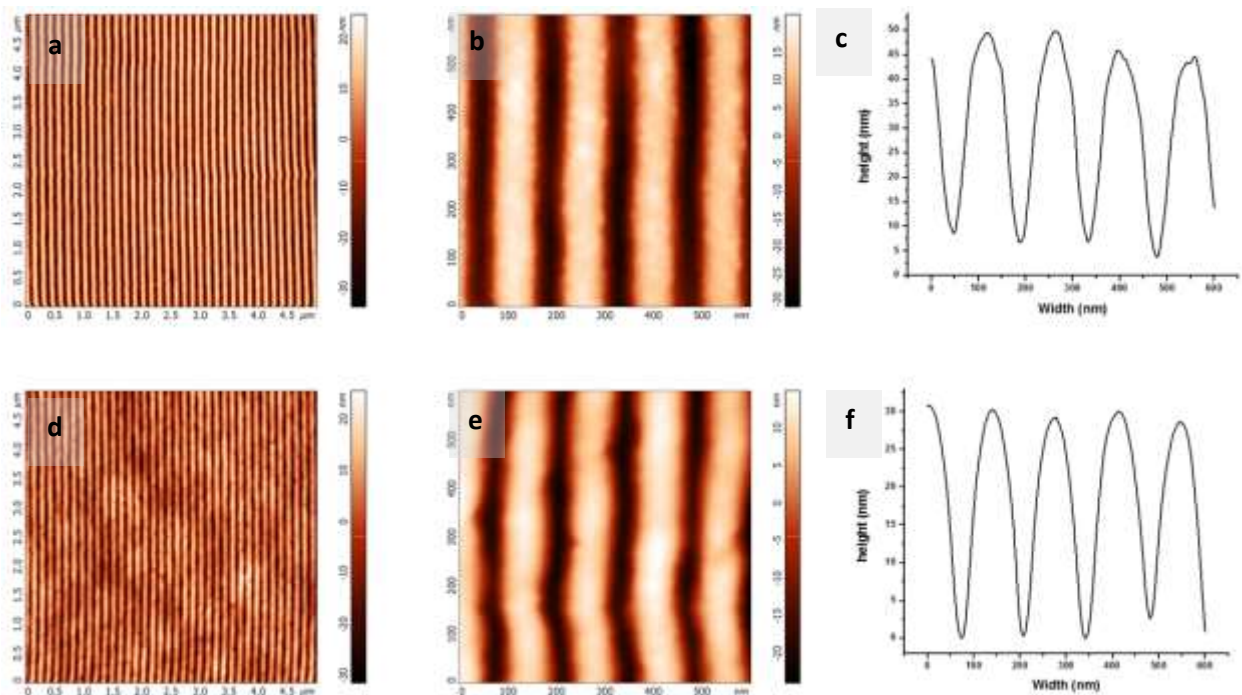


Figure 4. AFM images. (a) & (b) Nano-patterned PDMS replica. (d) & (e) Nano-patterned PEDOT:PSS. (c) Profile of (b); 42 nm height, and 87 nm linewidth. (f) profile of (e); 30 nm height, and 87 nm linewidth.

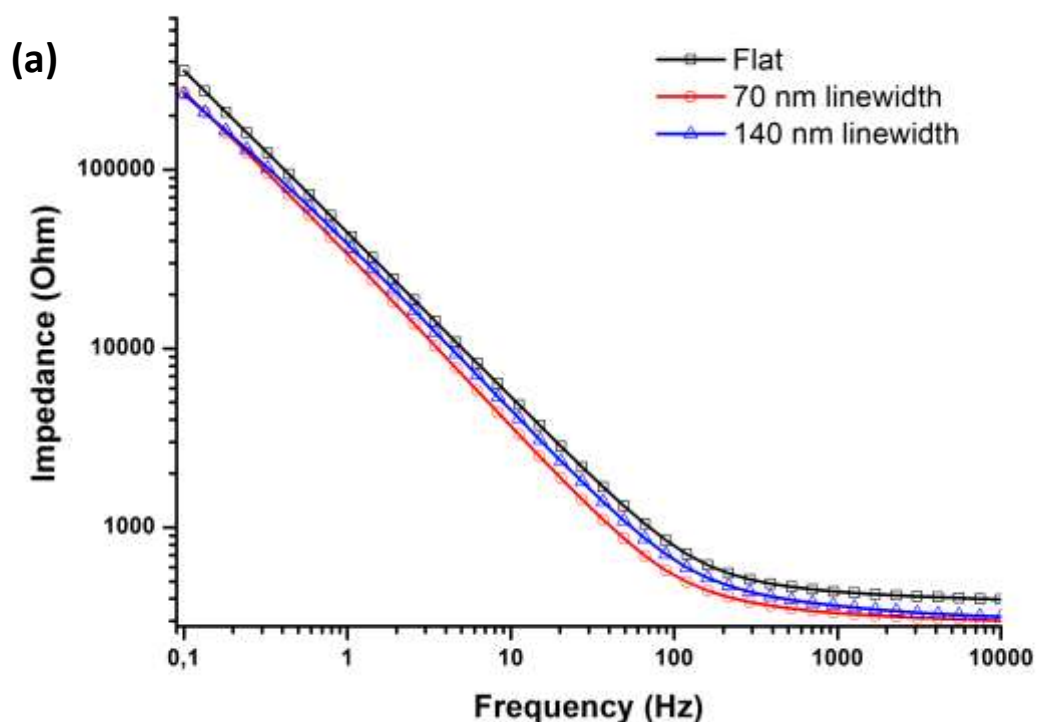
In our fabrication method the PEDOT:PSS solution is spin-coated directly on the PDMS replica (figure 1 (b)). And compared to CFL and T-NIL, the layers (PEDOT:PSS, and stamp) order is inverted which is a great advantage for several reasons. First, it allows the

PEDOT:PSS solution to fully fill in the nano-patterns for a higher replication yield. Second, and in comparison with T-NIL, it doesn't require applying pressure; hence no machines are needed to regulate the pressure. Third, it overcomes the problem of gas pressure (due to evaporation) introduced in the nano-features when placing a stamp on a PEDOT:PSS film and start heating, which is the case in T-NIL and CFL. Fourth, it overcomes the minor problem of gravity that counters the lifting forces that elevate the solution in the nano-features using T-NIL and CFL.

The fabrication strategy we presented using the epoxy supporting layer can be also applied in micro-patterning based on a PDMS mold patterned by the standard lithographic methods. Some materials such as PEDOT:PSS and other organic materials are difficult to pattern directly using the optical lithography because of their incompatibility with most of the developing and lifting solvents. Our fabrication technique opens the way for patterning such materials with convenience. Other advantages of our fabrication strategy include the easy processing, reliability, and reproducibility, as well as the ability to pattern electrodes with a large area. The obtained nano-patterned PEDOT:PSS and PEDOT:PSS/Au electrodes were tested for stability in aqueous media by soaking the electrodes for 48 hours in DI water, and by sonicating for 2 hours. No delamination or damages were observed on the nano-patterned PEDOT:PSS films, which makes the electrodes reliable enough for electrochemical measurements.

Figure 5 (a) shows the electrochemical impedance (Z) bode plot ($\log Z$ vs \log frequency) of the nano-patterned PEDOT:PSS/Au electrodes (circular shape; 87 nm linewidth, and 30 nm depth, and triangular shape; 157 nm linewidth, and 26 nm depth) vs a flat PEDOT:PSS/Au electrode (rectangular shapes) of the same surface area (1 x 1 mm) using electrochemical impedance spectroscopy. The details of the measurements setup is mentioned in the experimental section. The impedance of the nano-patterned PEDOT:PSS/Au electrodes was found to be lower than the impedance of the flat PEDOT:PSS/Au electrodes. And by fitting

the data with an RC circuit model (**Figure S4**), we are able to extract the film capacitance (C) and the solution resistance (R_s). Koutsouras et al. have shown that the electrode/electrolyte interface of PEDOT:PSS films is dominated by R_s and C .^[11] They have systematically studied the effect of increasing the surface area of planar PEDOT:PSS-coated gold electrodes on the electrochemical impedance.^[11] They have found that the impedance scales with $A^{-1/2}$ at the high frequency range and with A^{-1} at the low frequency range. For our electrodes, we have fixed the electrode size and the volume of the PEDOT:PSS layer, while only changing the effective surface area which takes in account the extra area introduced by the nano-features.



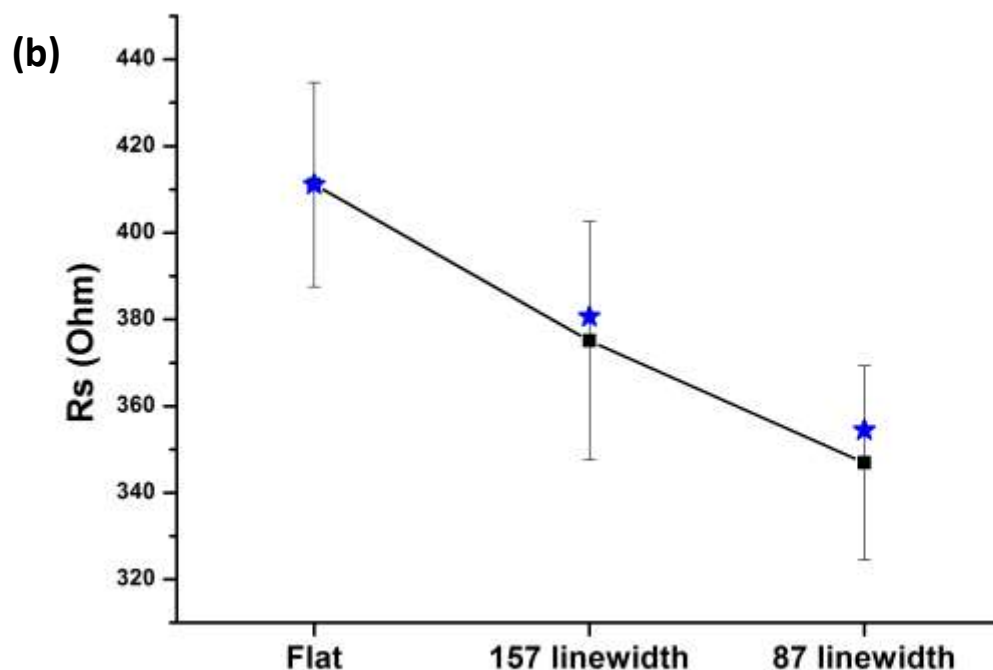


Figure 5. (a) The electrochemical impedance of the nano-pattered PEDOT:PSS compared to the flat film. (b) The spreading resistance as a function of PEDOT:PSS surface patterning; stars represent the theoretical estimation of R_s assuming having the same R_s for the flat films.

Figure 5 (b) shows the solution resistance decreasing with nano-patterning as the surface area increases. R_s drops by 15.6% in the case of 87 nm linewidth patterning and by only 8.8 % in the case of 157 nm linewidth patterning compared to the flat electrode. Theoretically, increasing the surface area of the electrodes results in decreasing R_s (R_s decreases as $A^{-1/2}$).^[11] In fact, this reduction in R_s appears in the high frequency domain which is dominated by the resistance (R_s). While the low frequency domain is dominated by the capacitance, and the two domains are determined by a characteristic frequency (f_c ; $f_c = 1/2\pi R_s C$). On the plot (figure 5 (b)), the stars represent the theoretical estimation of R_s as a function of the real change in the surface area of PEDOT:PSS by nano-patterning. We calculated the real gain in the surface area (A_{gain}) for the nano-pattered electrodes as $A_{\text{effective}}/A_{\text{flat}}$ based on the dimensions from the AFM characterization, based on which we estimated the theoretical gain in R_s from the

relation $R_s \sim A^{-1/2}$ (**Table S1**). The theoretical estimation of $R_{s \text{ gain}}$ ($R_{\text{gain}} = (A_{\text{eff}}/A_{\text{flat}})^{1/2}$ are 1.079 and 1.16 for 87 and 157 nm patterns respectively) compared to 1.09 and 1.19 based on the measured gain in R_s ($R_{\text{flat}}/R_{\text{patterned}}$).

Figure S5 shows the change in capacitance as a function of patterning PEDOT:PSS surface. There are variations in the C values between the three samples due to slight changes in the thickness values of PEDOT:PSS when spin coated on a nano-patterned PDMS mold vs a flat PDMS mold. However, R_s is not affected by the increase of PEDOT:PSS film thickness as shown by Cui et al. and affected only by the surface area.^[10,11] In fact, the capacitance of PEDOT:PSS films is governed by the film volume and can be discussed in terms of volumetric capacitance (C^* , with the unit F/cm^3).^[24] This is arising from ion penetration into the volume of the film.^[25] In an electrochemical cell setup, the ions from the electrolyte diffuse in the PEDOT:PSS films close to the holes sites on the PEDOT polymer chains to replace them. Proctor et al. have proposed a model for the volumetric capacitance and charge transport with in the PEDOT:PSS films.^[24] For validating the use of the RC equivalent circuit to model the impedance curves, we used the method suggested by Koutsouras et al.^[11] for obtaining a universal curve (f/f_c vs Z/R_s) as shown in **figure S6** which proves that the impedance behavior is predominantly consisting of the R_s and C components. The nano-patterned PEDOT:PSS obtained using our fabrication technique is limited by the replication of PDMS replica from a master mold. Higher aspect ratios would result in a higher effective surface area and subsequently lower electrochemical impedance. This fabrication method can be applied on bigger surface area ($2.5 \times 7.5 \text{ cm}^2$) as well as smaller electrode sizes however the latter is limited by the cutting efficiency of sub-millimeter carrier substrate such as polyimide.

The nano-patterned PEDOT:PSS obtained using our fabrication technique is limited by the replication of PDMS replica from a master mold. Higher aspect ratios would result in a higher

effective surface area and subsequently lower electrochemical impedance. This fabrication method can be applied on bigger surface area ($2.5 \times 7.5 \text{ cm}^2$) as well as smaller electrode sizes however the latter is limited by the cutting efficiency of sub-millimeter carrier substrate such as polyimide.

3.3 Conclusion

We have presented easy fabrication strategies for nano-patterning PEDOT:PSS with and without an underlying gold layer. These strategies have overcome some of the limitations introduced by using other patterning techniques such as nano-imprint lithography and capillary force lithography. We used our fabrication technique for obtaining nano-patterned PEDOT:PSS/Au electrodes for studying the electrochemical impedance. Our results show a decrease in the impedance with nano-patterning due to an increase in the surface area. These results open up the way for incorporating nano-patterning of PEDOT:PSS for biomedical applications in which, reducing the impedance is a necessity.

3.4 Experimental Section

Mold Replication: Single crystal silicon Master molds were bought from LightSmyth Technologies Inc. The size of the first mold is $25 \times 25 \times 0.8 \text{ mm}$, with patterns; $\sim 140 \text{ nm}$ period, 50 nm groove depth, and $\sim 70 \text{ nm}$ linewidth, while the size of the second mold is $12.5 \times 12.5 \times 0.7 \text{ mm}$, with patterns; $\sim 280 \text{ nm}$ period, $\sim 140 \text{ nm}$ linewidth. For testing a third Si mold was also used (size of $20 \times 20 \times 0.8 \text{ mm}$, with patterns; $\sim 205 \text{ nm}$ pitch, 165 nm groove depth, and $\sim 250 \text{ nm}$ linewidth). Before PDMS replication, the molds' surfaces were fluorinated by 1H,1H,2H,2H-perfluorodecyltrimethylchlorosilane (FDTS; $\text{C}_{10}\text{H}_4\text{Cl}_3\text{F}_{17}\text{Si}$) for anti-sticking. The process was done using the molecular layer deposition methods (Nanonex Ultra-100, from Nanonex Corporation). Double layer h-PDMS/PDMS replicas were made as described by Odom et al., and the materials were

bought from the same suppliers.^[22] The same replication was applied on a flat single crystal substrate to obtain a flat PDMS replica for comparison.

Solution preparation: A mixture of PEDOT:PSS (Clevios PH-1000 from Heraeus Holding GmbH.), ethylene glycol (EG; 5 vol%), and dodecyl benzene sulfonic acid (DBSA; 0.002 vol%) was made and sonicated for 20 minutes. Then Divinyl sulfone (DVS; 3 wt%), and 3-glycidoxypropyltrimethoxysilane (GOPS; ranging from 0.01 wt%) were added to the mixture and stirred for a minute. The new mixture was then filtered using 0.8 μm filters (Minisart, from Sartorius Stedim Biotech).

Electrodes Fabrication: The PDMS replicas were activated by plasma oxygen for 60 seconds at 100 Watts and 50 sccm. Then The PEDOT:PSS solution was spun on the replicas at 1100 rpm for 35 seconds (film thickness ~ 110 nm). After which the coated replicas were heated at 90°C for 10 minutes. The samples were next activated with plasma oxygen for 30 seconds at 100 Watts and 50 sccm before evaporating a 55 nm thick gold layer on the top of the PEDOT:PSS. The top gold layer was also activated by plasma oxygen for 60 seconds at 100 Watts and 50 sccm before spin-coating a UV-curable epoxy layer (Ossila encapsulation Epoxy, from Ossila Ltd.) at 3000 rpm for 50 seconds on its top. Then, a Laser-cut polyimide layer (thickness = 125 μm , and carrying size from 1 x 1 mm to 1x 1 cm) was placed over the epoxy layer while it was still in the liquid state, then UV-light (wavelength = 365 nm) was exposed on the samples for 2 minutes to cure the epoxy. Finally, the electrodes were demolded from the PDMS replicas and insulated the contact lines.

Surface characterization Atomic force microscopy (AFM) imaging was performed using an NTEGRA system from NT-MDT. All measurements were realized using amplitude

modulation mode of AFM. Cantilever (NSC35, Mikromash) with resonant frequency at 300 kHz and spring constant of 16 N/m were used in all experiments. Tips radius was 8 nm as verified by scanning electron microscopy. Images were taken at a frequency of 1Hz.

Electrochemical Impedance Characterization and Electrochemical Deposition: The impedance was measured using an electrochemical spectroscopy (EIS; potentiostat/galvanostat, Metrohm Autolab B.V.) with a three-electrode configuration; standard silver/silver chloride (Ag/AgCl) reference electrode, platinum (Pt) mesh as a counter electrode (size; 20 x 20 mm), and the flat or nanopatterned-PEDOT:PSS coated gold electrodes as working electrodes. The electrodes were immersed with a constant depth in a sodium chloride (NaCl) solution with a concentration of 0.1 M. The working electrodes were immersed at the same length in the electrolyte and at the same distance from the counter electrode. The data was analyzed using NOVA software (version 1.10.4, from Metrohm Autolab B.V.). The same setup (3-electrodes configuration) was used for electro-depositing PEDOT:PSS by using a solution of 0.1 M PSSNa and 0.01 M EDOT in DI water. The deposition was done in the galvanostatic mode.

References

- [1] D. T. Simon, E. O. Gabrielsson, K. Tybrandt, M. Berggren, *Chem. Rev.* **2016**, *116*, 13009.
- [2] A. Facchetti, *Chem. Mater.* **2011**, *23*, 733.
- [3] I. Roman LS, Mammo W, Pettersson LAA, Andersson MR, *Adv Mater* **1998**, *10*, 774.
- [4] F. R. Granstrom M, Petritsch K, Arias AC, Lux A, Andersson MR, *Nature* **1998**, *395*:257.
- [5] R. J. Groenendaal LB, Jonas F, Freitag D, Pielartzik H, *Adv Mater n.d.*, 481.
- [6] C. F. Kim JS, Lagel B, Moons E, Johansson N, Baikie ID, Salaneck WR, Friend RH, *Synth Met* **2000**, 311.
- [7] N. K. Guimard, N. Gomez, C. E. Schmidt, *Prog. Polym. Sci.* **2007**, *32*, 876.
- [8] D. T. Simon, E. O. Gabrielsson, K. Tybrandt, M. Berggren, *Chem. Rev.* **2016**, *116*, 13009.
- [9] J. Rivnay, R. M. Owens, G. G. Malliaras, *Chem. Mater.* **2014**, *26*, 679.
- [10] X. Cui, D. C. Martin, *Sensors Actuators B Chem.* **2003**, *89*, 92.
- [11] D. A. Koutsouras, P. Gkoupidenis, C. Stolz, V. Subramanian, G. G. Malliaras, D. C. Martin, *ChemElectroChem* **2017**, DOI 10.1002/celc.201700297.
- [12] J. Rivnay, P. Leleux, M. Ferro, M. Sessolo, A. Williamson, D. A. Koutsouras, D. Khodagholy, M. Ramuz, X. Strakosas, R. M. Owens, C. Benar, J.-M. Badier, C. Bernard, G. G. Malliaras, *Sci. Adv.* **2015**, *1*, e1400251.
- [13] J. Rivnay, S. Inal, B. A. Collins, M. Sessolo, E. Stavrinidou, X. Strakosas, C. Tassone, D. M. Delongchamp, G. G. Malliaras, *Nat. Commun.* **2016**, *7*, 11287.
- [14] J. Choi, H. Choi, J. Shin, H. Kim, J. Jang, H. Lee, *Org. Electron.* **2013**, *14*, 3180.
- [15] V. A. Online, J. Kwon, V. Ganapathy, Y. H. Kim, K. Song, H. Park, Y. Jun, P. J. Yoo, J. H. Park, **2013**, 7838.
- [16] L. Petti, M. Rippa, R. Capasso, G. Nenna, A. De Girolamo, D. Mauro, G. Pandol, M. G. Maglione, C. Minarini, **2013**.
- [17] Y. Yang, K. Lee, K. Mielczarek, W. Hu, A. Zakhidov, **n.d.**, 485301, 1.
- [18] J. B. Emah, R. J. Curry, S. R. P. Silva, J. B. Emah, R. J. Curry, S. R. P. Silva, **2013**, 103301, 2006.
- [19] B. K. Suh, M. C. Park, P. Kim, **2009**, 2699.
- [20] N. Sanetra, V. Feig, B. Wolfrum, A. Offenha, D. Mayer, **2011**, 1289, 1284.
- [21] M. R. Abidian, D. C. Martin, *Biomaterials* **2008**, *29*, 1273.
- [22] T. W. Odom, J. C. Love, D. B. Wolfe, K. E. Paul, G. M. Whitesides, **2002**, 5314.
- [23] M. ElMahmoudy, S. Inal, A. Charrier, I. Uguz, G. G. Malliaras, S. Sanaur, *Macromol. Mater. Eng.* **2017**, *302*, 1600497.
- [24] C. M. Proctor, J. Rivnay, G. G. Malliaras, *J. Polym. Sci. Part B Polym. Phys.* **2016**, *54*, 1433.
- [25] M. Elmahmoudy, S. Inal, A. Charrier, I. Uguz, G. G. Malliaras, S. Sanaur, *Macromol. Mater. Eng.* **2017**, DOI 10.1002/mame.201600497.

Supporting Information

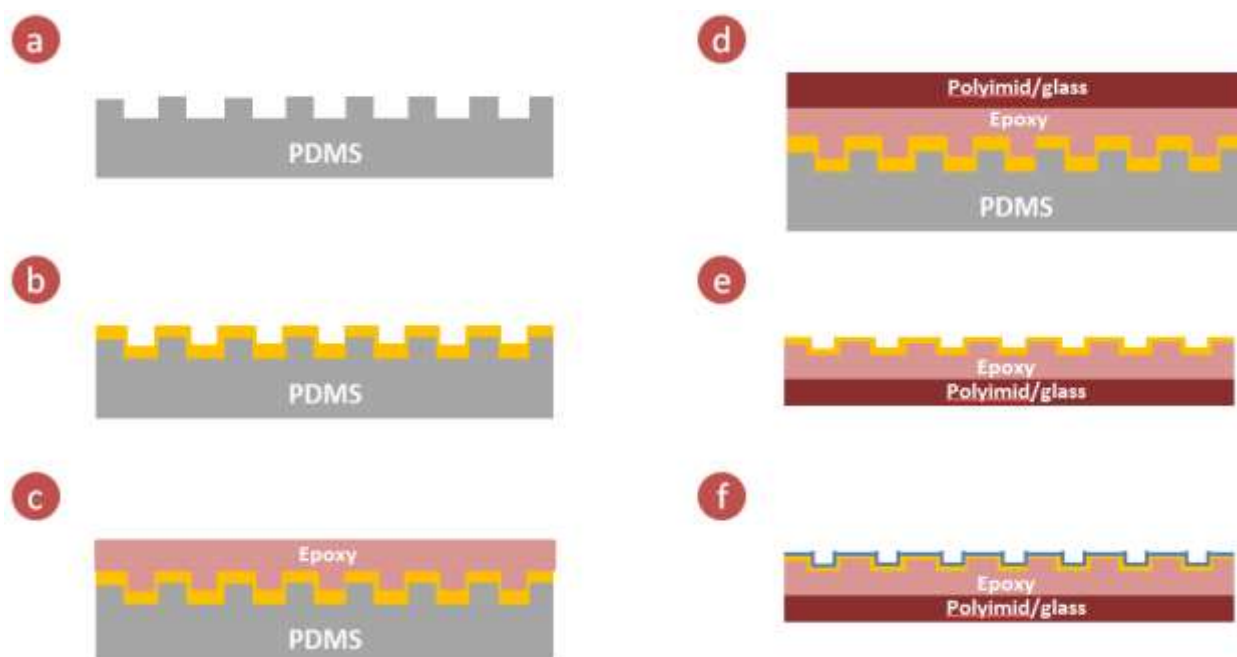


Figure S1. Schematic of gold nano-patterning and coating by an electrochemically deposited PEDOT:PSS layer (a) PDMS nano-patterned replica. (b) Gold evaporation on the PDMS replica. (c) Spin-coating epoxy on the gold layer. (d) Placing a polyimide or glass substrate on the epoxy and exposing to UV-light to cure the epoxy layer. (e) Demolding the layers stack from the PDMS replica. (f) Electro-deposition of PEDOT:PSS on the nano-patterned gold.

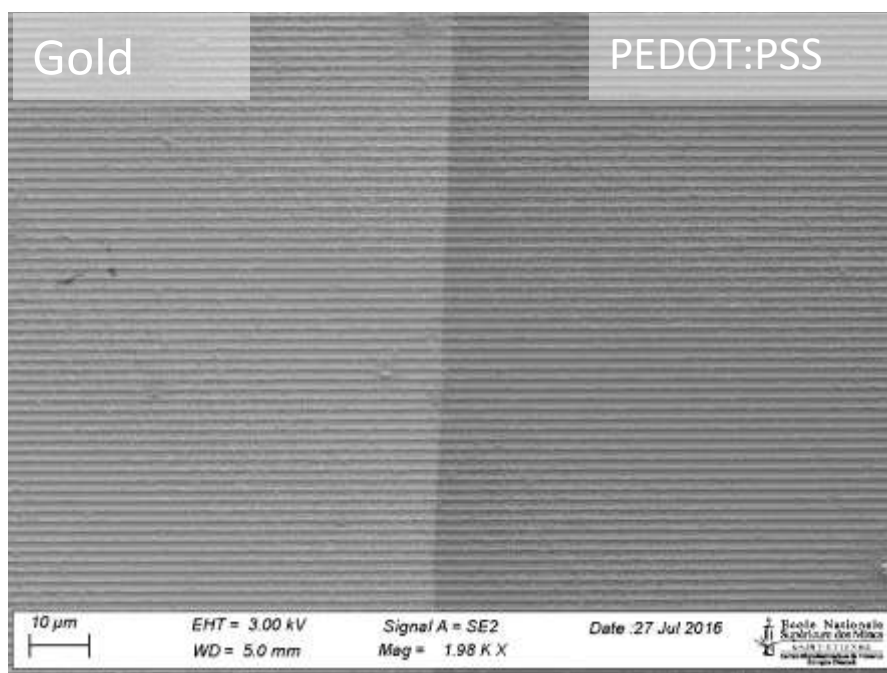


Figure S2. Electro-deposited PEDOT:PSS on nano-patterned gold. The left side (bright grey) is only gold, and the right side (dark grey) is the deposited PEDOT:PSS on gold.

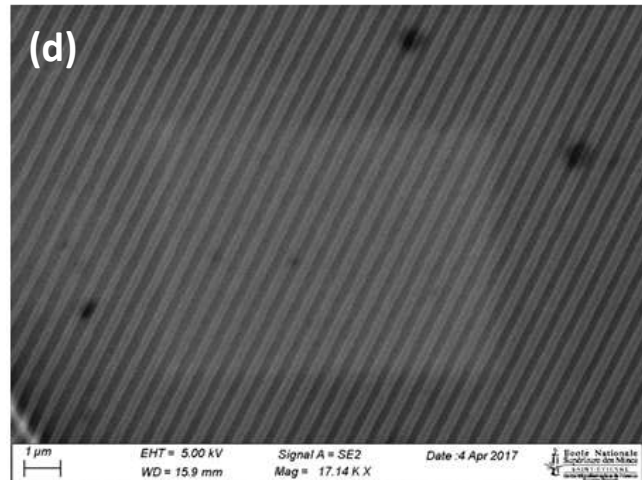
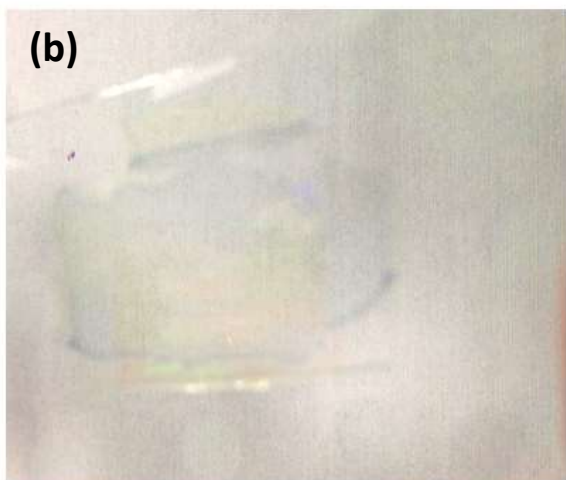
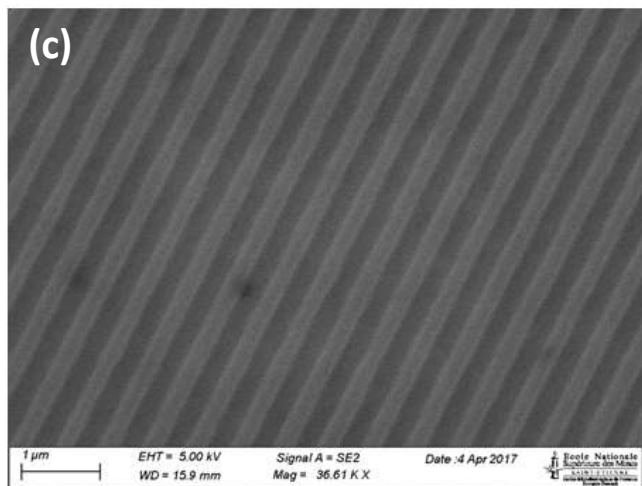
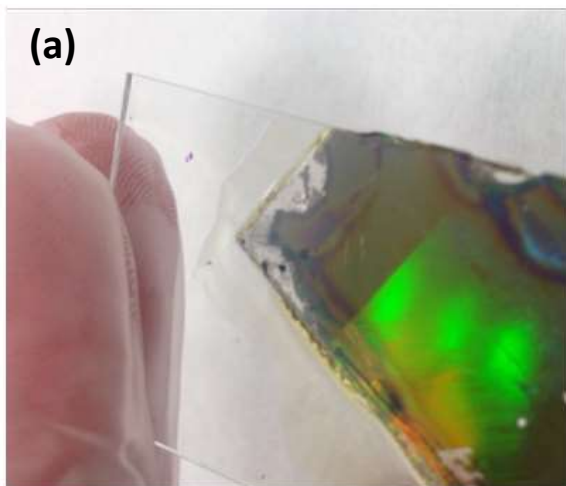


Figure S3. Patterns dimensions; ~ 205 nm pitch, 165 nm groove depth, and ~ 250 nm linewidth. (a) Nano-patterned PEDOT:PSS/Au demolded on glass using epoxy. (b) Nano-patterned PEDOT:PSS demolded on glass using epoxy. (c) & (d) SEM images of nano-

patterned PEDOT:PSS.

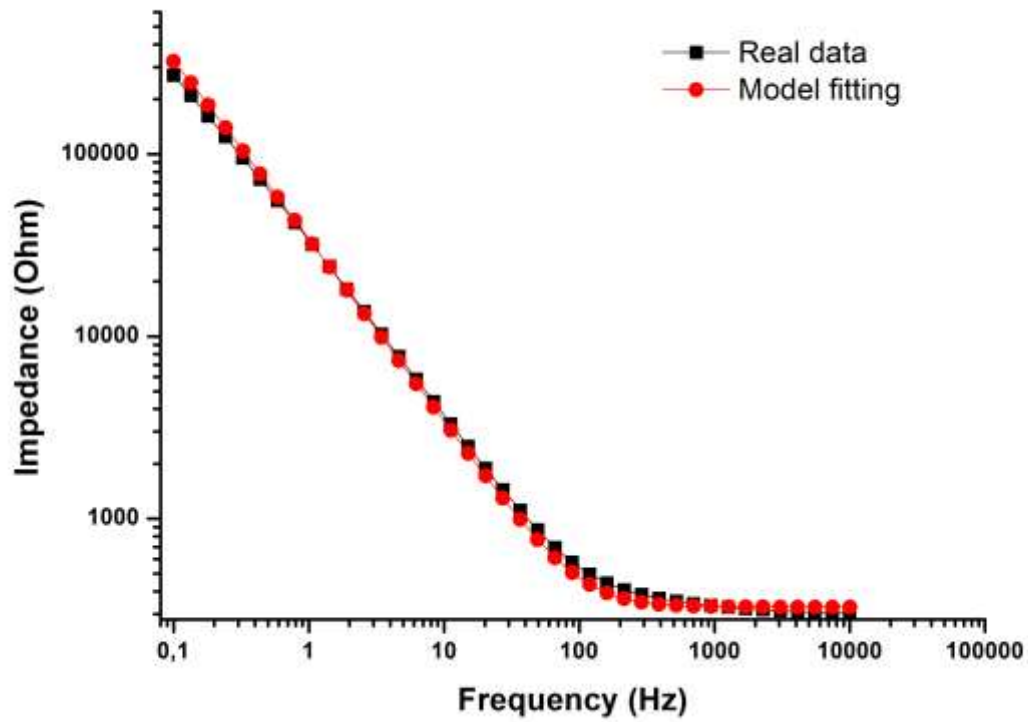


Figure S4. Electrochemical impedance of PEDOT:PSS/Au film modeled with an RC equivalent circuit.

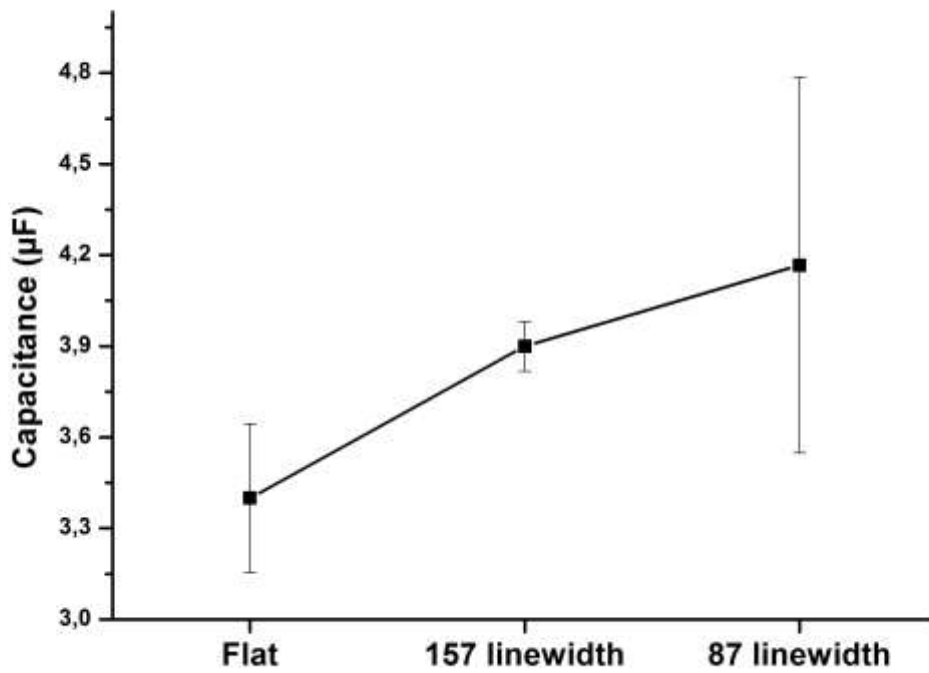


Figure S5. Capacitance of PEDOT:PSS film; nano-patterned vs a flat.

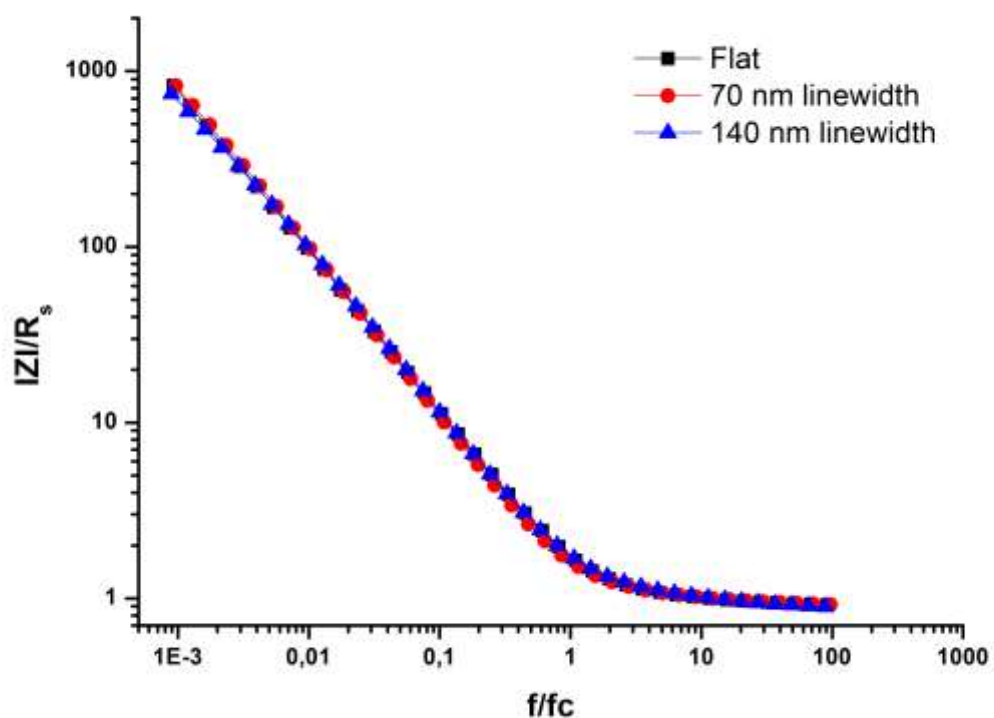


Figure S6. Normalized impedance ($|Z|/R_s$) vs frequency (f/f_c) for flat and nano-patterned PEDOT:PSS electrodes.

Table S1. Summary of the theoretical and measured gain in area and solution resistance for the flat and nano-patterned PEDOT:PSS electrodes.

Sample	R_s (Ohm)	A_{gain} (measured)	R_{gain} (estimated)	R_{gain} (real measured)
	measured	A_{eff}/A	$\text{Sqr}(A_{\text{gain}})$	$R_{\text{flat}}/R_{\text{patterned}}$
Flat	411.1	1	1	1
157 nm linewidth	375.1	1.17	1.08	1.09
87 nm linewidth	346.9	1.35	1.16	1.19

Chapter 4

Designing Low Impedance Amorphous PEDOT:PSS Electrodes For Neural Recordings

4.1 Introduction

In the field of neuroscience major progress had been made as a result of ground-breaking technologies extensively employed in research to study the dynamics of neural circuits. This may then be translated it to clinical studies for treatment of neurological disorders or to advance brain machine interfaces.^[1-3] Among existing technologies, multi electrode arrays (MEAs) form the basis of research conducted for extracellular engagement with neural networks. These are primarily based on metallic electrodes made of platinum, gold, tungsten, etc..^[4] In order to obtain a more fundamental understanding of neural signaling processes, stimulation or recording experiments require the electrode dimensions to approach those of individual neurons.^[5,6] This necessitates electrode miniaturization at the neural interface, while keeping the impedance of the system low to ensure accurate recording of the underlying networks.^[7] However, metallic electrodes have limitations in their ability to accurately record the local neural populations at micron resolution as the signal quality dramatically decreases, or even diminishes, due to increased impedance.^[7] The impedance of an electrode is governed by the double layer capacitance formed by the charge accumulation at the electrode/electrolyte interface, which is in turn limited by the exposed surface area. Therefore, the morphology and the micro/nano-structure of the electrode surface play a crucial role in its characteristics.^[8] In order to decrease the impedance and obtain a better signal to noise ratio

(SNR), surface optimization is of a great interest in order to enhance the non-faradaic interface. Extensive research has been conducted regarding this interface to introduce surface topography, such as sintering of metal nanoparticles and introducing fractal nanostructures. However, such efforts require complicated fabrication techniques and offers limited performance increase.

Recently, metallic electrodes coatings made up of high surface area chemical composites such as conducting polymers (CPs) or carbon nanotubes (CNTs) have received considerable attention for optimization of the neural interface.^[9-11] Among these poly(3,4-ethylenedioxythiophene)/poly(4-styrenesulfonate) (PEDOT:PSS) has emerged as a promising candidate due to the highly reproducible, biocompatible and chemically stable nature of this material. CPs offer the potential to interface solid-state electronics with living cells at the cellular level^[12,13] which has already been shown with PEDOT:PSS coated electrodes in many applications through demonstration of the ability to record single neuron activity *in vivo* both in animal models and human patients in clinical studies.^[14,15] The high performance recordings obtained using PEDOT:PSS are largely due to the exceptional chemical and mechanical properties, which can be modified based on the application. This possibility to control properties, such as the ionic conductivity, provides the chance to further enhance performance at the neural interface.^[16] A recent study on the working mechanism of PEDOT:PSS shows each PEDOT chain in the deposited film can be modeled as an individual plane capacitor contributing to the total impedance of the system.^[12] The hydration of the polymer provides means of ion transport within the bulk of the film to charge the capacitors and effectuates an ionic resistance.^[17,18] Therefore, PEDOT:PSS coatings offer a 3D sensing platform and the impedance of the bulk is directly proportional to the amount of PEDOT:PSS.^[17] However, when limited to a small area for single neuron coupling, increasing the film thickness results in high resistance for ion injection and prevents the uniform charging of each capacitor, especially in depths of the film. In the equivalent circuit, ionic

resistance (R) becomes dominant and constitutes a high pass (RC) filter, eliminating high frequency components of the recorded neural signals. Thus, when coated as a thick film on a micron scale working electrode, the beneficial aspects of PEDOT:PSS coatings are lost, preventing good recordings of the full neural spectrum (0.5Hz to 1kHz). To deal with this issue, a possible approach is to induce porosity and variety of topologies in the film which would facilitate ion injection, therefore minimizing the resistance.^[19] The morphology of PEDOT:PSS can be tuned through several techniques, one of which is freeze-drying.^[19,20] This process relies on removing crystallized solvent within the deposited film upon sublimation, leaving behind micro-pores while keeping the structure intact. Enhanced signal amplitude and stimulation capabilities of PEDOT:PSS have been demonstrated by *in vitro* studies taking advantage of the increased surface area on large scale.^[20]

In this report, we provide a system with the ability to minimize the impedance at the cellular level by using micro-porous PEDOT:PSS coatings on micron-scale electrodes. To validate this approach, electrodes coated with small surface area and large volume composites were fabricated, a process that has been investigated by Hofmann et al. for gold electrodes.^[21] The final device structure was designed to have a small aperture on the active area over a large PEDOT:PSS electrode. As a result of the low ionic resistance of the film due to induced porosity, the electrolyte is able to drift inside film in all directions efficiently. Electrochemical impedance spectroscopy (EIS) was utilized to demonstrate the improved impedance of small aperture electrodes with large underlying PEDOT:PSS volumes. The electrodes were tested *in vitro* using an extracted hippocampus in order to validate the potential of this electrode design for neural interfacing applications. Superior SNR was observed through sharp wave discharges (SWDs) which occur as a result of induced pathophysiological activity using the neurotoxin 4AP.

4.2 Results and Discussion

Devices were fabricated on a glass substrate with gold interconnects patterned through lithography techniques (**Figure 1**; Fabrication details are described in the experimental section). A layer of parylene C was deposited on the gold as insulation and etched selectively to expose the electrode surface for subsequent patterning of PEDOT:PSS. PEDOT:PSS was later freeze-dried without being annealed when still in aqueous form. Finally, a layer of SU8 was deposited over the hydrated film and developed to create micron scale apertures over the electrode surface. To be able to characterize the drift of ions inside the film, three types of electrodes were fabricated: electrodes with 40 μm or 200 μm diameters and a 200 μm electrode with a 40 μm aperture. The sets of electrodes were fabricated for both standard spin-cast PEDOT:PSS and freeze-dried porous PEDOT:PSS.

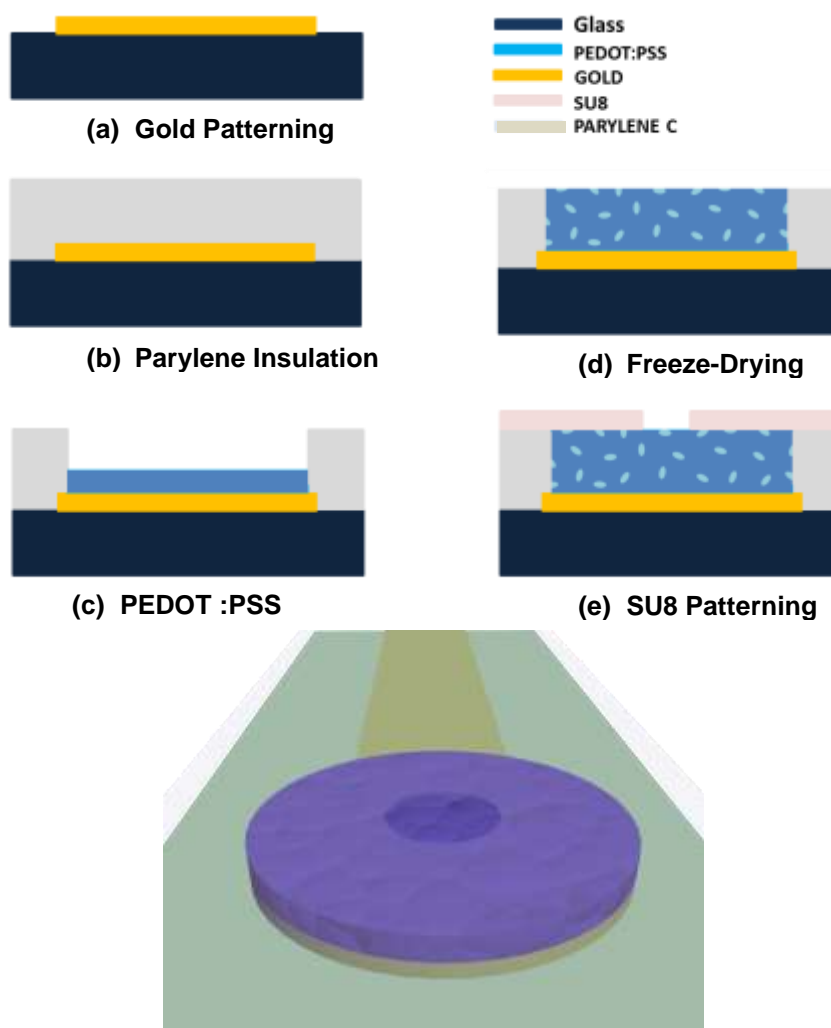
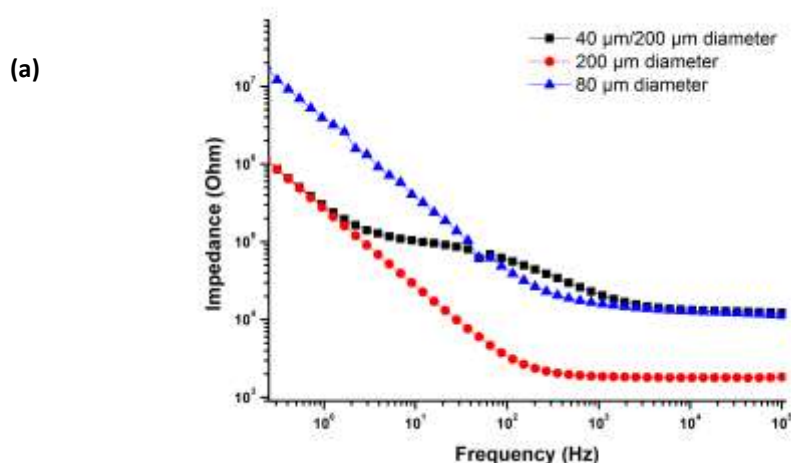


Figure 1. Fabrication Scheme of freeze-dried PEDOT:PSS micro-patterned electrodes by photolithography. (a) Gold patterning. (b) Parylene C deposition. (c) PEDOT:PSS patterning. (d) Freeze-drying PEDOT:PSS. (e) Su8 Patterning.

The electrode coating for each method of film deposition (standard spin-cast or freeze dried porous) was achieved using the same deposition parameters, therefore the electrodes possess the same amount of PEDOT:PSS. The freeze-drying method creates porosity in the film, which results in an increase in its physical volume and swelling when immersed in aqueous environment. Electrochemical impedance spectroscopy of all devices was measured and the results are compared in **Figure 2**. The electrochemical impedance of both amorphous and spin-cast PEDOT:PSS gold-coated electrodes can be modeled using a simple RC circuit (**Figure S1**) where R represents the solution resistance (R_s) and C represents the film capacitance (C). In the low frequency domain, the impedance is dominated by the capacitance, while in the high frequency range the resistance is the dominating parameter.^[17] Both normal and amorphous PEDOT:PSS electrodes with smaller aperture result in EIS spectra which overlap that of the 200 μm electrode, but only at low frequencies (<1 Hz) as shown in Figure 2 (a) & (b).



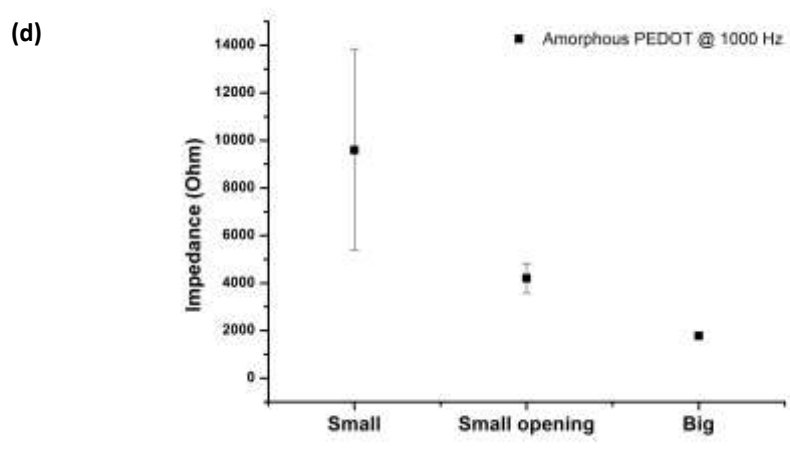
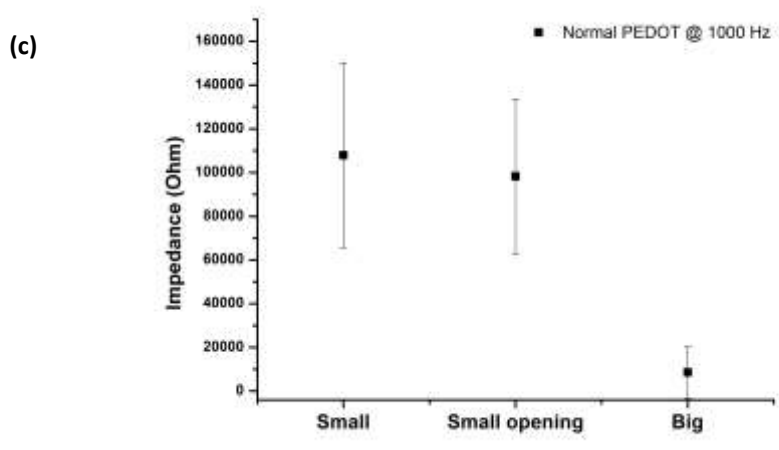
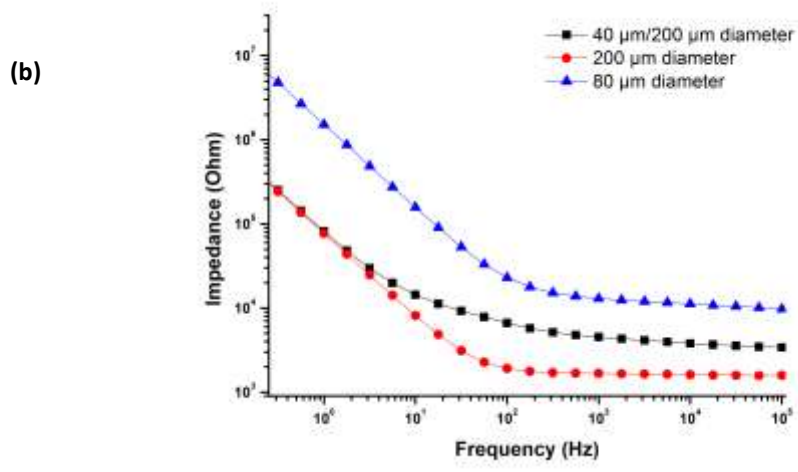


Figure 2. Electrochemical impedance of PEDOT:PSS electrodes. (a) Bode plot of normal PEDOT:PSS. (b) Bode plot of freeze-dried PEDOT:PSS. (c) Impedance at 1000 Hz of the normal PEDOT:PSS electrodes. (d) Impedance at 1000 Hz of the freeze-dried PEDOT:PSS electrodes.

This behavior shows that the capacitance is governed by the amount of PEDOT:PSS on the electrode. This is in complete agreement with our understanding of the *volumetric* capacitance (C^* ; capacitance per unit volume), which indicates that the capacitance is dependant on the volume of the PEDOT:PSS film.^[12] For higher frequency regimes, on the other hand, the impedance of the big electrodes with small aperture follows the same behavior as the small electrodes in the case of the normal PEDOT:PSS films (Figure 2 (a)). This indicates a high ionic resistance despite the known swelling of the normal PEDOT:PSS.^[16,18] Hence, introducing the small aperture to minimize the surface contact with the electrolyte has an effect on the electrode performance by increasing the ionic resistance compared to the big electrodes. In contrast, when amorphous PEDOT:PSS is employed, the impedance of the electrodes with small aperture in the high frequency range is lower than the impedance of the small electrodes. In this case the electrolyte can drift inside the film more efficiently due to high porosity and swelling of the film. Alwan et al. characterized the pore size of the freeze-dried PEDOT:PSS to be $39.1 \pm 2.7 \mu\text{m}$ in diameter (median value).^[19] Indeed the micro structuring allows for the increase of surface area in contact with the electrolyte, which leads to a decrease in the solution resistance value. However, the impedance spectra of electrodes with small aperture do not overlap those of the big electrodes in the high frequency range, due to some resistance introduced by the insulated areas of the PEDOT:PSS electrode. Figure 2 (d) shows the decrease of the impedance (at 1000 Hz) of the amorphous PEDOT:PSS electrodes of large volume and small aperture compared to small and big electrodes. The impedance of the electrodes with small aperture decreases by 2.3 times compared to the impedance of the small electrodes and increases by 2.4 times compared to the big electrodes. While in the case of normal PEDOT:PSS, the impedance (at 1000 Hz) of the impedance of the electrodes with aperture is 1.1 times less than the small electrodes and 11.5 times higher than the big electrodes as shown in Figure 2 (c).

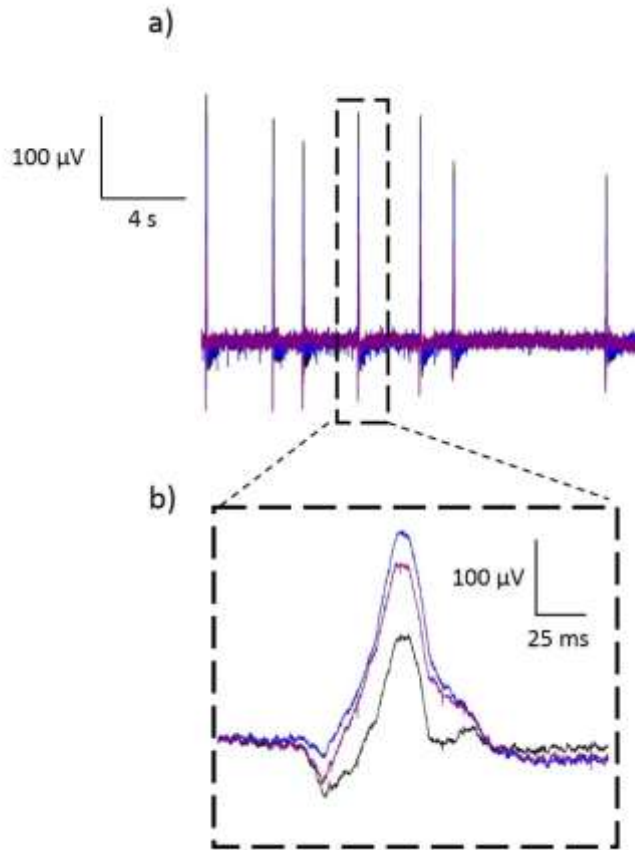


Figure 3. Improving device performance while increasing spatial resolution, demonstrated by a) a neural recording of hippocampal tissue with induced pathological SWD activity. B) The zoomed in view of a single SWD shows the obtained SNR for large area (blue), small area (black) and small area with large volume (purple) electrodes. The good performance of the latter is seen through the close SNR performance compared to the large area electrode trace.

Through *in vitro* neural recordings with extracted hippocampi from mice (postnatal day 14 through 18), the advantage of this small-aperture electrode with porous PEDOT:PSS was validated. In this way, the benefit of reduced electrode impedance, and therefore improved recording or stimulation of tissue, can be shown while the small aperture allows for improved spatial resolution. Here, the tissue was placed on the device in a perfusion bath with the recording sites located together directly under the dorsal hippocampus to ensure no difference in recordings as a result of placement. Sharp wave discharges (SWDs) as seen in **Figure 3 (a)** are typical of pathophysiological activity induced by the application of the neurotoxin 4-aminopyridine (4AP) to neural tissue *in vitro*. 4AP selectively blocks subsets of potassium

channels, which result in a widening of neural action potentials. Such a widening subsequently causes individual neurons to remain over the threshold potential to delivery vesicles to down-stream neurons. This means that cells affected by 4AP continue to deliver excitatory neurotransmitters for a longer period of time, and as a result when the concentration is high enough, as presented here, large scale pathophysiological activity of large populations of neurons is created. In the magnified view of a single SWD (Figure 3 (b)) the various amplitudes of the three electrode designs are evident. The small volume PEDOT:PSS trace (black) exhibits the lowest SNR, while the large volume (blue) shows the highest. The large volume with small aperture (purple) exhibits good performance, following closely to the large volume electrode trace, thereby demonstrating effective use of the PEDOT:PSS volume. This is the case of all SWDs shown here, demonstrating the expected results when considering the EIS spectra.

4.3 Conclusion

Here, we demonstrated a sensing platform capable of recording neural signals with a state of the art signal to noise ratio, facilitated by the 3D motion of ions inside the film due to induced porosity. The electrodes offer the ability to decrease the impedance at the neural interface particularly for high frequency activity. The approach can be utilized for improved spatial resolution of the current electrode technology to couple with smaller populations of cells or single neurons more accurately. The thickness and the size of the aperture can be tuned for the frequency range of targeted neural activity.

4.4 Experimental Section

Device Fabrication: 1x3 inch glass slides were cleaned by sonication first in a soap-water solution, then in acetone. These were used as substrate to coat the positive photoresist, S1813 Shipley. The ultraviolet (UV) mask aligner SUSS MJB4 was used to expose the photoresist using a mask with the pattern of gold interconnects. The photoresist was developed and the

substrates were loaded into an Alliance Concept EVA450 to deposit 10 nm of chromium to promote adhesion, followed by a 100 nm thick gold layer. Utilizing a liftoff process performed in an acetone bath, the gold patterning was completed. A layer of parylene C with a thickness of 1 μm was deposited over gold interconnects by chemical vapor deposition using a SCS Lab coater 2. A dilute soap-water solution was spin-coated onto the insulating PaC layer, followed by the deposition of a second sacrificial layer of parylene C (1.5 μm). The positive photoresist AZ9260 was spin-cast, exposed to define the electrode area and developed. This AZ9260 provides an etch mask for the subsequent reactive ion etching using an Oxford 80 plus plasma etcher resulting in etching of the parylene C to open the gold contacts. Following this step the PEDOT:PSS was deposited onto the electrodes by two strategies :

Thin film PEDOT:PSS (PH 1000 from H.C. Stark) containing 5 vol% of ethylene glycol, 0.1 vol% dodecyl benzene sulfonic acid and 1 wt.% of 3-glycidoxypropyltrimethoxysilane (GOPS), in aqueous form was spin-coated onto the electrode array at 400 rpm for 15 seconds. The devices were exposed to a soft baking step (110°C for 1 min) followed by peeling off the sacrificial layer of parylene, leaving PEDOT:PSS only on the surface of electrodes. Devices were baked at 110°C for one hour to cure the PEDOT:PSS.

Porous PEDOT:PSS was fabricated utilizing an aqueous dispersion of PEDOT:PSS (PH-1000, Clevios) were realized via freeze drying technique. 3-glycidoxypropyltrimethoxysilane (GOPS, Sigma-Aldrich) was added to the PEDOT:PSS solution as a crosslinker (3 wt%) to improve the mechanical robustness and stability in water. Further, dodecylbenzenesulfonic acid (DBSA, 0.5%) was added to the PEDOT:PSS/GOPS dispersion in order to improve the conductivity of the resulting porous structures. Prior to freeze drying the solution was spread evenly over the lithographically patterned electrodes via custom made doctor blade. The top sacrificial parylene-C layer enabled the confinement of PEDOT:PSS solution inside the electrode domains. We assume that the capillary forces drive the solution flow towards the

cavity formations. After the deposition of PEDOT:PSS solution onto the substrates, the samples were placed inside freeze-dryer (Cryotec) where they were frozen from 5 to $-40\text{ }^{\circ}\text{C}$ at a controlled rate of $-0.9\text{ }^{\circ}\text{C min}^{-1}$, at which point the ice phase was sublimed from the scaffolds, as described by Wan et al.^[19] After, the samples were kept in DI water over 24 h to enable the diffusion of low molecular components.

All devices were kept in DI water over 24 hours to remove the excess of PSS and to reach maximum swelling prior the deposition of SU8 2002 photoresist. A $2\text{ }\mu\text{m}$ thick SU8 layer was spin-coated onto the substrate at 3000 rpm for 35 seconds, followed by soft baking at 95°C for 1 minute. The SU8 negative photoresist was then exposed with UV-light (365 nm wavelength; 80 mJ/cm^2) for patterning. Afterwards the resist was post baked at 95°C for 1 minute. Finally, the resist was developed by SU8 developer for 1 minute, then rinsed with water.

Characterization: All the electrodes were characterized in phosphate buffer solution (PBS) using an Autolab PGSTAT equipped with an FRA module. As counter and reference electrode, Ag/AgCl and Pt electrodes were employed respectively. The thickness of porous PEDOT:PSS ($1.3\text{ }\mu\text{m}$) of the PEDOT:PSS coatings were measured using a Dektak mechanical profilometer.

Neural Recording: Hippocampus Preparation: All protocols have been approved by the Institutional Animal Care and Use Committee of INSERM. After decapitation of anesthetized mice, the brains were rapidly extracted (postnatal day 14 through 18). The brain was cut into the left and right hemisphere in a chilled and perfused bath. The complete hippocampus, including the septum, was extracted from each hemisphere. This preparation maintains the entire 3D hippocampal architecture, preserving cellular and axonal integrity.^[22,23] Freshly extracted preparations were placed in a chamber and perfused with oxygenated ($95\%\text{ O}_2/5\%\text{ CO}_2$) ACSF (126 mM NaCl , 3.5 mM KCl , 2 mM CaCl_2 , 1.3 mM MgCl_2 , $1.2\text{ mM NaH}_2\text{PO}_4$, 26.2 mM NaHCO_3 , and 10 mM glucose). The tissue was maintained in the chamber at room

temperature and allowed to recover for 1 h before experimental use. After this period of recovery, preparations were transferred with a pipette to the surface of the device. Recording sites were located together directly under the dorsal hippocampus to ensure no difference in recordings due to tissue placement. The chamber containing the hippocampus was continuously perfused with oxygenated ACSF warmed at 33 °C.

Note: my contribution in this chapter is helping designing electrodes, measuring and analysing impedance.

References

- [1] E. C. Leuthardt, G. Schalk, J. R. Wolpaw, J. G. Ojemann, D. W. Moran, **2004**, *63*, DOI 10.1088/1741-2560/1/2/001.
- [2] M. A. Lebedev, M. A. L. Nicolelis, **2017**, 767.
- [3] V. S. Polikov, P. A. Tresco, W. M. Reichert, *J. Neurosci. Methods* **2005**, *148*, 1.
- [4] J. C. Williams, R. L. Rennaker, D. R. Kipke, **1999**, 303.
- [5] M. E. Spira, A. Hai, *Nat. Nanotechnol.* **2013**, *8*, 83.
- [6] F. Santoro, S. Dasgupta, J. Schnitker, T. Auth, G. Panaitov, G. Gompper, A. Offenhausser, **2014**.
- [7] S. F. Cogan, **2008**, DOI 10.1146/annurev.bioeng.10.061807.160518.
- [8] S. Paik, Y. Park, D. D. Cho, **n.d.**, 373.
- [9] X. Cui, D. C. Martin, *Sens. Actuat B-Chem* **2003**, *89*, 92.
- [10] X. Luo, C. L. Weaver, D. D. Zhou, R. Greenberg, X. T. Cui, *Biomaterials* **2011**, *32*, 5551.
- [11] T. Gabay, M. Ben-david, I. Kalifa, R. Sorkin, **2007**, *35201*, DOI 10.1088/0957-4484/18/3/035201.
- [12] C. M. Proctor, J. Rivnay, G. G. Malliaras, *J. Polym. Sci. Part B Polym. Phys.* **2016**, *54*, 1433.
- [13] J. Rivnay, G. G. Malliaras, **2014**.
- [14] D. Khodagholy, T. Doublet, P. Quilichini, M. Gurfinkel, P. Leleux, A. Ghestem, E. Ismailova, T. Hervé, S. Sanaur, C. Bernard, G. G. Malliaras, *Nat. Commun.* **2013**, *4*, 1575.
- [15] D. Khodagholy, J. N. Gelinas, T. Thesen, W. Doyle, O. Devinsky, G. G. Malliaras, G. Buzsáki, *Nat. Neurosci.* **2014**, *18*, 310.
- [16] M. Elmahmoudy, S. Inal, A. Charrier, I. Uguz, G. G. Malliaras, S. Sanaur, *Macromol. Mater. Eng.* **2017**, DOI 10.1002/mame.201600497.
- [17] D. A. Koutsouras, P. Gkoupidenis, C. Stolz, G. G. Malliaras, V. Subramanian, D. C. Martin, *ChemElectroChem* **2017**, DOI 10.1002/celec.201700297.
- [18] E. Stavriniidou, P. Leleux, H. Rajaona, D. Khodagholy, J. Rivnay, M. Lindau, S. Sanaur, G. G. Malliaras, *Adv. Mater.* **2013**, *25*, 4488.
- [19] A. M.-D. Wan, S. Inal, T. Williams, K. Wang, P. Leleux, L. Estevez, E. P. Giannelis, C. Fischbach, G. G. Malliaras, D. Gourdon, *J. Mater. Chem. B* **2015**, *3*, 5040.
- [20] S. Inal, A. Hama, M. Ferro, C. Pitsalidis, J. Oziat, D. Iandolo, A. Pappa, M. Hadida, M. Huerta, D. Marchat, P. Mailley, R. M. Owens, **2017**, *1700052*, 1.
- [21] B. Hofmann, K. Enno, M. Schottdorf, A. Offenh, B. Wolfrum, **2011**, 1054.
- [22] I. Khalilov, M. Esclapez, I. Medina, D. Aggoun, K. Lamsa, X. Leinekugel, **1997**, *19*, 743.
- [23] M. L. Davies, S. A. Kirov, R. D. Andrew, **2007**, *166*, 203.

Chapter 5

Linear Cell Migration on Micro-Patterned Conducting Polymers

5.1 Introduction

Cell migration is involved in many biological functions such as wound healing, tumor metastasis, and morphogenesis.^[1-3] Several strategies were used to control cell migration such as chemical gradients (chemotaxis),^[5-7] surface-anchored biochemical gradients (haptotaxis), light intensity gradients (phototaxis),^[4] gravitational gradients (geotaxis),^[8] stiffness gradient (durotaxis),^[9] and electrostatic potential (galvanotaxis).^[10] [There is a great interest in developing in-vitro platforms for controlling and studying these processes, and such platforms often rely on innovative materials solutions. Organic electronic materials are currently being investigated for their biological applications, and there is significant interest also in their use as tissue engineering scaffolds.^[11,12] Conducting polymers (CPs) such as PEDOT:PSS provide great chemical and mechanical properties to interface with biological systems. Compared to metal substrates, the soft nature of CPs is closer to the mechanical properties of the tissues, hence less foreign interactions. This is in addition to the ability to tailor the chemical structure, and the electrical and mechanical properties of these polymers to fit with the study of interest.^[13] Another advantage of using CPs is the mixed ionic and electronic conduction, which provides enhanced communication between cells and devices.^[14,15]

Wong et al. have shown that the shape and the growth of cells can be controlled noninvasively using conducting polymers, by applying an electrical bias and changing the redox state of the polymer film.^[16] In their investigation they used the conducting polymer polypyrrole, and observed that aortic endothelial cells adhere and function differently on the reduced and the

oxidized films. This study has paved the way for several studies focusing on the effect of electrochemical state of conducting polymers on cell growth and stimulation.^[17,18] In order for the adjacent cells to attach to each other or to a surface, anchoring molecules (integrins, proteins, and actins) are used. The chemistry of a surface impacts the adsorption of these molecules and varies their density.^[19] Salto et al. have demonstrated the use of conducting polymer PEDOT:tosylate as an electronic switch (reduced/oxidized) to monitor neural stem cell adhesion.^[20] They used human serum albumin (HSA) for promoting cell adhesion, and they have reported an increase in HAS adsorption in the reduced state compared to the oxidized and neutral states. A similar study was done by Wan et al. who studied cell (normal and cancerous) density control on conducting polymer surface poly(3,4-ethylenedioxythiophene) p-toluenesulfonate (PEDOT:TOS) by creating electrochemical gradient along the polymer film.^[21] In their experiment, they used fibronectin as an adhesion protein, in the growth medium serum, and they could observe an increase in the fibronectin adsorption in the reduced area compared to the other states. These changes in cell adhesion molecules had a direct impact on the cell density distribution. Gumus et al. have used conducting polymers to control the migration of bovine aortic endothelial cells (BAEC).^[22] By depositing Fn, and creating electrochemical gradient on PEDOT:TOS surface, they observed a change in the trajectories and speed of BAEC cells depending on the redox state (reduction/oxidation) of the film. These changes are based on the Fn gradient initiated by the electrochemical gradient.

Beside the electrochemical gradient, surface topography (micro- and nano-patterning) is another key factor for cell adhesion, migration, growth, proliferation, and differentiation.^[19,23-27] Mahoney et al. have used micro-channels (polyimide walls; 20-60 μ m) to study the cell neurite growth, and they have found that the neurites grow and orient themselves parallel to the patterns.^[28] Teixeira et al. have done a similar investigation for studying the human corneal epithelial cells adhesion to micro- and nano-patterned substrates (silicon oxide), and

in effect cells showed alignment and elongation to the patterns or rounding.^[27] However, and to the best of our knowledge, micro-pattered CPs were not applied for studying cell migration. In this work, we micro-pattern PEDOT:PSS film in the form of micro-stripes using photolithography to study the alignment and motion of the hCMEC cells in relation to these stripes. We also investigate the effect of the electrochemical gradient on directionality of the hCMEC cells along the micro-stripes. Hence, collectively we are combining the soft nature of the CPs with the electrochemical gradient, and micro-patterning in one platform to study cell response. Our study shows the ability of controlling the migration of hCMEC cells which opens the way for more studies on the effect of patterning conducting polymers for cell migration.

5.2 Results and discussion

Figure 1 presents the fabrication scheme of PEDOT:PSS micro-patterning. The fabrication details are explained in the experimental section. The devices were chosen to be fabricated on ITO (indium tin oxide) substrates to combine conductivity (for biasing the device) and transparency (for microscope imaging) at the same time. The ITO surface was functionalized using GOPS to have a stronger adhesion to the spin-coated PEDOT:PSS film (**figure S1**; experimental section). The patterning is done using photolithography technique. Using conventional lithography has been limited to pattern organic materials because of the chemical incompatibility between the organic materials and the process chemicals.^[29] In our case we employ a fluorinated orthogonal photoresist which is chemically benign to PEDOT:PSS.^[30,31] The photoresist was spin-coated and patterned directly on the top of PEDOT:PSS film. After developing, the patterns were transferred to the PEDOT:PSS film by dry etching. Eventually the photoresist residual layer was stripped off the micro-patterned PEDOT:PSS. The thickness of the PEDOT:PSS patterns is determined by the initial thickness of the PEDOT:PSS (~ 400 nm), the thickness of the orthogonal photoresist layer ($1.2 \mu\text{m}$),

and the etching rate of each layer. The PEDOT:PSS patterns depth we obtained is ~ 250 nm.

The features patterned on the PEDOT:PSS film are micro-stripes of varying widths (linewidth; 10, 15, 20, and 30 μm , and period; 20, 30, 40, and 60 μm respectively).

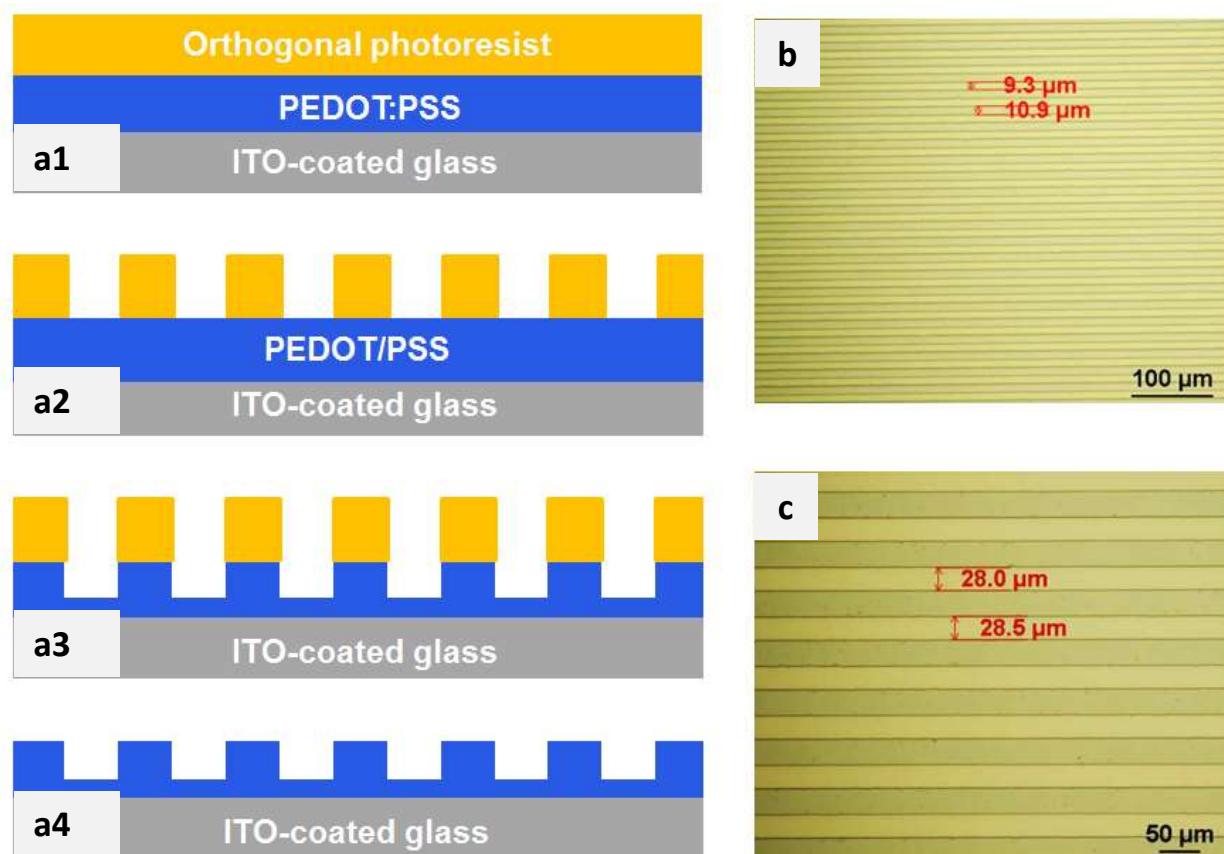


Figure 1. Fabrication scheme of micro-patterned PEDOT:PSS. (a1) Stacking PEDOT:PSS and photoresist layers on ITO by spin-coating. (a2) Micro-patterning the photoresist by photolithography. (a3) Dry etching PEDOT:PSS layer. (a4) Stripping off the photoresist residual layer. (b-c) microscope images of micro patterned PEDOT:PSS (10 μm , and 30 μm linewidths respectively).

Figure 2 represents the device architecture and the states of operation. Linear electrical gradient cannot be created directly on PEDOT:PSS film by applying potential along the film because the charge transfer in conjugated polymers is not linear due to their charge transfer mechanism and polymeric chains structure. The electrical gradient was rather created on ITO-coated substrate by applying positive (+ve) and negative (-ve) voltages at its two ends. Due to the big difference in conductivity between PEDOT:PSS (0.1 S cm^{-1}) and ITO ($4 \times 10^3 \text{ S cm}^{-1}$), the potential values along the ITO surface area replicated vertically to the PEDOT:PSS film.

It should be mentioned that the typical conductivity of PEDOT:PSS is a lot higher ($\sim 500 \text{ S cm}^{-1}$) than the values we obtained. This damping in conductivity was made in purpose by adding 3-glycidoxypropyltrimethoxysilane (GOPS; 3.5 wt.%)^[13] to the PEDOT:PSS mixture solution and without adding ethylene glycol (EG) or Dimethyl sulfoxide (DMSO) or other polar solvents or additives that enhance the film conductivity.^[32] To oxidize or reduce or create an electrochemical gradient on PEDOT:PSS film, a reference/ground electrode is immersed in the electrolyte or media. This configuration enables to force ions to move in or out of the PEDOT:PSS film by applying a bias. When applying only a -ve bias, the positive ions in the electrolyte move into the PEDOT:PSS film then it becomes reduced and the color change to a dark blue as shown in figure 2 (c) due to the electrochromic property of PEDOT:PSS. In contrast, when applying a +ve bias, the positive ions move out of the film and the film becomes oxidized, and the color change to be transparent. While when applying a potential along PEDOT:PSS film, the redox state (oxidation/reduction) at every point along the film (on the x-axis) have a different potential, starting from a highly reduced (at the -ve end) to a highly oxidized (at the +ve end) passing by the neutral state at the central line of the device. The bias we applied on our devices is -1.3 V and +1.3 V at the contacts, and -0.5 V and +0.5 V at the two ends of the stripes.

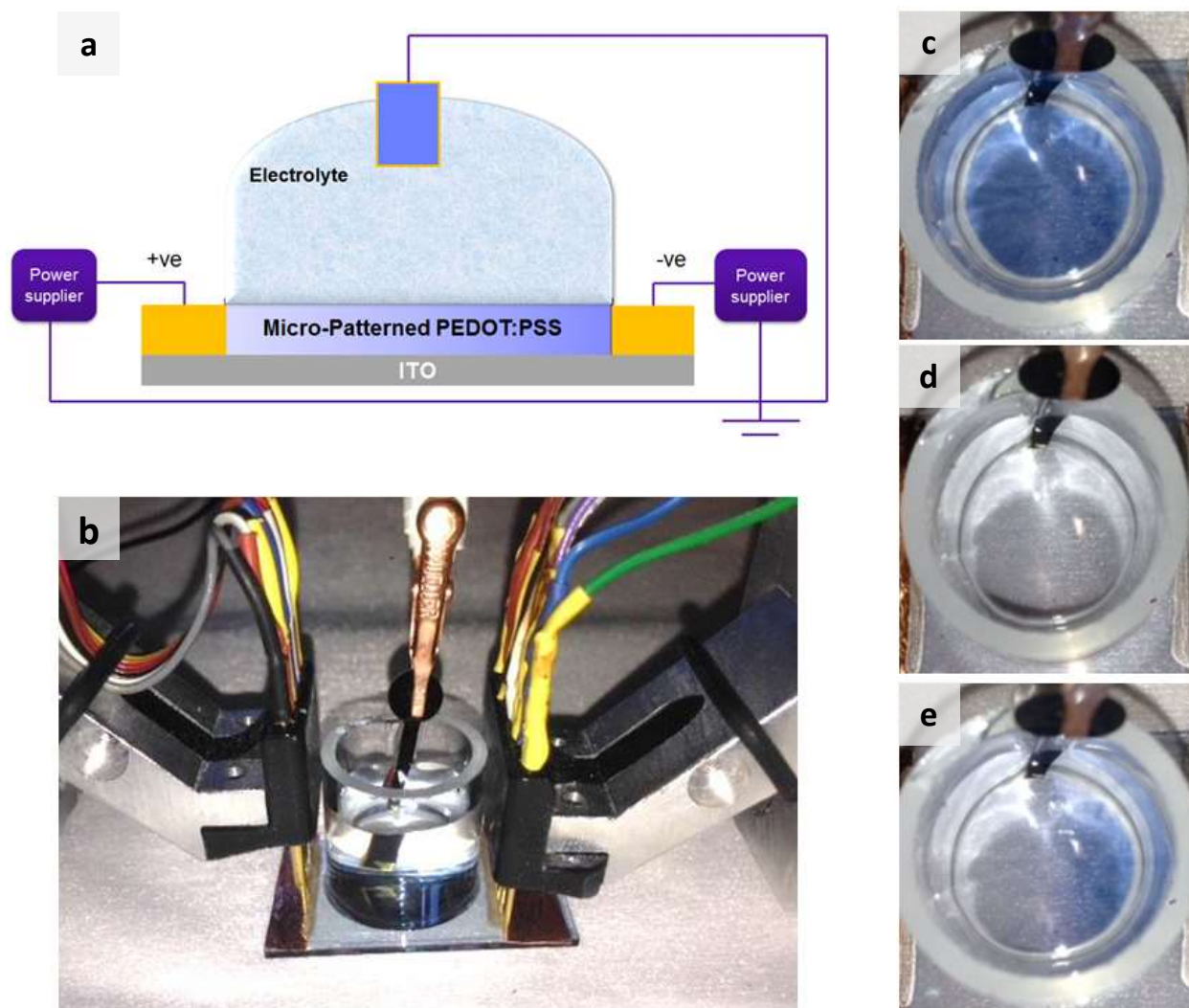
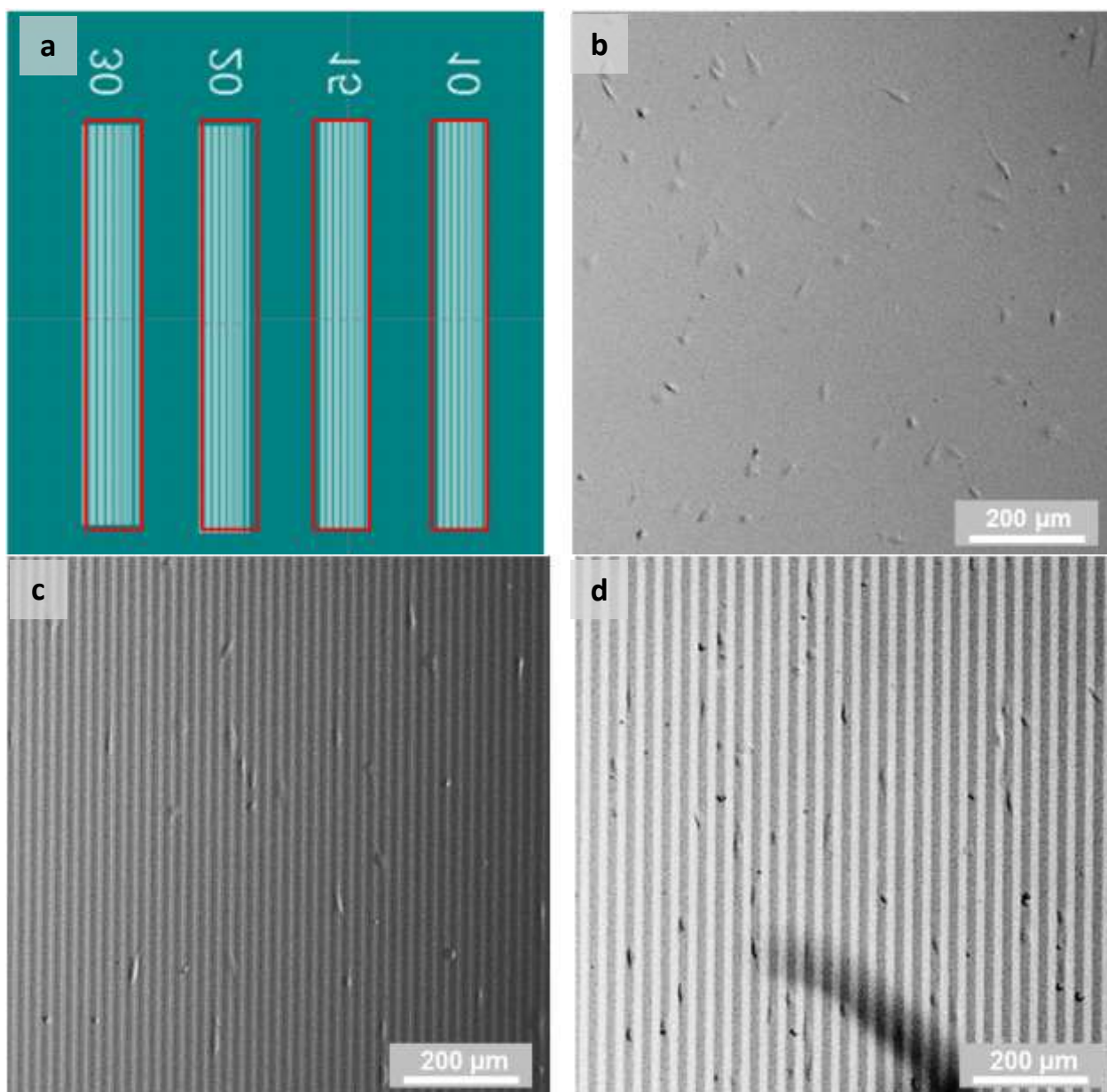


Figure 2. (a) Scheme of device configuration. (b) Image of the wired device with the well filled with electrolyte. (c) The device in the reduction state ($-ve$ bias). (d) The device in the oxidation state ($+ve$ bias). (e) The device in the gradient state ($+ve$ and $-ve$ bias).

PEDOT:PSS films were patterned into 4 groups of micro-strips of varying widths (10, 15, 20, and 30 μm) as shown in **figure 3 (a)**. The length of the lines is 12 mm, and the width of each group is 2 mm, while the distance between lines is also 2 mm. The average size of hCMEC cells is $\sim 15 \mu\text{m}$ wide and between 80-165 μm in length. The cells have shown alignment to the micro-strips of all dimensions as shown in figure 3. The dark grey strips in the images (figure 3 (b-f)) represent the higher level of PEDOT:PSS patterns while the bright grey represents the lower level. ON all linewidths hCMEC cells have shown preferential adhesion to the upper level of the micro-patterned PEDOT:PSS film. When the lines get wider

(20 and 30 μm), the cells tend to adhere to the edges of these dark lines implying their affinity to the 3D structure of the film. The micro-patterns were also tested on the fibroblast (TIF) cells, and cells showed alignment to the micro-stripes as shown in **figure S2**, however this was a side experiment and is not the focus of this work, however it proves the potential of using our platform with different kind of cells.



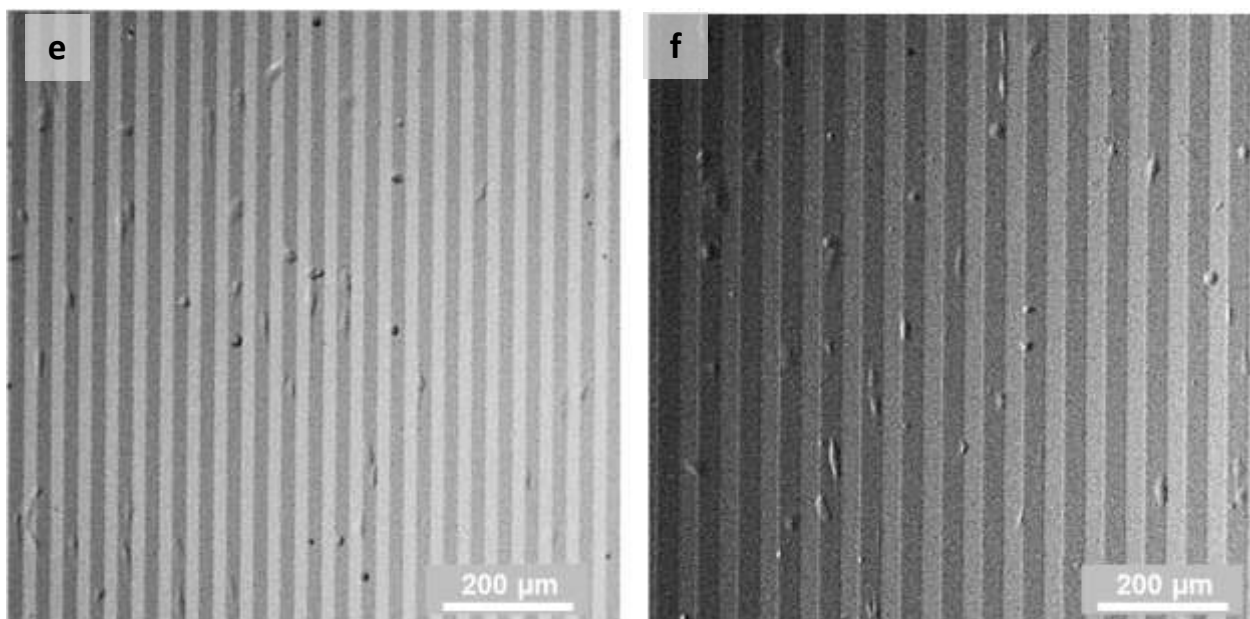
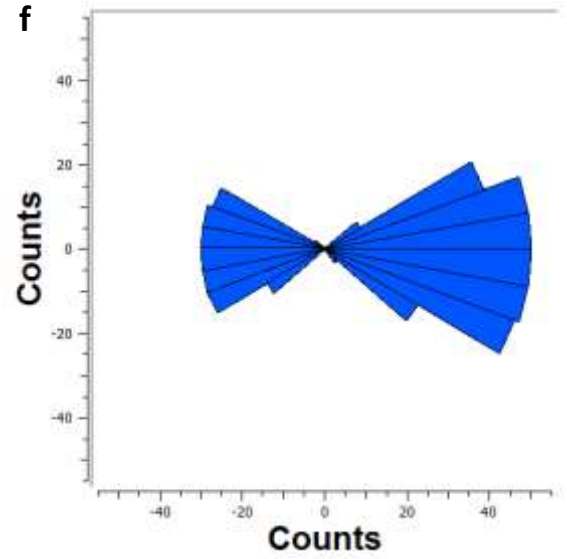
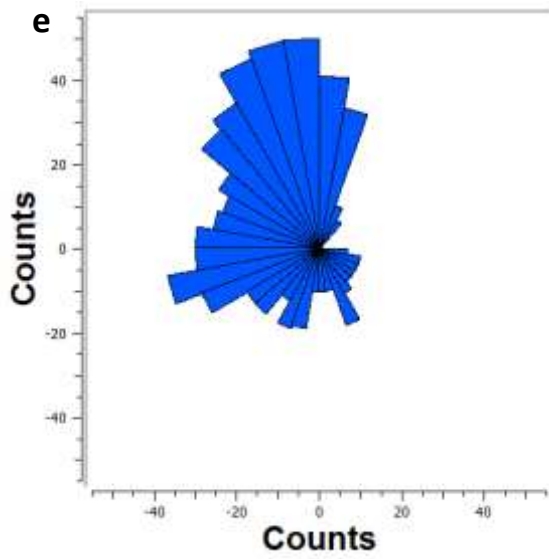
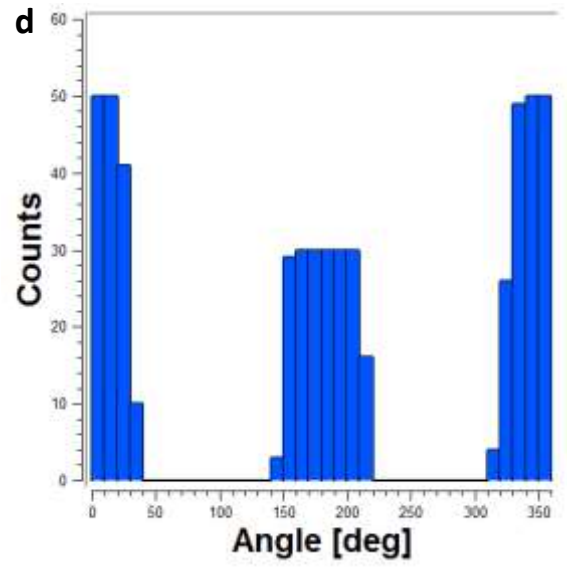
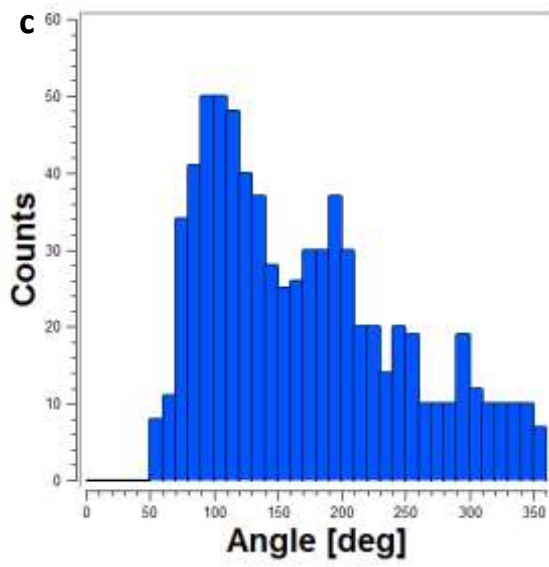
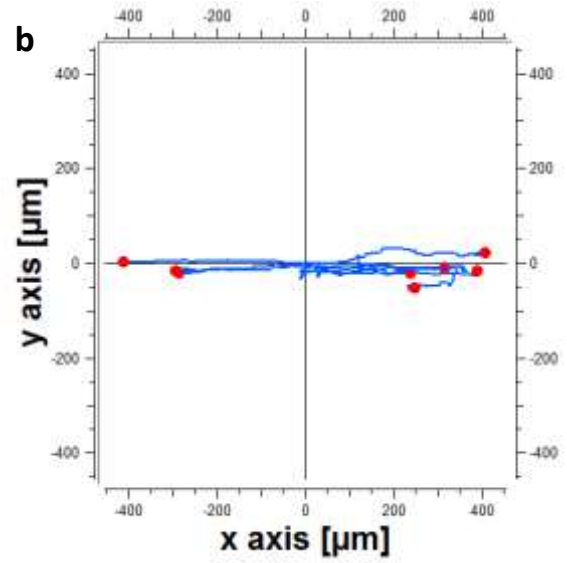
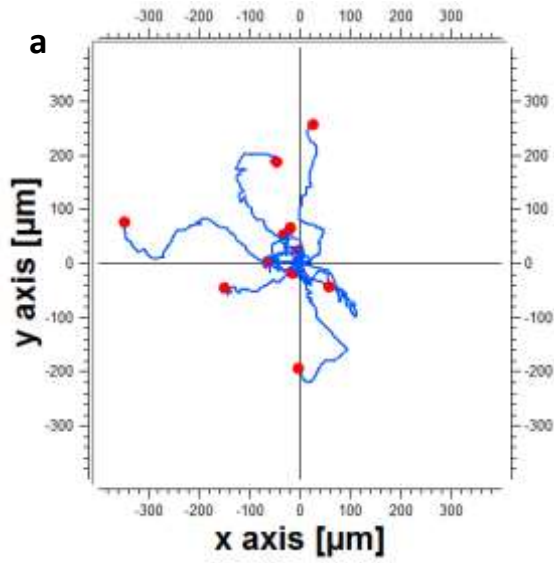


Figure 3. (a) Scheme of the device surface from a top view containing 4 groups of micro-strips of varying linewidths. (b-f) hCMEC cells aligned on PEDOT:PSS micro-strips (linewidths 10, 15, 20, and 30 μm respectively).

Figure 4 demonstrates the motion analysis of hCMEC cells on flat vs micro-patterned PEDOT:PSS films (with no bias) in terms of trajectories, angles of motion, and velocity. The trajectories of hCMEC cells on a flat PEDOT:PSS film showed a random motion as shown in figure 4(a) compared to a linear motion along the x-axis in the case of micro-patterned PEDOT:PSS film as illustrated in figure 4(b). In these plots, all the motion data was processed to have the same start point $(x, y) = (0, 0)$, and the end of the trajectories (blue lines) for every cell is indicated by the red point. The average accumulated distance travelled by the cells during the period of the experiment (~ 17 hours) is $344.1 \pm 139 \mu\text{m}$ on the flat PEDOT:PSS film, and $522.9 \pm 64.4 \mu\text{m}$ on the micro-patterned PEDOT:PSS films (**Table S1**). However the average Euclidian distance (the distance between the start and the end points) travelled by the cells was $134.5 \pm 107.3 \mu\text{m}$ on the flat film compared to $324.4 \pm 70 \mu\text{m}$ on the micro-patterned film (Table S1).



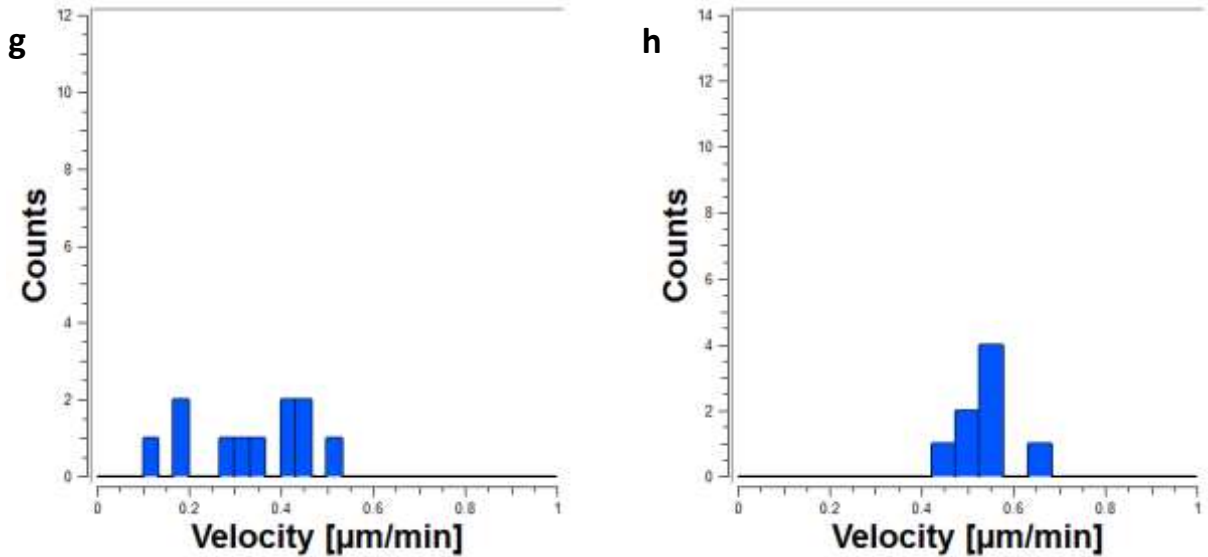


Figure 4. Analysis plots of hCMEC cells migration on flat (left column) vs micro-patterned (right column) PEDOT:PSS films with no bias. (a-b) Spatial plot of cells trajectories over 17 hours. (c-d) Histogram of cells angles of motion. (e-f) Rose diagram of the cells migration orientation. (g-h) Histogram of cells migration velocities.

The average directness (D) of the cell trajectories (n) was calculated by comparing the Euclidian to the accumulated distances as in **equation (1)**.^[33] The theoretical maximum value of D is 1, which represents a straight line. The average directness of hCMEC cells on the micro-patterned PEDOT:PSS is 0.64 compared to 0.38 on the flat PEDOT:PSS film.

$$D = \frac{1}{n} \sum_{i=1}^n \frac{d_{i,euclidian}}{d_{i,accumulated}} \quad (1)$$

Histograms of angles of motion of hCMEC on flat vs patterned PEDOT:PSS films are demonstrated in figure 4 (c) & (d) respectively. The histogram shows the angles taken by all cells along their trajectories. The plot demonstrates more divergence in cells orientation on flat PEDOT:PSS film compared to the micro-patterned film. In Figure 4 (e) & (f), the rose diagrams show the distribution of migration angles (from start to end points) with intervals of 10 degrees. The radius of the wedges indicates the number of cells. Rose diagram visualizes the orientation of cell migration independently of cell velocity. The circular distribution of the end points was confirmed to be uniform by doing Rayleigh uniformity test; $P = 0.13$ and 0.62 for cells on the flat film and micro-patterned film respectively, which are above the median

value at 0.05.^[34] The average velocity of hCMEC cells on the flat PEDOT:PSS devices was measured $0.33 \pm 0.13 \mu\text{m min}^{-1}$ ($= 19.8 \pm 7.8 \mu\text{m h}^{-1}$) vs $0.533 \pm 0.07 \mu\text{m min}^{-1}$ ($= 32 \pm 4.2 \mu\text{m h}^{-1}$) for the cells moving on the micro-patterned film as shown in figure 4 (g) & (h) (Table S1). This increased speed (by ~ 1.6 folds) of the hCMEC cells on the micro-patterned PEDOT:PSS films shows that the facilitated linear motion of the cells along the micro-strips allows higher velocities. That also show that the random motion of cells on flat PEDOT:PSS, which requires re-orientation, slows down the overall cell motion and decreases the accumulated and Euclidian distances migrated by the cells. Indeed, this platform incorporating micro-patterning provide a way for controlling cells migration orientation and speed.

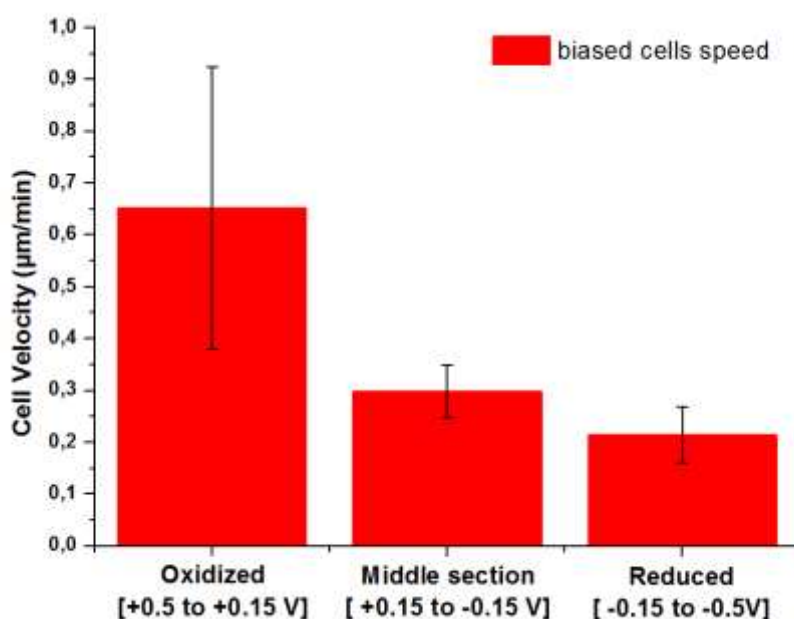


Figure 6. Speed of hCMEC cells on biased PEDOT:PSS micro-strips.

By applying electrical bias as shown in figure 2, the speed of cells could be tuned gradually along the device as shown in **figure 6** (reduced: $0.215 \mu\text{m min}^{-1} = 12.9 \mu\text{m h}^{-1}$ vs oxidized: $0.652 \mu\text{m min}^{-1} = 39.1 \mu\text{m h}^{-1}$). The speed increases by 3 folds on the oxidized region compared to the reduced region. This change in speed is arising from the gradual change of

the redox state of PEDOT:PSS films based on the electrical gradient (0.1 V mm^{-1}) created on the underlying ITO layer. Our results are comparable with what Alwin et al. found; an increase in the EC cells speed by 3 folds on the oxidized PEDOT:TOS ($32.5 \pm 3.8 \mu\text{m h}^{-1}$) compared to the control (neutral) PEDOT:TOS film ($11.5 \pm 1.6 \mu\text{m h}^{-1}$), while it didn't vary between the neutral and reduced sections of the PEDOT:PSS film. In our case the average cells speed at the central section of the biased micro-patterned device was lower than the average speed on the unbiased micro-patterned devices ($17.9 \mu\text{m h}^{-1}$ vs $32 \pm 4.2 \mu\text{m h}^{-1}$). This could be due to some unknown changes between cells batches seeded on two times for the two sets of devices. More experiments could be done to elaborate more on this specific comparison. However our results confirm the capability of controlling cells speed electrically and the migration trajectories by creating 3D patterns on PEDOT:PSS films. Cell migration is mediated by the fibronectin adhesion to the device surface. The fibronectin is adsorbed gradually on the surface as a result of the electrochemical gradient (low density at the oxidized regions vs high density at the reduced regions) as discussed in the introduction leading to a stronger adhesion of the cells on the reduced parts, hence more difficulty to break attachments at the rear side of the cells to form new ones at the front side of the cell while moving forward.

5.3 Conclusion

In this work we have shown the fabrication of micro-patterned PEDOT:PSS film using photolithography incorporating fluorinated photoresist. The fabricated micro-patterned PEDOT:PSS films were used as a substrate for hCMEC cells. The cells showed adhesion and alignment to PEDOT:PSS micro-stripes of different widths ($10 \mu\text{m}$ to $30 \mu\text{m}$). The cells migration speed on the micro-stripes was found to be 1.6 folds higher than its speed on flat PEDOT:PSS film, and the Euclidian distance was increased by 2.4 folds. When creating electrochemical gradient along the PEDOT:PSS films by applying a bias, the velocity of the

cells on the oxidized region was increased by 3 folds compared to the reduced region, and the speed of the cells was found to change along the film depending on its redox state. Future work using our platform may include studying the effect of the patterns dimensions and pitch on cells alignment and motion, as well as the effect of changing the mechanical properties (by varying GOPS percentage in PEDOT:PSS film composition) on cells adhesion and migration.

5.4 Experimental Section

Materials and Samples Preparation: PEDOT:PSS water dispersion (Clevios PH-1000 from Heraeus Holding GmbH.) was added to dodecyl benzene sulfonic acid (DBSA; 0.002 vol%) and sonicated for 15 minutes. Then 3-glycidoxypropyltrimethoxysilane (GOPS; ranging from 3.5 wt%) was added to the mixture solution followed by one minute stirring. The solution was filtered (0.8 μm filters; Minisart, from Sartorius Stedim Biotech) and spin-coated (2 layers at 3000 rpm, then 750 rpm for 35 seconds) on the ITO-coated substrates (from Solems SA, ITOSOL30). The PEDOT:PSS-coated substrates were then baked for 1 hour at 140 °C. The adhesion of the PEDOT:PSS films to ITO is known to be weak and when immersed in solution the films deform making wrinkles and delaminate off the ITO surface (**Figure S1**). Hence a surface functionalization step was performed on the ITO before spin-coating PEDOT:PSS by using GOPS. First, ITO substrates were plasma-activated (50 sccm, 100 W for 3 minutes). The substrates were then immersed in a solution (95:5 v/v ethanol:DI water, and 3 wt% GOPS) for 30 minutes, followed by washing with ethanol/water/ethanol, and eventually annealed for 20 minutes at 110°C. GOPS was chosen for functionalization to bond with the already existing GOPS in the PEDOT:PSS film composition.

Micro-patterning: PEDOT:PSS films were patterned using photolithography. The substrate were spin-coated by fluorinated photoresist (Oscar 5001, from Orthogonal Inc.) at 1200 rpm for 35 seconds, the soft-baked 65°C for 1 minute, and exposed by 63 mJ/cm² UV-light (365

nm) through a photo-mask to transfer the features of interest. After exposure, the samples were hard-baked for 1 minute at 70°C, and finally developed (developer 100, Orthogonal Inc.) for 120 seconds. The samples were etched afterwards by plasma reactive ion etching (RIE; plasmalab80plus, from Oxford Instruments) for 3 minutes (50 sccm O₂, 100 W, 10 °C). Finally, the samples were put in the stripper (Stripper 903, Orthogonal Inc.) for 3 hours to remove photoresist residuals, then were dried using nitrogen gun. The micro-pattered PEDOT:PSS was characterized using an optical microscopy (Olympus BH3-MJL4A), and a mechanical profilometer (Ambios XP-2).

Device preparation: Glass wells (diameter 12 mm) were fixed around the micro-patterned PEDOT:PSS by PDMS (Sylgard 184) and let cure overnight at 50°C. Gold electrodes coated (by drop-casting) by a thick layer of PEDOT:PSS were used as ground electrodes. The ground electrodes were fixed to the wells using PDMS (70°C for 2 hours) and then were let to cure overnight. The devices were then soaked in water for 2 hours to assure removing any contamination of any extra content in the PEDOT:PSS film and PEDOT:PSS ground electrodes. Finally the devices were dried using a nitrogen gun. Two conducting tapes made of copper were fixed at the two ends of the device for connecting to the power supply. The contacts were assured to completely stick to the ITO substrate by pressing and measuring the resistance using a multi-meter.

Cell Culture: Human cerebral microvascular endothelial cells (hCMEC/D3) immortalised with human telomerase reverse transcriptase catalytic subunit and Simian vacuolating virus 40 (hTERT/SV40) Large T antigen were kindly donated by Dr. Ignacio Romero (Department of Biological Sciences at The Open University, Milton Keynes), and first described by Weksler et al.^[35] hCMEC/D3 cells line is used in a wide range of in vitro models of the human blood-brain-barrier^[36–39] due to its morphological characteristics of primary brain endothelial cells

and the presence of specific brain endothelial markers and cell surface adhesion. hCMEC/D3 cells were grown in endothelial basal medium-2 (EBM-2; Lonza Group Ltd.) supplemented with SingleQuots (Lonza Group Ltd. UK). The hCMEC/D3 cells used in the experiments were between passage 29 and 32.

TIF cells were kindly provided by Ellen Van Obergghen Schilling (IBV Valrose, Nice) and transfected with p^{cmv}LifeAct-TagRFP (ibidi GmbH) using Lipofectamine®3000 in Opti-MEM Reduced Serum Medium. The transfection conditions were in accordance to the Lipofectamine®3000 reagent protocol (Invitrogen). A clone was selected and cultivated in Dulbecco's Modified Eagle's Medium (DMEM; Invitrogen) supplemented with 10% FBS and 50 µg mL⁻¹ of Geneticin® (Invitrogen) to establish a stable clone having a good expression of fluorescent labelling of actin cytoskeleton. Cells were used between passage 32 and 35.

Devices were seeded with TIF LifeAct or hCMEC/D3 both at very low density to reach 15% confluency after spreading. Before seeding the hCMEC/D3 cells, devices were coated with fibronectin (4 µg/cm², Sigma) during 1h at room temperature. Cells were maintained in a 5% carbon dioxide 95% saturated air atmosphere at 37°C for 24hrs before being used in time-lapse experiment.

Time-Lapse Microscopy and motion analysis: The devices were moved to the fluorescent microscope/incubation system (Axio Observer Z1 Carl Zeiss) at 37 °C and 5% CO₂, 2 hours after the system was stabilized. The microscope works in the transmission mode, hence the devices were placed with the cells side facing up. The media-containing wells were covered by a Para film to reduce evaporation. The microscope was set to take images of the devices every 20 minutes over the course of 15 hours (magnification 5x, and 10x over area 12 x 2 mm, and 12 x 14 mm respectively). The motion tracking was done using imageJ (Fiji image processing package) free software, and the motion analysis and diagrams were done using Ibidi (chemotaxis and migration free tool) software.

Electrical Bias Setup: The devices in the incubator were wired to a two-channel power supply (Keithley 2612B, Keithley Instruments). The three terminals (ground electrode, +ve electrode, and -ve electrode) were connected so that the +ve electrode is connected to one channel, and the -ve electrode is connected to the other channel, while the ground electrode (PEDOT:PSS-coated gold electrode) is connected to the two grounds from the two channels. The bias was set on during the whole time of the experiment.

References

- [1] P. Martin, P. Martin, **2012**, 75, DOI 10.1126/science.276.5309.75.
- [2] R. L. Juliano, S. Haskill, N. Carolina, **1993**, 120, 577.
- [3] R. L. Juliano, S. Haskill, N. Carolina, **1993**, 120, 577.
- [4] K. Saranak, Jurepan; Foster, **1997**, 387:465.
- [5] SB Carter, *Nature* **1967**.
- [6] Albert HARRIS, *Exp. Cell Res* **1973**, 77:285.
- [7] F. S. F. ELIZABETH J. PETTIT, *Physiol. Rev.* **1998**, Vol. 78, 949.
- [8] B. Lowe, **1997**, 1606, 1593.
- [9] C. Lo, H. Wang, M. Dembo, Y. Wang, *Biophys. J.* **2000**, 79, 144.
- [10] C. A. Erickson, R. Nuccitelli, **1984**, 98.
- [11] J. Rivnay, R. M. Owens, G. G. Malliaras, *Chem. Mater.* **2014**, 26, 679.
- [12] D. T. Simon, E. O. Gabrielsson, K. Tybrandt, M. Berggren, *Chem. Rev.* **2016**, 116, 13009.
- [13] M. Elmahmoudy, S. Inal, A. Charrier, I. Uguz, G. G. Malliaras, S. Sanaur, *Macromol. Mater. Eng.* **2017**, DOI 10.1002/mame.201600497.
- [14] C. M. Proctor, J. Rivnay, G. G. Malliaras, *J. Polym. Sci. Part B Polym. Phys.* **2016**, 54, 1433.
- [15] J. Rivnay, S. Inal, B. A. Collins, M. Sessolo, E. Stavrinidou, X. Strakosas, C. Tassone, D. M. Delongchamp, G. G. Malliaras, *Nat. Commun.* **2016**, 7, 11287.
- [16] J. Y. Wong, R. Langert, D. E. Ingber, **1994**, 91, 3201.
- [17] R. O. L. Anger, **1997**, 94, 8948.
- [18] N. K. Guimard, N. Gomez, C. E. Schmidt, *Prog. Polym. Sci.* **2007**, 32, 876.
- [19] R. E. M. Coby C. Larsena, Faina Klighmanb, Kandice Kottke-Marchanta, b, **n.d.**, DOI 2006.05.009.
- [20] C. Salto, E. Saindon, M. Bolin, A. Kanciurzevska, M. Fahlman, E. W. H. Jager, P. Tengvall, E. Arenas, M. Berggren, **2008**, 14133.
- [21] A. M. D. Wan, D. J. Brooks, A. Gumus, G. G. Malliaras, **2009**, 5278.
- [22] A. Gumus, J. P. Califano, A. M. D. Wan, J. Huynh, C. A. Reinhart-King, G. G. Malliaras, *Soft Matter* **2010**, 6, 5138.
- [23] P. Roach, T. Parker, N. Gadegaard, M. R. Alexander, *Surf. Sci. Rep.* **2010**, 65, 145.
- [24] L. M. Y. Yu, N. D. Leipzig, M. S. Shoichet, *Mater. Today* **2008**, 11, 36.
- [25] W. Zheng, W. Zhang, X. Jiang, **2012**, 1.
- [26] A. Blau, *Curr. Opin. Colloid Interface Sci.* **2013**, 18, 481.
- [27] A. I. Teixeira, G. A. Abrams, P. J. Bertics, C. J. Murphy, P. F. Nealey, **2003**, DOI 10.1242/jcs.00383.
- [28] M. J. Mahoney, R. R. Chen, J. Tan, W. M. Saltzman, **2005**, 26, 771.
- [29] J. Huang, R. Xia, Y. Kim, X. Wang, J. Dane, O. Hofmann, A. Mosley, A. J. De Mello, J. C. De Mello, D. D. C. Bradley, **2007**, 1043.
- [30] B. P. G. Taylor, J. Lee, A. A. Zakhidov, M. Chazichristidi, H. H. Fong, J. A. Defranco, G. Malliaras, C. K. Ober, **2009**, 1501, 2314.
- [31] B. A. A. Zakhidov, J. Lee, H. H. Fong, J. A. Defranco, M. Chazichristidi, P. G. Taylor, C. K. Ober, G. Malliaras, **2008**, 3481.
- [32] H. Shi, C. Liu, Q. Jiang, J. Xu, *Adv. Electron. Mater.* **2015**, 1, 1.
- [33] V. Semmling, V. Lukacs-kornek, C. A. Thaiss, T. Quast, K. Hochheiser, U. Panzer, J. Rossjohn, P. Perlmutter, J. Cao, D. I. Godfrey, P. B. Savage, P. A. Knolle, W. Kolanus, I. Förster, C. Kurts, *Nat. Publ. Gr.* **2010**, 11, 313.
- [34] N. I. Fisher, *Statistical Analysis of Circular Data*, Cambridge University Press, Canberra, **1993**.
- [35] B. B. Weksler, E. A. Subileau, N. Perriere, P. Charneau, K. Holloway, M. Leveque, H.

- Tricoire-Leignel, A. Nicotra, S. Bourdoulous, P. Turowski, *FASEB J.* **2005**, *19*, 1872.
- [36] K. Hatherell, P.-O. Couraud, I. A. Romero, B. Weksler, G. J. Pilkington, *J. Neurosci. Methods* **2011**, *199*, 223.
- [37] C.-H. Chou, J. D. Sinden, P.-O. Couraud, M. Modo, *PLoS One* **2014**, *9*, e106346.
- [38] X. Shao, D. Gao, Y. Chen, F. Jin, G. Hu, Y. Jiang, H. Liu, *Anal. Chim. Acta* **2016**, *934*, 186.
- [39] G. Adriani, D. Ma, A. Pavesi, R. D. Kamm, E. L. K. Goh, *Lab Chip* **2017**, DOI 10.1039/C6LC00638H.

Supporting Information

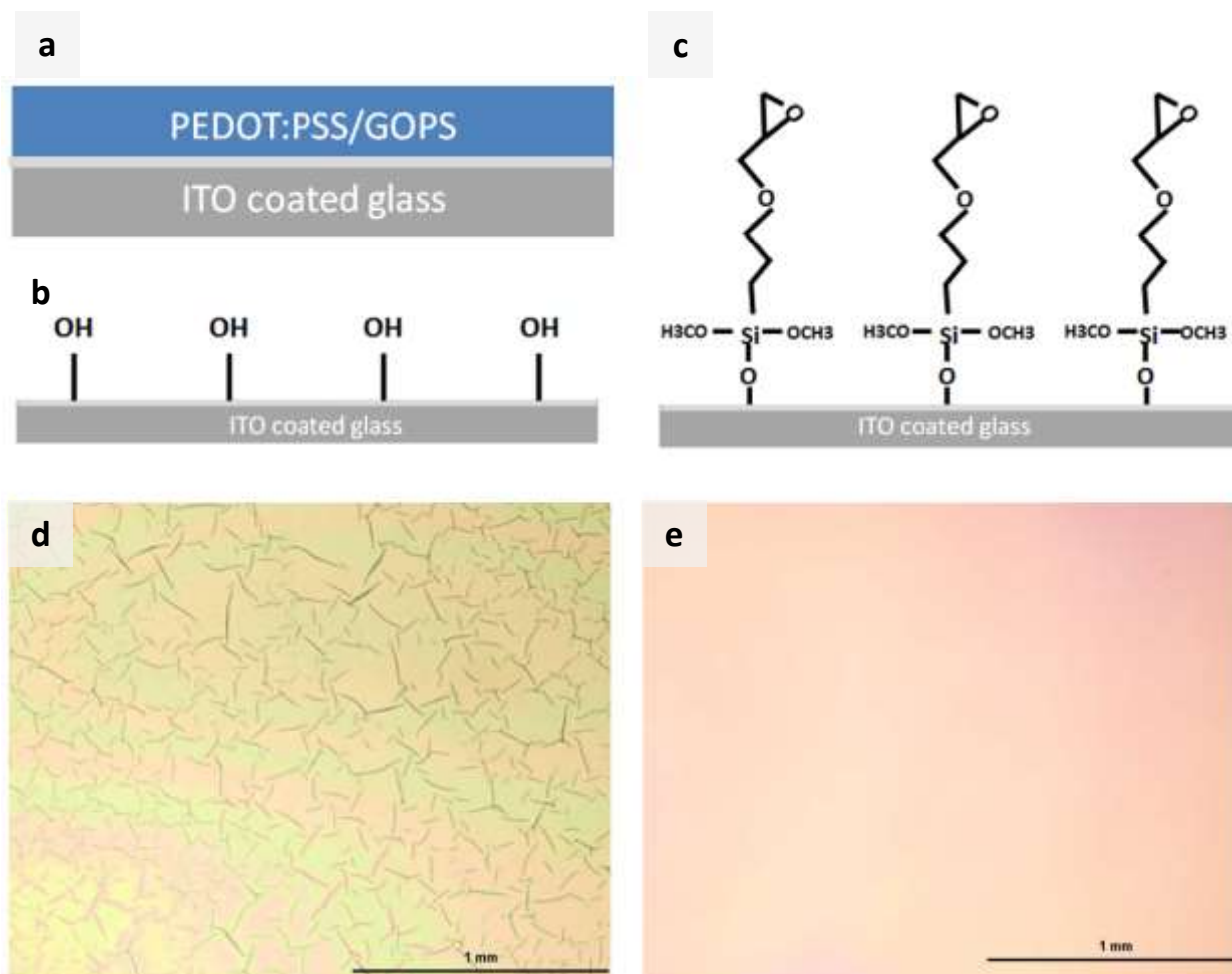


Figure S1. (a) Scheme of the PEDOT:PSS/GOPS spincoated on ITO surface. (b) Hydroxyl groups on the ITO surface after plasma activation. (c) GOPS functionalized ITO surface. (d) Spin-coated PEDOT:PSS on ITO without prior surface functionalization. (e) Spin-coated PEDOT:PSS on ITO with surface functionalization.

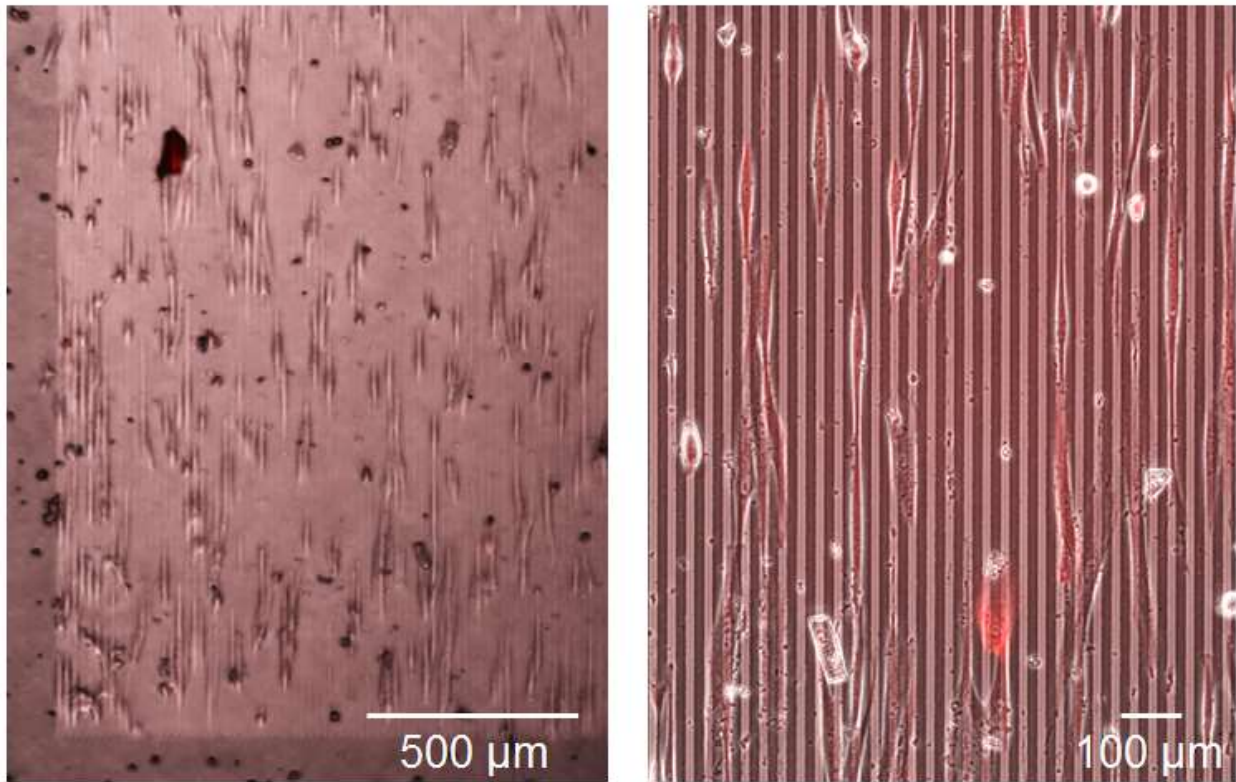


Figure S3. Fibroblast cells adhesion and alignment along PEDOT:PSS micro-stripes (15 μm width).

Figure S1. Summary of the motion analysis of hCMEC cells on flat vs patterned PEDOT:PSS films

Measured value	PEDOT:PSS	Min	Max	Mean	Std Dev
Accumulated distance [μm]	Flat	124.339	548.172	344.101	138.969
	Patterned	425.31	645.233	522.913	64.4439
Euclidean distance [μm]	Flat	23.7164	358.056	134.502	107.291
	Patterned	236.862	414.108	324.443	69.9719
Velocity [$\mu\text{m}/\text{min}$]	Flat	0.119557	0.527088	0.330866	0.133624
	Patterned	0.43399	0.658401	0.533585	0.0657591

Chapter 6

Conclusion and outlook

In this thesis the capabilities and potentials of conducting polymers (CPs) in biomedical applications have been demonstrated. Indeed, the soft nature of CPs makes them a superior candidate for biological interfaces when compared to inorganic materials since they induce reduced foreign body response from cells and biological tissue. Poly (3,4-ethylenedioxythiophene) doped with polystyrene sulfonate (PEDOT:PSS) was used as a prototypical CP due to its outstanding electrical, mechanical, and electrochemical properties, as well as its ease of processing, and the ability to tailor these properties to match the purpose of different biomedical applications.

Chapter 1 titled “PEDOT:PSS for Biomedical Applications” gives an introduction to PEDOT:PSS material properties and examines the literature for several approaches which have been used to improve or alter these properties. Through the use of advanced characterization technologies scientists are pushing the limits to understand the relationship between the changes in PEDOT:PSS film properties and the morphology and structure of these films. This chapter additionally covers synthetic routes of PEDOT:PSS, the various deposition and processing methods, and the resulting effect on the material properties. Finally it covers a wide range of biomedical applications using PEDOT:PSS, highlighting emerging subjects such as electrophysiology, bio-sensing, tissue engineering, and drug delivery.

Chapter 2 titled “Tailoring the Electrochemical and Mechanical Properties of PEDOT:PSS Films for Bioelectronics” is aimed at investigating the electrical, electrochemical, and swelling and mechanical properties of PEDOT:PSS thin films with varying amounts of the

cross-linker 3-glycidoxypropyltrimethoxysilane (GOPS). GOPS showed a dramatic impact on all of these properties, which gives us a wide range of choices when trying to tailor one of these. The increase of GOPS percentage in PEDOT:PSS solution resulted in a decrease in the conductivity, electrochemical impedance at 1 KHz, and swelling. This decrease is countered by an increase in the mechanical strength and aqueous stability of the PEDOT:PSS films. However, these trade-offs and optimizations of PEDOT:PSS film properties make it possible to match many applications and purposes. As a demonstration, organic electrochemical transistors (OECTs) were used to investigate the impact of various GOPS quantities in PEDOT:PSS films (used as the channel) on their performance. The figure of merit of the OECTs is the transconductance, which decreases gradually when increasing GOPS, due to the reduced conductivity and increased impedance. However at 1 wt.% GOPS, the conductivity of the PEDOT:PSS was still high and the mechanical stability in liquid is sufficient to demonstrate stable performance of the OECTs. This was shown by measuring the transconductance over 21 days. This study and quantification of the effect of GOPS on PEDOT:PSS film properties is essential to the rest of the research carried out in this thesis. This importance is indicated in every chapter, particularly regarding the control of mechanical properties and/or the conductivity for certain applications, including micro- and nano-patterning in order to understand the reasons behind these changes and their effect on the film performance and structure.

Chapter 3 titled “Facile Nano-Patterning of PEDOT:PSS thin films” presents a straightforward fabrication technique for nano-patterning PEDOT:PSS by using a UV-curable epoxy as a supporting layer to transfer the patterns from a polydimethylsiloxane (PDMS) mold to a carrier substrate; rigid or flexible. This technique overcomes some of the limitations introduced when patterning PEDOT:PSS using other patterning techniques such as thermal nano-imprint lithography or capillary force lithography. The epoxy-assisted fabrication method allows also obtaining nano-patterened PEDOT:PSS on gold layer, hence making

electrodes suitable for neural recordings and stimulation and other biomedical applications. A great advantage of using nano-patterned PEDOT:PSS electrodes is the reduced electrode impedance. Our investigation has shown that the electrochemical impedance of nano-patterned PEDOT:PSS electrodes was lower than the flat PEDOT:PSS electrodes. This reduction in impedance is due to an increase of the surface area at the interface with the electrolyte compared to a flat electrode of the same size. Future work regarding this project would be to fabricate nano-patterned sub-millimeter electrodes, which would make the use of these electrodes with reduced impedance possible in *in-vivo* applications such as neural probes. Also by using molds with a higher aspect ratio, the impedance of an electrode would decrease more as the surface area will increase. The described fabrication method can be also used to micro-pattern materials that are not compatible with lithography process solvents as an alternative technique. Moreover, this nano-patterning technique can be used to fabricate nano-wire OECT devices, simply by etching the thin layer between PEDOT:PSS grooves. The interest of making such nanowires is the confinement of the polymer chains that might result in increasing the conductivity by forcing the charge carriers to move linearly.

Chapter 4 titled “Designing Low Impedance Amorphous PEDOT:PSS Electrodes for Neural Recordings” introduces a sensing platform for neural recordings with low impedance. In this investigation electrodes with a large volume and small exposed surface area to the electrolyte designed and fabricated. This was accomplished by opening a small aperture above the insulated PEDOT:PSS coated electrodes. In addition, we used a highly porous PEDOT:PSS film obtained by a freeze-drying method. Indeed, the very high porosity of the films allowed for a higher contact surface between the electrolyte and the PEDOT:PSS. With standard, non-porous films, the impedance is damped by 2.3 folds at 1000 Hz, thus hindering the ability to record neural activity with millisecond temporal resolution. As a proof of concept, these small-aperture devices were used to record signals from hippocampus in an *in vitro* setup and have shown a higher signal to noise ratio compared to a small electrode of the same

surface/electrolyte contact area. Our devices can be utilized to record signals from a single neuron more accurately as a result of its small size but lower impedance. Another future application involves the use of these electrodes in *in vivo* applications for neural stimulation or recording to enhance the signal to noise ratio.

Chapter 5 titled “Linear Cell Migration on Micro-Patterned Conducting Polymers” introduces a platform for cell guidance and controlled migration. In this work micro-patterned (parallel micro-strips) PEDOT:PSS films were used as a substrate for cell adhesion to induce alignment and linear motion. As a result the cells have shown alignment parallel to the micro-strips (10-30 μm). By studying the motion of the cells on these stripes it was found that the cells migration velocity was increased by 1.6 fold compared to their motion on a flat PEDOT:PSS film. Similarly, the Euclidian distance (the straight distance between the start and end points) taken by the cells moving on the micro-strips was increased by 2.4 fold when compared to a flat PEDOT:PSS film. In addition, an electrochemical gradient was created along the device (along the stripes) by biasing the device electrically to gradually vary the redox state of the PEDOT:PSS film along the device from a highly oxidized to a high reduced ends. As a result the cells showed varying speeds based on the their position on the device, which provides a higher level of electrical control of the cell migration. Future work on this could involve studying the effect of varying mechanical properties of PEDOT:PSS films and the pattern dimensions on cell motion. Additionally, investigating the effect of creating a steeper electrochemical gradient (sub-millimeter length devices) on the cell migration may allow a directional migration of cells between two points. Finally, nano-patterned PEDOT:PSS can be used to study cell adhesion and motion behavior.

Appendix

A1. Free-Standing Micro-/nano-patterned PEDOT:PSS

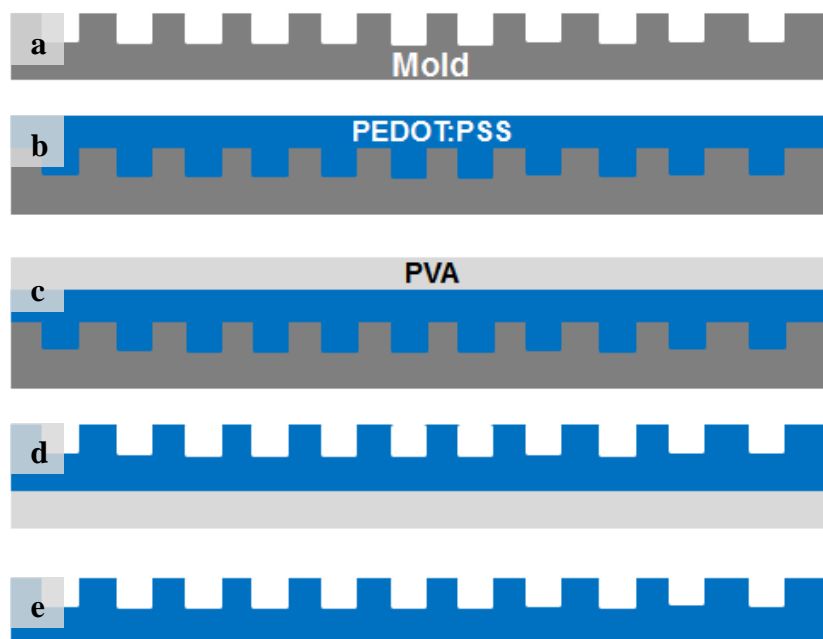


Figure A.1. Fabrication scheme of patterning PEDOT:PSS using poly vinyl alcohol PVA. (a) PDMS master replica from a silicon or quartz master mold as described in chapter 3. (b) Drop-casting or spin-coating PEDOT:PSS on the PDMS mold then baking at 110°C for 1 hour. (c) Drop-casting PVA on PEDOT:PSS and leaving it dry overnight. (d) Peeling off the PVA/PEDOT:PSS layers from the PDMS with tweezers. (e) Free-standing patterned PEDOT:PSS after dissolving PVA in DI water.



Figure A.2. Macroscopic images of big area patterned PEDOT:PSS film demolded from a PDMS mold using PVA layer.

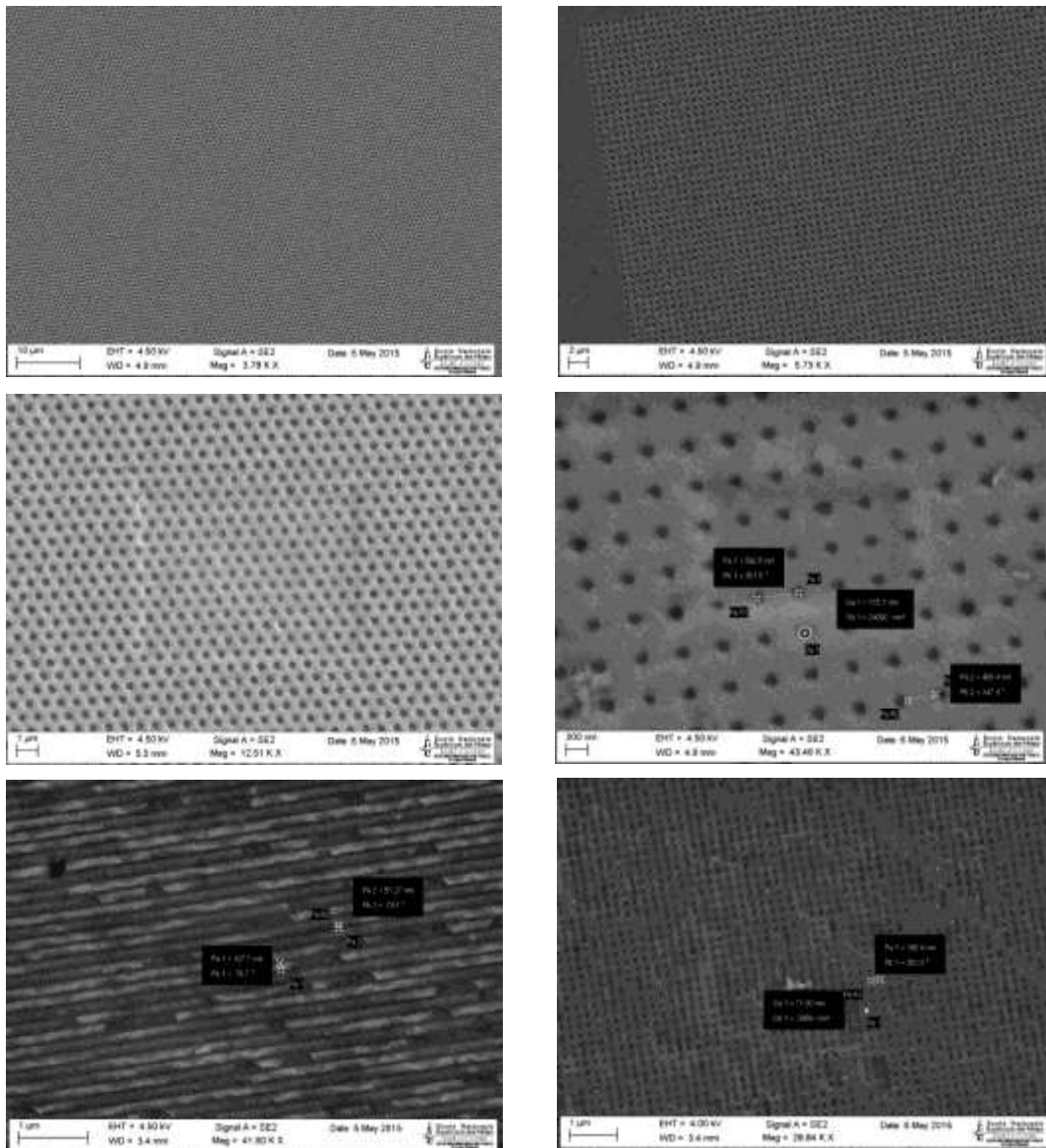


Figure A.3. SEM images of patterned PEDOT:PSS of varying dimensions.

A2. Micro-/Nano-Patterned PEDOT:PSS Using Nano-Imprint Lithography (T-NIL) on a Transfer Layer

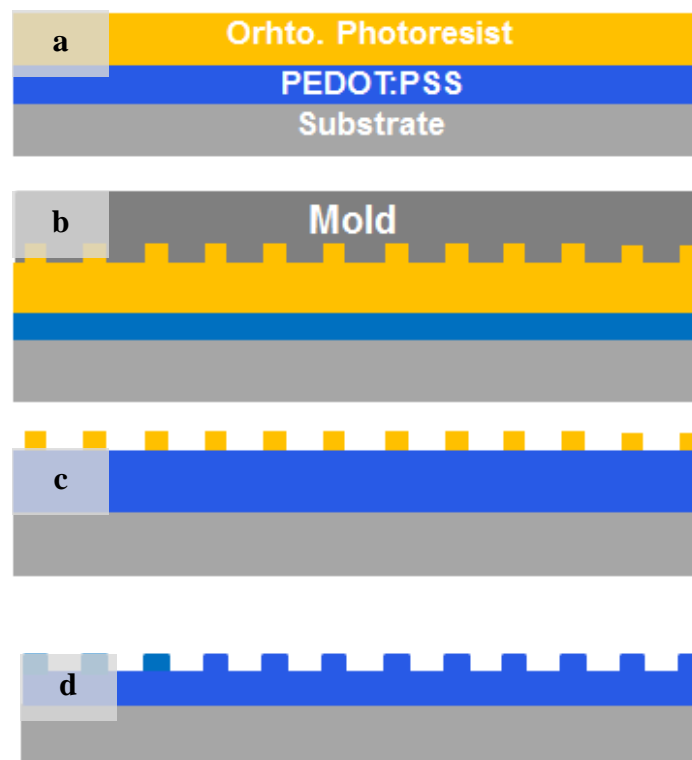


Figure A.4. Fabrication scheme of nano-patterned PEDOT:PSS using orthogonal photoresist. (a) Spin-coating PEDOT:PSS followed by baking at 110°C for 1 hour, then spin coating orthogonal photoresist; Oscar 5001 at 120 rpm for 35 seconds. (b) Applying the PDMS mold with some pressure using tweezers while soft baking at 65°C for 1 minute, and finally exposing the substrate to UV-light for curing the photoresist (as described in chapter 5). (c) Transferring the micro- or nano-features to the PEDOT:PSS by etching (as described in chapter 5). (d) Patterned PEDOT:PSS after stripping of the photoresist residual layer.

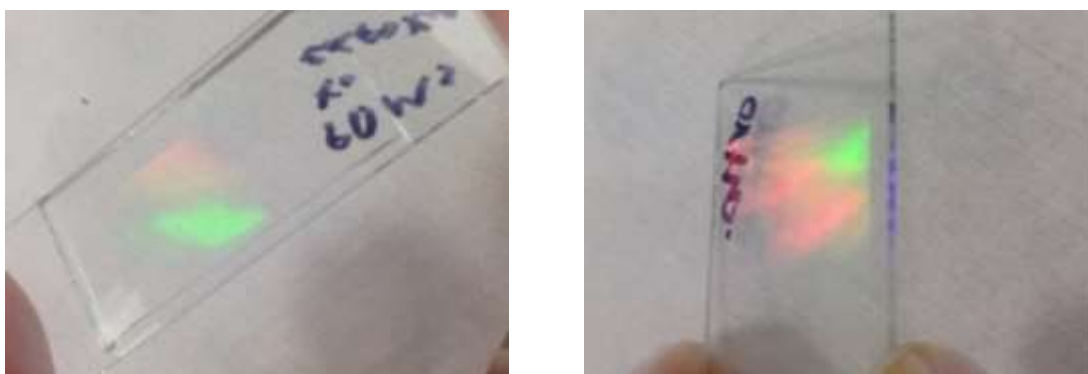


Figure A.5. Macroscopic images of nano-patterned (a) PDMS. (b) Orthogonal photoresist.

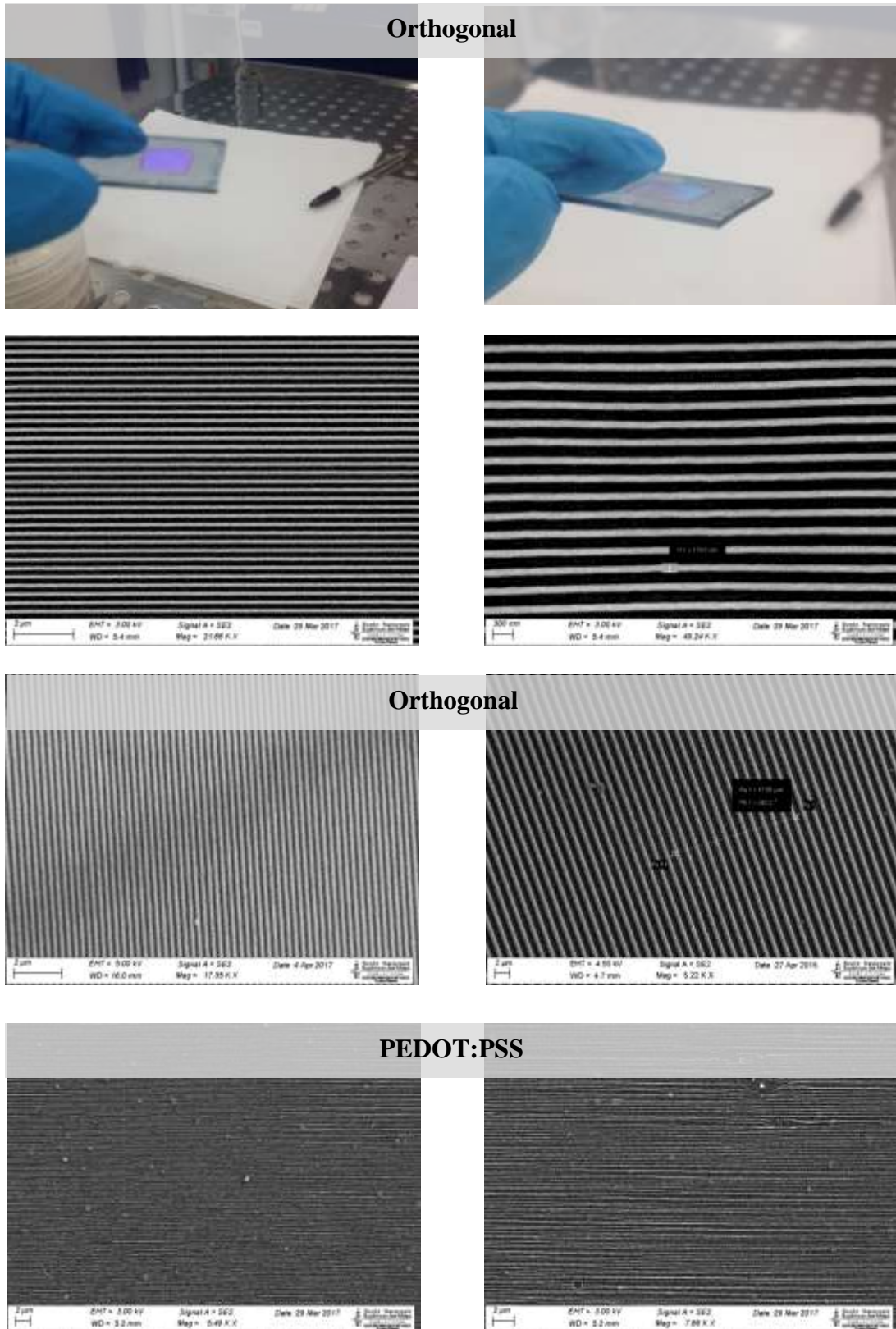


Figure A.6. (a-b) Macroscopic images of nano-patterned orthogonal photoresist. SEM images of nano-patterned: (c-d) PDMS. (e-f) Orthogonal photoresist. (g-h) PEDOT:PSS.

A3. Micro-/Nano-Patterned PEDOT:PSS Using Capillary Force Lithography (CFL)

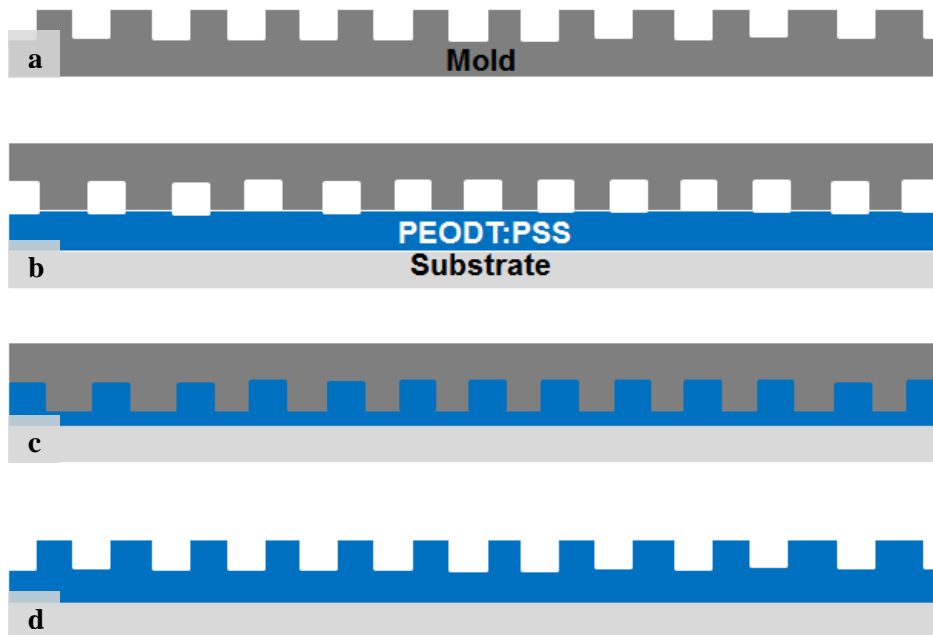


Figure A.7. Fabrication scheme of PEDOT:PSS using CFL. (a) PDMS replica (as described in chapter 3) based on quartz mold. (b) PEDOT:PSS spin-coated on a glass substrate at 200 rpm. (c) Applying the PDMS mold on the PEDOT:PSS without applying pressure (the PEDOT:PSS elevated to fill the features by the capillary forces) and baking for 5 minutes at 90°C. (d) Demolding the patterned PEDOT:PSS and continuing baking at 110°C for 1h.

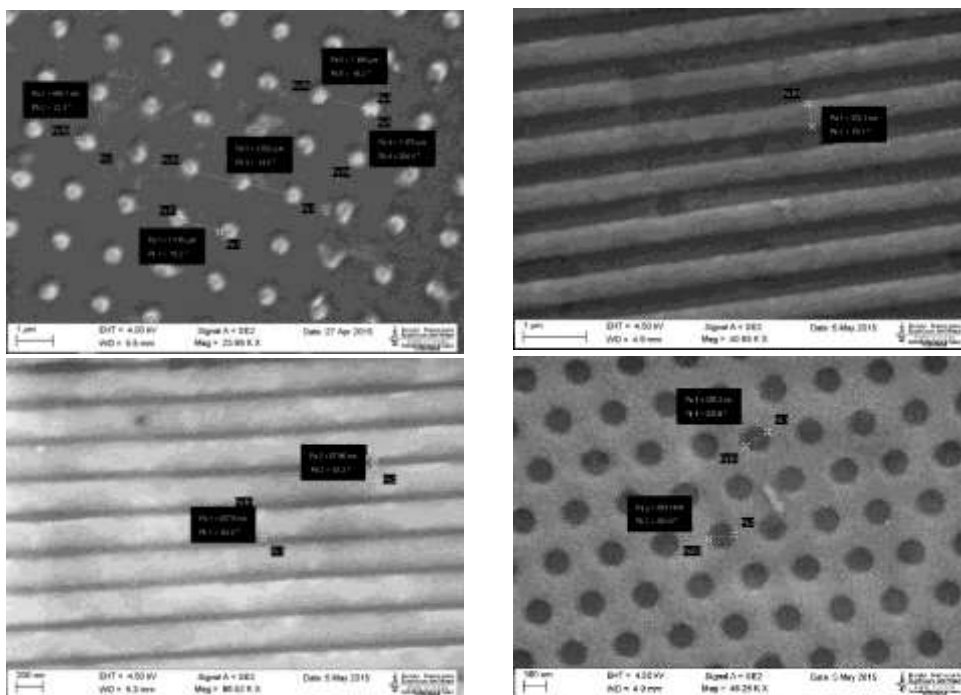


Figure A.8. Patterned PEDOT:PSS with varying dimensions using CFL.

List of Publications and Conferences

1. **Elmahmoudy, M.**, Inal, S., Charrier, A., Uguz, I., Malliaras, G. G., & Sanaur, S. (2017). Tailoring the Electrochemical and Mechanical Properties of PEDOT:PSS Films for Bioelectronics. *Macromolecular Materials and Engineering*, (March). <https://doi.org/10.1002/mame.201600497>
2. **Elmahmoudy M.**, Rutz A. L., & Malliaras G. G. PEDOT:PSS for BioMedical Applications. *Advanced BioSystems*. Review article in the submission process.
3. **ElMahmoudy, M.**, Charrier, A., Malliaras, G. G., & Sanaur, S. Facile Nano-Patterning of PEDOT:PSS Thin Films. Journal article in the submission process.
4. **ElMahmoudy, M.**, Curto, V., Ferro, M., Hama, A., O'Connor, R., Malliaras, G. G., & Sanaur, S. Cell Migration on Micro-Patterned Conducting Polymer Stripes. Journal article in preparation.
5. Schmidt, M. M., **ElMahmoudy, M.**, Malliaras, G. G., Inal, S., & Thelakkat, M. (2017). Smaller counter cation for better transconductance in anionic conjugated polyelectrolytes. *Macromolecular Chemistry and Physics*. Submission number: macp.201700374.
6. UGUZ, I., **ElMahmoudy, M.**, Khodagholy, D., Pitsalidis, C., Williamson, A., Bernard C., Malliaras, G. G., & DONAHUE, M. Micro-Porous PEDOT:PSS Micro-Electrodes Designed for Improved Neural Recordings. Journal article in preparation.
7. Mantione, D., del Agua, I., Schaafsma, W., **ElMahmoudy, M.**, Uguz, I., Sanchez-Sanchez, A., Sardón, H., Castro, B., Malliaras, G. G., & Mecerreyes, D. (2017). Low-Temperature Cross-Linking of PEDOT:PSS Films Using Divinylsulfone. *ACS Applied Materials & Interfaces*, acsami.7b02296. <https://doi.org/10.1021/acsami.7b02296>
8. **ElMahmoudy, M.**, & Sanaur, S. (2015). Fabrication and Properties of Micro/Nano-Structured Conducting Polymers for Electrophysiological and Biological Applications. Poster at the MRS Fall Meeting, Boston, United States of America.
9. **ElMahmoudy, M.**, Inal S., & Sanaur, S. (2016). Enhancing The Mechanical and Electrochemical Properties of PEDOT:PSS Thin Films. Poster at the International Winterschool on Bioelectronics 2016, Kirchberg, Austria.
10. **ElMahmoudy, M.**, Curto, V., Ferro, M., Hama, A., Malliaras, G. G. , Sanaur, S. (2017). Micro/Nano-patterned Conducting polymers towards low impedance contacts and cell guidance. EMRS, Strasbourg, France.
11. **ElMahmoudy, M.**, Curto, V., Ferro, M., Hama, A., Sanaur, S., Malliaras, G. G. (2017). Micro/Nano-Patterning for Organic Bioelectronics. Poster at the Journées de la recherche, Saint-Etienne, France.
12. **ElMahmoudy, M.**, Curto, V., Ferro, M., Hama, A., Sanaur, S., Malliaras, G. G. (2017). Organic Bioelectronic Devices for Cells Guidance and Control. Poster at the Journées de la recherche, Gardanne, France.
13. **ElMahmoudy, M.**, Inal S., & Sanaur, S. (2016). Enhancing The Mechanical and Electrochemical Properties of PEDOT:PSS Thin Films. Poster at the future of Microelectronics Symposium, Gardanne, France.
14. **ElMahmoudy, M.**, & Sanaur, S. (2015). 3D Patterned Conducting Polymer Arrays for Biological Applications. Poster at NaMiSCeB Workshop, Grenoble, France.
15. **ElMahmoudy, M.**, Malliaras G. G. (2016). ELBYSER Summer School, Chania, Greece. Participation.
16. **ElMahmoudy, M.**, & Sanaur, S. (2015). Bruker AFM Workshop, Bordeaux, France. Participation.